THE USE OF VARIOUS FAILURE CRITERIA
AS APPLIED
TO HIGH SPEED WEAR

THESIS

David A. Huber, Civilian

AFIT/GAE/ENY/11-D01

DEPARTMENT OF THE AIR FORCE
AIR UNIVERSITY

AIR FORCE INSTITUTE OF TECHNOLOGY

Wright-Patterson Air Force Base, Ohio

AFIT/GAE/ENY/11-D01

THE USE OF VARIOUS FAILURE CRITERIA
AS APPLIED
TO HIGH SPEED WEAR

THESIS

Presented to the Faculty

Department of Aeronautical and Astronautical Engineering

Graduate School of Engineering and Management

Air Force Institute of Technology

Air University

Air Education and Training Command

In Partial Fulfillment of the Requirements for the

Degree of Master of Science in Aeronautical Engineering

David A. Huber, B.S.M.E

Civilian

December 2011

APPROVED FOR PUBLIC RELEASE; DISTRIBUTION UNLIMITED.

The Use of Various Failure Criteria
As Applied
To High Speed Wear

David A. Huber, B.S.M.E

Civilian

Approved:

/signed/		- DATE -

Dr. Anthony N. Palazotto   date
(Chairman)

/signed/   - DATE -

Dr. William P. Baker   date
(Member)

/signed/   - DATE -

Chad S. Hale, Lt Col, USAF   date
(Member)

/signed/   - DATE -

Stephen P. Meador   date
(Member)

AFIT/GAE/ENY/11-D01

Abstract

This research has been aimed at developing methods to predict mechanical wear of sliding bodies at high velocities. Specifically, wear of test sled slippers at the Holloman High Speed Test Track at Holloman AFB, NM, is being considered. Developing a numerical model to represent the velocity range achieved at the test track is infeasible, so numerical modeling techniques must be adopted. Previous research has made use of finite element codes to simulate the high velocity sliding event. However, the extreme velocities at the test track can create numerical errors in the finite element codes. To avoid the numerical errors, an Eulerian-Lagrangian hydrocode called CTH has been used to allow for a velocity range of 200 to 1,500 meters per second. The CTH model used in this research performs plane strain analysis of a slipper colliding with a 6 μm radius semi-circular surface asperity.

The slipper-asperity collision event creates pressure waves in the slipper which leads to failed cells and worn material. Equations have been derived to represent the onset of plasticity and elastic wave speed through a material under plane strain conditions. These equations were validated using the CTH model. Several failure criteria were evaluated as possible methods to estimate damaged material from the sliding body. The Johnson and Cook constitutive model was selected because of its ability to handle high strains, strain rates, and temperatures. The model developed in this thesis calculates total mechanical wear between 49.31% and 80.87% of the experimental wear from the HHSTT January 2008 test mission.

Acknowledgements

There are many people I need to thank for helping to make this research possible. First and foremost, my advisor Dr. Anthony Palazotto. I truly would have been lost without his guidance throughout the research and writing process. His ability to process and interpret all the research and answer all the questions asked has been a true inspiration to acheive better results academically. The countless discussions of wave mechanics, and how to extend existing characterizations to the plane strain scenario, have been crucial for my contributions to this ongoing area of research. I also need to thank Mr. Stephen Meador for all his help in understanding the CTH modeling process. He helped to provide a solid foundation to start researching the wear phenomenon. Additionally, I need to thank the Air Force Office of Scientific Research for funding this research work through the STTR phase I grant. I would also like to thank the professors at the great and wonderful Miami University who helped me to realize the possibility of grad school. My undergraduate education was a truly significant experience that prepared me for graduate level courses.

The support of my family has been extremely helpful in my pursuit for a Master's degree. There isn't one thing I have done in my life that I can't attribute to their support. Finally, the unwaivering support of my fiancé throughout my time in grad school has consistently helped me stay focussed on my research and to realize future possiblities.

David A. Huber

Table of Contents

List of Figures

List of Tables

List of Symbols

List of Abbreviations

The Use of Various Failure Criteria

As Applied

To High Speed Wear

I. Introduction

The purpose of this research is to examine the interactions of sliding bodies at high velocities that lead to wear. In order to accomplish this, the wear of test sled slippers at the High Speed Test Track, (HHSTT), at Holloman Air Force Base (AFB) is being considered. Principle concepts of impact and wave propagation are used to evaluate different failure criterion within the material. This chapter will discuss the goals of this thesis, as well as provide a background on the HHSTT. Also, previous research in the formulation of wear models will be discussed.

1.1   Objective of Research

The HHSTT performs a variety of tests at high velocities using a rocket sled system that rides on a set of rails. The sled is attached to the rails using slippers, which are described in greater detail in Section 1.2. The rail is composed of AISI 1080 steel, whereas the slippers are made of VascoMax 300, a maraging steel. The HHSTT engineers would like to be able to estimate the amount of wear of each slipper to check whether it will reach a critical thickness before the end of the test run. The goal of this research is to develop a numerical model to predict mechanical wear of an HHSTT slipper as it slides down the track. These numerical models take advantage of known viscoplastic characteristics to quantify an amount, or volume, of material that has reached a prescribed failure criterion.

1.2   Holloman High Speed Test Track

The HHSTT is a rocket powered sled test track located at Holloman AFB in New Mexico. This test track facility is used for a variety of experiments including ground

level aerodynamic studies, investigating hypersonic conditions, munitions testing, and egress systems. In April 2003, a land speed record of 2,885 m/s (6,453 miles per hour) was set at the facility.

A rocket sled train used for these high speed experiments typically consists of several pusher stages and one forebody stage. Rockets are attached to each sled to accelerate the train to the desired velocity. The forebody sled carries the test payload and required instrumentation along with the final rocket. The setup shown in Figure 1.1 is the configuration used for a mission conducted in January 2008.
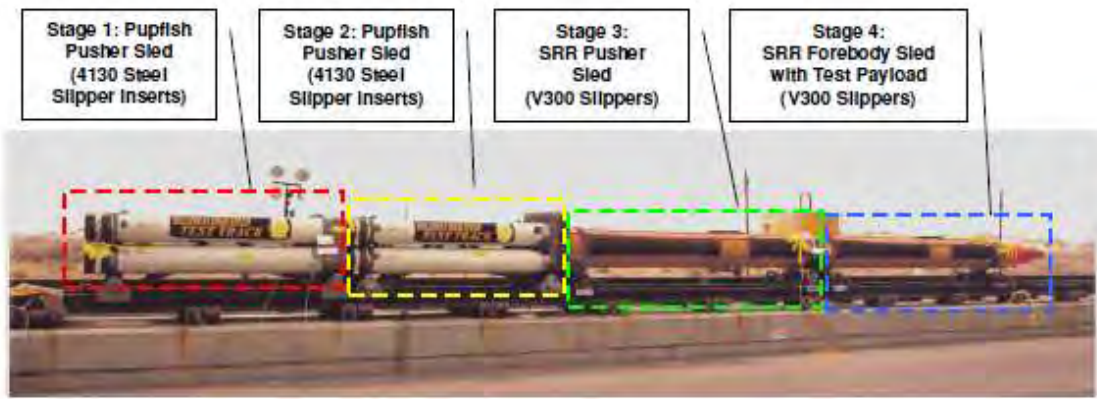
Figure 1.1:   January 2008 Rocket Test Sled

The sleds ride on parallel AISI 1080 steel rails approximately 6,000 meters long. Each sled is attached to the track by four slippers that wrap around the rail. Figure 1.2 shows the forebody sled attached to the rail for the record-setting mission in April 2003.

Slipper material is selected based on the maximum velocity of each slipper. The first two pusher sleds in the January 2008 configuration use AISI 4130 steel inserts placed between the rail and slipper housing, as shown in Figure 1.3. The steel inserts are discarded after each test, whereas the slipper housings are reused. The third pusher sled and forebody sled do not use the steel inserts, they only use slippers fabricated from VascoMax 300. These slippers are discarded after each test due to the amount of wear. Figure 1.4 shows the VascoMax 300 slippers attached to the rail.

2

Figure 1.2:   HHSTT Rocket Sled System
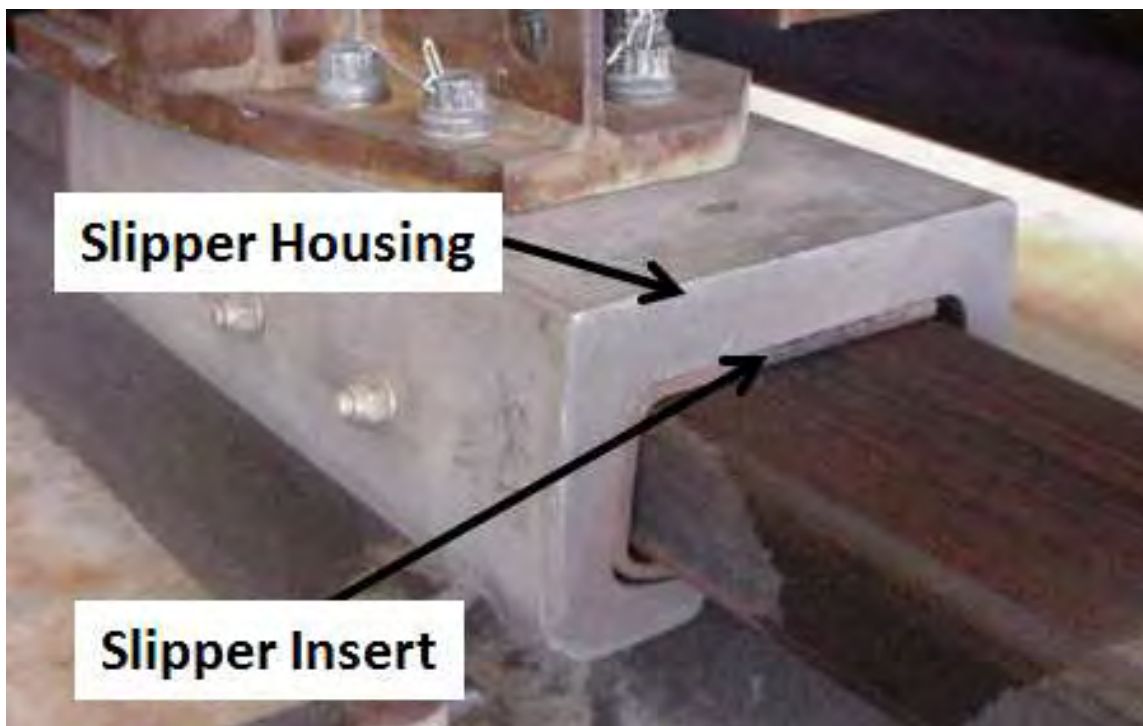
Figure 1.3:   VascoMax 300 Slipper with AISI 4130 Steel Insert

3

Figure 1.4:   VascoMax 300 Slipper without Steel Insert

Sled designers have considered several variables that may lead to poor data collection, or failed experiments. One concern is the amount of wear within the slippers as they reach desired velocities. Figure 1.5 shows the standard dimensions of the slippers used for the last pusher sled and forebody sled. The designers would like to be able to estimate the amount of wear of each slipper to check whether it will reach a critical thickness before the end of the test run.
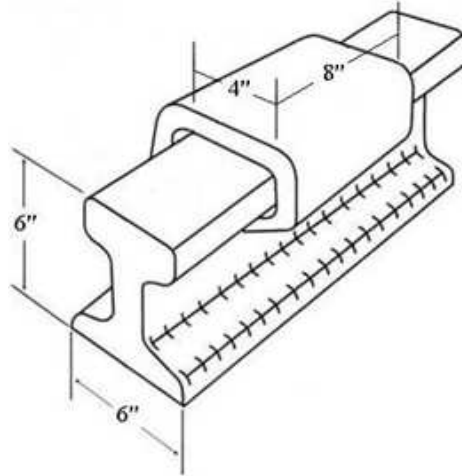
Figure 1.5:   HHSTT Slipper-Rail Dimensions

1.3   Summary of Previous Research

Research into the mechanics of wear has been ongoing for several decades. This research has led to several definitions of wear. The American Society for Testing and Materials, (ASTM), defines wear as "damage to a solid surface, generally involving progressive loss of material, due to relative motion between that surface and a contacting substance or substances" [5]. Researchers have developed various methods and experiments to define the rate at which material is removed as it slides against another surface.

One type of experiment is the pin on disk experiment. This experiment uses a rotating disk, or ring, and pin placed on the surface of the rotating disk. A force is applied to the pin and the material removed is measured. Figure 1.6 is a schematic of a pin on disk experiment.
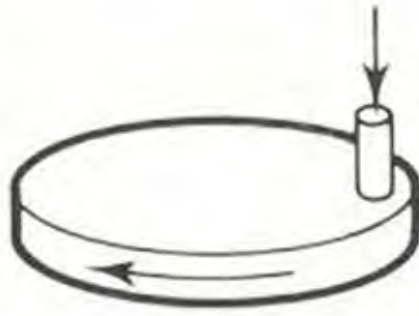
Figure 1.6:   Pin On Disk Experiment [13]

In 1956, Archard and Hirst [4] used a pin on disk experiment to study the wear of metals under unlubricated conditions. From their research, Archard and Hirst concluded that wear rate was initially dependent on time, until interface equilibrium was reached and the wear rate became constant.

In 1960, Wolfson [36] studied the wear of materials in high speed track applications. Sixty tests were performed at varying velocities, bearing pressures, track conditions, and sliding materials. The test allowed a sled to accelerate down a track. Once the desired velocity was reached, a pin was dropped into contact with the rail with a pneumatic device. This pin was held in contact with the rail at a constant bearing pressure during the test. The pin was removed from the rail once a specified sliding distance was reached. The amount of worn material was determined by comparing final dimensions and weights to initial values. Wear rates were determined by dividing the volume of worn material by the sliding distance. A conversion method was applied to Wolfson's data to compare results to the analytical model developed in this thesis. This conversion method and application of Wolfson's data is described in greater detail in Section 4.6.

In 1970, Farrell and Eyre [19] used pin-on-disk wear experiments to characterize wear between two steels. Their work provided distinction between mild wear and severe wear, the transition between the two states, and its dependence on both sliding

speed and applied load. Mild wear "involves the relatively slow removal of the tops of the highest contacting asperities with little substrate distortion," while severe wear shows a greater scale of surface damages and "the wear rate increases by some two orders of magnitude from that of mild wear and the maximum size of the wear particles increases suddenly at the transition load." Their work also showed that the coefficient of friction, μ, is dependent on both the sliding velocity and applied load, as shown in Figure 1.7.
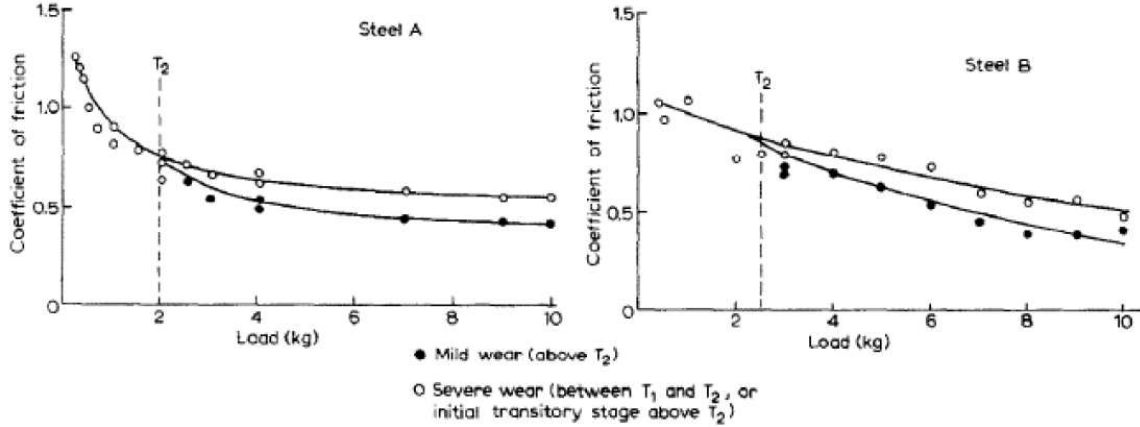
Figure 1.7:   Variation of Coefficient of Friction with Load [19]

The pin-on-disk experiments by Archard and Hirst, and Farrell and Eyre considered velocities on the order of 10 m/s. In 1976, Montgomery [30] published the friction and wear of metals in high muzzle velocity weapons. A pin-on-disk experiment was used with a velocity range of 3 to 550 m/s. In order to keep the pin from running over the same path on each rotation of the disk, the pin was moved radially. Strain gauges were used to measure the frictional and normal forces during the experiment. Similar to Farrell and Eyre, Montgomery's experiments showed that the coefficient of friction was dependent on both the sliding velocity and applied load, or pressure. The coefficient of friction was plotted as a function of the product of pressure and velocity, Pv, in Figure 1.8.

At low Pv values, the coefficient of friction was higher. As the Pv value increased, the coefficient of friction decreased exponentially to an asymptotic value.

7
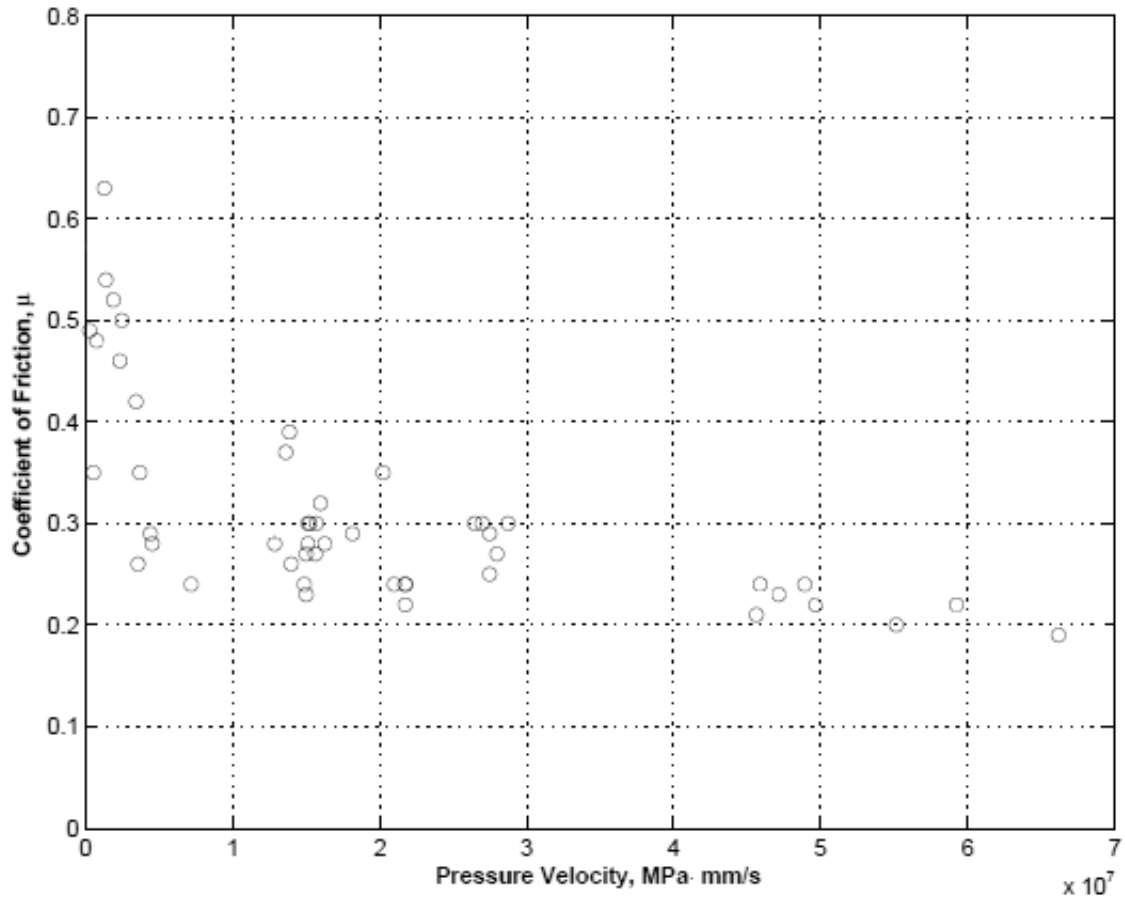
Figure 1.8:   Variation of Coefficient of Friction with Pv [30]

According to Montgomery, "the mechanism of wear at high sliding speeds is almost certainly surface melting followed by subsequent removal of a portion of the melted surface layer." This surface melting creates a film of molten material along the sliding interface, and effectively lowers the coefficient of friction to the asymptotic value in Figure 1.8.

In 1987, Lim and Ashby [26] published a paper describing the various mechanisms of wear. This paper formulated wear-mechanism maps showing the relationship between wear mechanisms and test conditions, sliding velocity and pressure. These wear mechanism maps were generated by applying two converging approaches. The first approach was to plot experimental results, and identify the mechanisms by observation. The second approach was to use numerical equations describing each mechanism. The two methods generate a map showing the total wear rate and define the contribution of each wear mechanism. Figure 1.9 shows the wear-mechanism map for steel.

Contours of constant normalized wear rates were superimposed on fields showing the regimes of dominance of different wear mechanisms. There were discontinuities in the contours when they cross the field boundaries into the regimes of severe-oxidational wear and melt wear. The wear rates given in parentheses were the values when mild wear takes place. The shaded regions indicated a transition between mild and severe wear [26]. The parameters were normalized to allow specimens of various sizes and shapes. Section 2.2 describes the normalization in greater detail. Very little work has been presented in the past that stresses the relationship between wear and wave mechanics, which is a goal of this research.

1.4   AFIT and HHSTT Wear Research

In 2007, Cameron [12, 13] used equations developed by Archard, and Lim and Ashby to characterize the wear of the HHSTT slipper from the 2003 test run. A code was written to analyze dynamic data and estimate mechanical and melt wear depths. The data was provided by Holloman using a program called Dynamic Analysis and
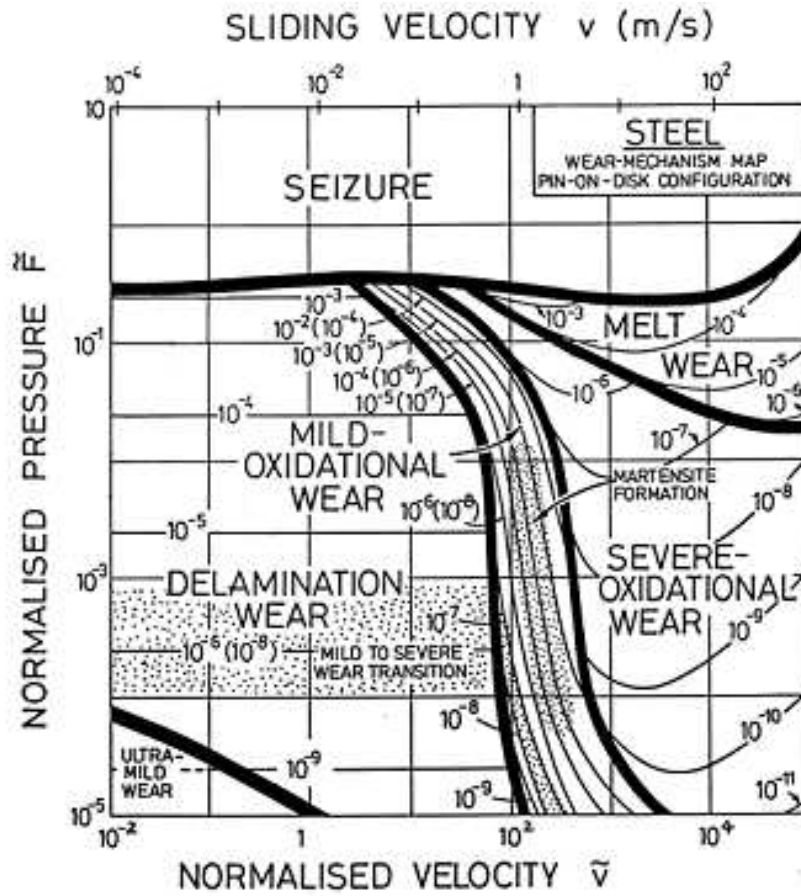
Figure 1.9:   Wear Mechanism Map for Steel [26]

10

Design System, (DADS). The DADS data is discussed in greater detail in Section 3.1. The test was a simulation of the forebody sled accelerating from 0 to 3,030 m/s at a constant acceleration for 2.5 seconds. Cameron's analysis calculated a mechanical wear depth of 0.27 cm and a melt wear depth of 0.08 cm. The total wear depth of 0.35 cm is less than the nominal thickness of the HHSTT slippers. The analysis was deemed an acceptable initial approximation of high velocity slipper wear depth because the slippers used at the track have never worn through the entire thickness due to a test run.

In 2008, Chmiel [14] used a finite element analysis, (FEA), approach to predict the wear of HHSTT slippers. Two methods were evaluated in the research. One method used equations developed by Archard on a macro-scale in incremental steps, and the second method utilized failure criterion based on material property on a micro-scale. The methods were evaluated at low velocities so results could be compared to previously published experiments. The incremental approach produced numerical errors during simulation that were deemed unacceptable. The failure method based on material properties was found to be a feasible solution.

In 2009, Burton [10, 11] studied the surface features of VascoMax 300 slipper and AISI 1080 steel rail samples. An optical profilometer was used to gain accurate measurements of the surface roughness. Figure 1.10 is a plot of recorded surface height data. The data was then filtered to remove surface waviness and microstructural features. Filtering the surface data was beneficial for modeling purposes because it removed sharp edges and sudden changes in profile which can lead to singularities when used in FEA models. Figure 1.11 is the FEA model of the slipper and rail specimens with scanned and filtered profile geometry used by Burton.

The FEA model was used to study the effect of mesh refinement on the coefficient of friction at the interface of the two sliding bodies. Burton stated: "If the key features of the surface irregularity are not represented in the model, the model coefficient of friction and the effective coefficient of friction for the macroscopic forces are essentially
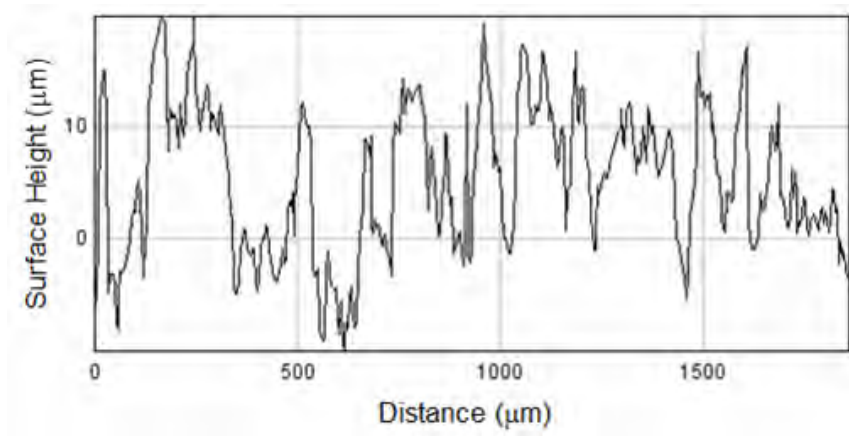
Figure 1.10:   VascoMax 300 Surface Height Data [11]
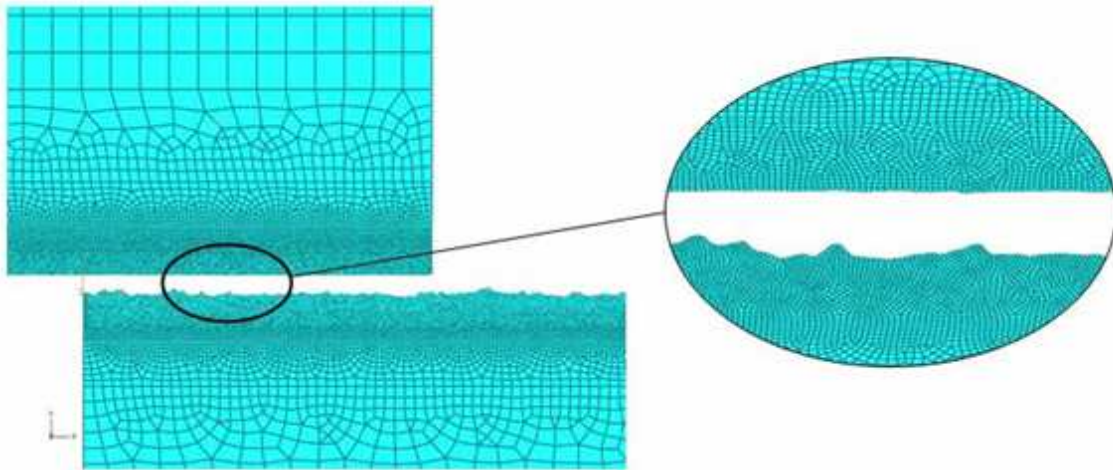
Figure 1.11:   Finite Element Model Used by Burton [11]

the same." This suggests that a precise measurement of the surface is not necessary to model the coefficient of friction.

In 2009, Hale [20] used a micro-scale FEA approach similar to Chmiel to model the mechanical wear rates of a hypothetical HHSTT test run. The velocity profile of the third stage from the January 2008 mission, Figure 1.12, was used for this research. The wear phenomenon is most accurately represented as a 3-dimensional problem. To simplify the model, a plane strain approach was used to simulate a VascoMax 300 test slipper sliding on a rail made of AISI 1080 steel and colliding with a semicircular surface asperity with a radius of 6 μm. The damage criterion used was based upon the viscoplastic behavior of the material defined by the Johnson-Cook [23] model, discussed in Section 2.4. The total damage accumulated by each finite element model (FEM) run was divided by the distance slid to achieve a plane strain wear rate.
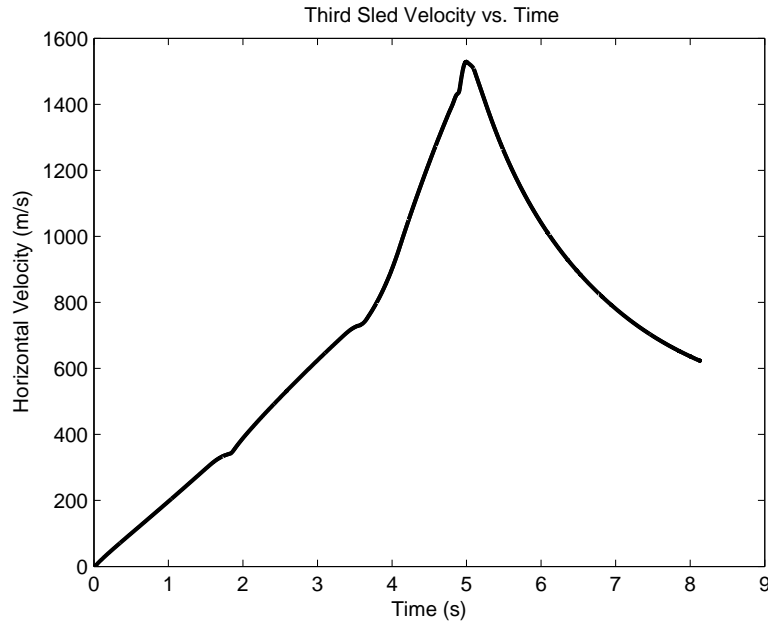
Figure 1.12:   HHSTT Third Stage Velocity Profile

Hale's model approximates the wear of HHSTT slippers by a collision with a single surface asperity under plane strain conditions. In a real test, the slipper bounces and slides across numerous asperities. In order to account for the multiple asperities, a scaling factor was developed. This scaling factor was determined by comparing

13

the calculated single asperity wear rates with the wear rate models developed by Archard [2–4]. Applying the scaling factor allows the HHSTT wear problem to be simplified to a simulation with a single asperity. The bouncing of the slipper was included in the calculation of total wear by multiplying the percentage of contact between the slipper and rail during a test run. The amount of slipper-rail contact, was determined from the DADS data. Additionally, a coefficient was applied to represent a semi-spherical surface asperity in the plane strain simulation. The Archard scaling factor, contact coefficient, and semi-spherical coefficient are described in greater detail in Sections 3.3 and 3.4.

In 2010, Meador [28] used a hydrocode to investigate the wear phenomenon. This model was also used to estimate the wear of a hypothetical HHSTT test run. However, Meador attempted to predict slipper wear of the fourth sled reaching a maximum velocity of 3,000 m/s. For this research, the velocity profile was identical to the third stage up to the point of max velocity and then accelerates to 3,000 m/s. Similar to Hale, a plane strain model was used to evaluate failure criterion due to the collision with a surface asperity.

Meador used the estimated wear rates to determine the total wear of an HHSTT slipper for an entire test run. The total wear calculation is described in greater detail in Section 3.4. The results of this calculation were compared to Hale's results and experimental data from the 2008 test mission. Figure 1.13 shows the total wear volume removed for a sliding distance of 5,186 meters, which is the length of the January 2008 test mission. Meador's predicted total wear was greater than Hale's, but was approximately 46% of the total measured wear from the 2008 test mission.

In 2010, Lodygowski [27] conducted research evaluating the temperature of two metals sliding relative to each other. The FEA model, shown in Figure 1.14 forces a plate made of VascoMax 300 to slide between two AISI 1080 steel surfaces. The temperatures of the material were calculated over a velocity range from 1 m/s to 200 m/s.
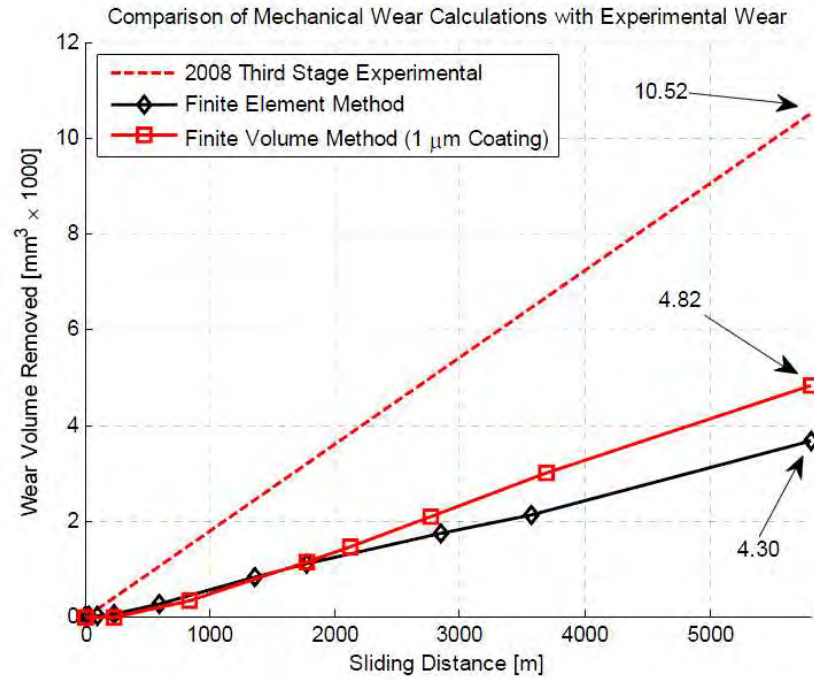
Figure 1.13:   Total Wear Predicted by Meador [31]
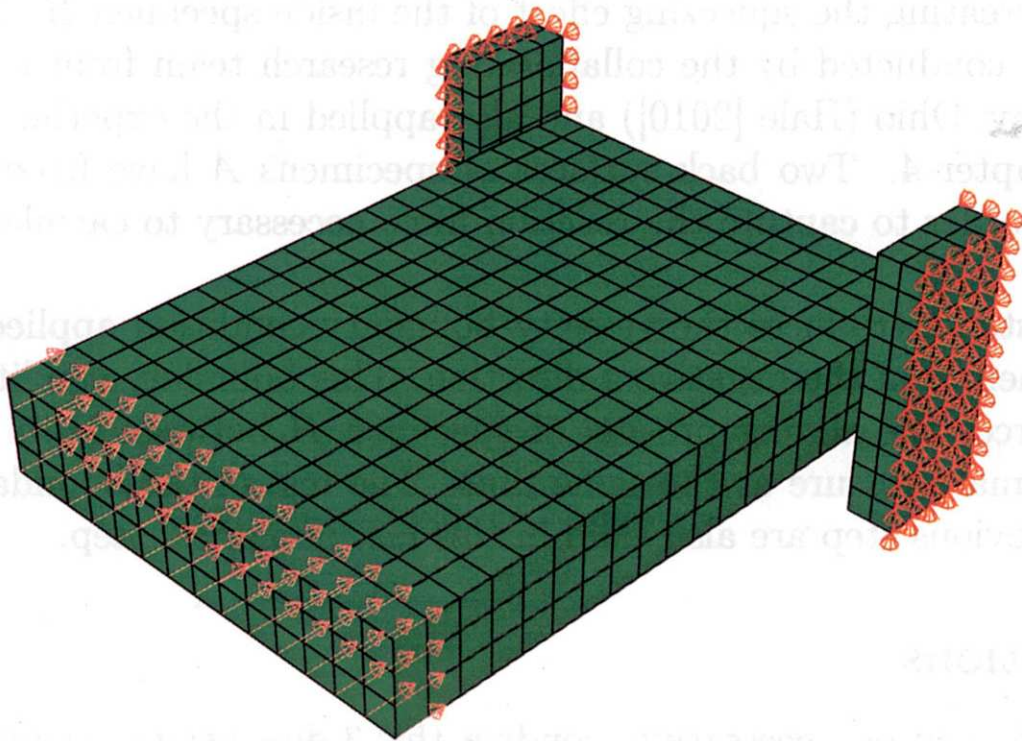
Figure 1.14:   Finite Element Model Used by Lodygowski [27]

15

Lodygowski's research provided two conclusions relevant to this thesis. The first conclusion states that the temperature of the VascoMax 300 plate does not change with sliding velocity. This is due to the fact that the entire VascoMax 300 plate is not in contact with the AISI 1080 steel throughout the whole simulation. However, the interfacing region of the AISI 1080 steel is in contact with the VascoMax 300 for the entire simulation, and the temperature of the AISI 1080 steel is affected by the sliding velocity. The model developed in this thesis maintains contact between the two materials during the entire simulation. As such, it is expected that the temperature of the materials will be affected by the sliding velocity. The second conclusion discusses the relationship between material temperature at the interface and sliding velocity. Figure 1.15 shows the average temperature of the AISI 1080 steel along the interface for a given sliding velocity. Lodygowski states that the relationship is not linear, but rather a logarithmic increase to a particular value.
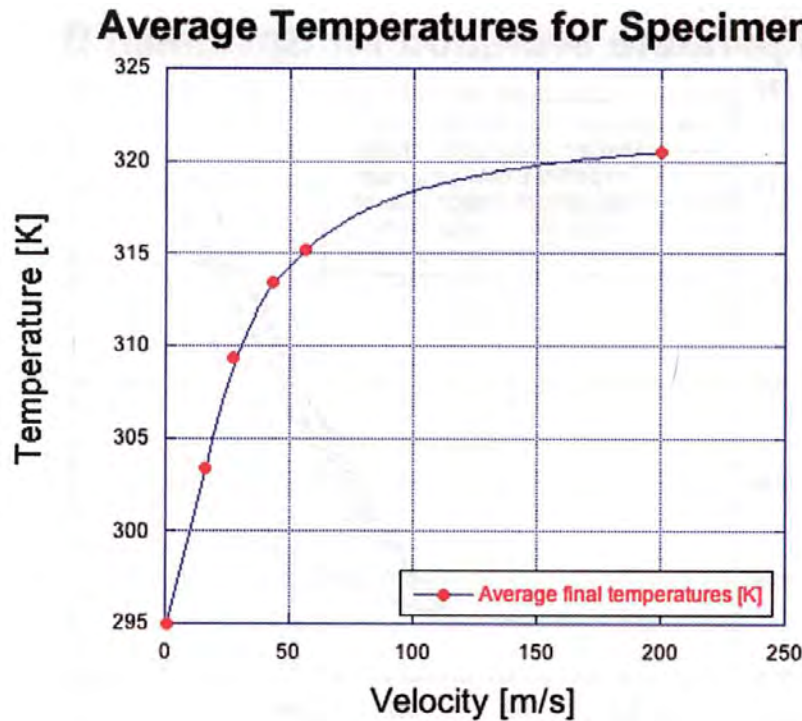
Figure 1.15:   Variation of Temperature with Sliding Velocity [27]

1.5 Direction For Current Research

In order to quantify wear of HHSTT slippers, it is necessary to investigate the mechanics of impact that lead pressure wave propagation through the material. There has been much consideration of impact under uniaxial strain conditions and the associated pressure waves that result [29, 37]. The goal here is to extend these understandings to plane strain scenarios to develop a model that represents HHSTT environments, but to stress the effect of wave mechanics in an associated wear environment. This is discussed further in Section 2.5.2.

The goal of this research is to create a model that will accurately predict mechancial wear of VascoMax 300 slippers colliding with a of 6 μm radius semicircular surface asperity made of AISI 1080 steel. Thus, the characteristics of wave mechanics play a formidable part of the analysis. A hydrocode, called CTH, discussed in Section 2.8, is used to simulate this scenario. The analysis is similar to the micro-scale model developed by Chmiel [14], and used by both Hale [20] and Meador [28]. Since a numerical model is used to evaluate field variables, such as pressure, stress, strain rate, etc. there are several failure criteria that could be used. Section 2.9 discusses the various failure criteria that are used for this research.

II. Theoretical Background

This chapter discusses the theoretical background required to develop the numerical models described in Chapter III and interpret the results presented in Chapter IV. A description of the various wear mechanisms are presented, along with a discussion of the coefficient of friction between sliding metals. This chapter will also discuss the use of a hydrocode, including the considerations of conservation equations, constitutive equations, and an equation of state. Various failure criteria used to quantify material damage related to wear is presented in this chapter. Fundamentals of wave mechanics, previously defined under uniaxial conditions are extended for application in a plane strain scenario. This chapter presents derived equations defining the onset of plasticity and elastic wave speed through a material under plane strain conditions.

2.1 Wear Rate

The model developed for this research is used to predict mechanical wear rates defined by Equation 2.1 due to a collision with a surface asperity, where W is the wear rate, V_w is the volume of worn material, and d_{slide} is the sliding distance into the asperity. Wear rate is simply defined as the volume of material worn per distance slid. Developing a model to predict wear rates, allows multiple scenarios to be run and compared. Specifically, the sliding velocity and boundary conditions can be changed. It was found by Hale [20] that the wear rate from a mechanical point of view is not history oriented. This suggests that the wear rate from an individual simulation is independent of wear at a previous simulation.

$$W = \frac{V_w}{d_{slide}} \tag{2.1}$$

It is important to note that wear is a system response influenced by both material properties and event conditions. These event conditions consist of the geometry

and material topography, the relative motion and contact, the loading scenario, and any environmental conditions including lubrication [6]. The onset of wear is a result of collisions between surface irregularities, such as those shown in Figure 2.1.
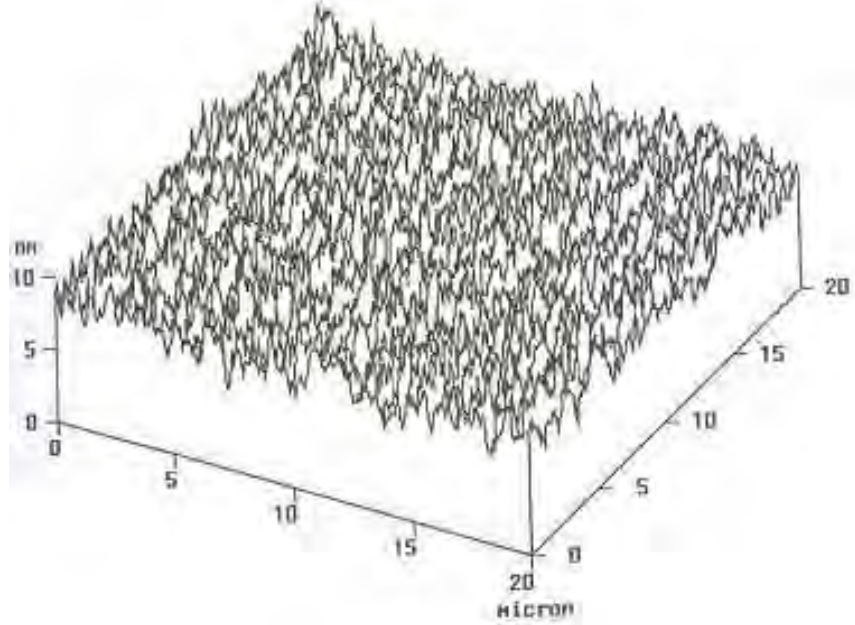
Figure 2.1:   Irregularities in Metal Surface Profile [9]

2.2   Wear Mechanisms

As mentioned earlier, there are several ways to define wear. In order to avoid confusion, for the purpose of this research, wear is defined in the simplest form as "the removal of material volume through some mechanical process between two surfaces" [31]. Furthermore, there are several mechanical processes that can lead to wear. Bayer [8] defines three ways to classify wear. In no significant order, the first is in terms of the appearance of wear. The surface may be described as scratched, polished, pitted, etc. The second classification is the physical mechanism leading to surface damage. Terms related to this classification are adhesion, abrasion, melting, and oxidation. The third classification describes the situation of the event including, dry sliding wear, lubricated wear, rolling wear, and metal-to-metal sliding wear.

As discussed in Section 1.3, Lim and Ashby [26] developed wear mechanism maps based on loading scenario and material properties. The wear rates were normalized, $\tilde{W}$, and plotted against the normalized pressure, $\tilde{F}$, and normalized velocity, $\tilde{v}$. The wear rate, pressure, and velocity were normalized using Equations (2.2, 2.3, and 2.4) respectively.
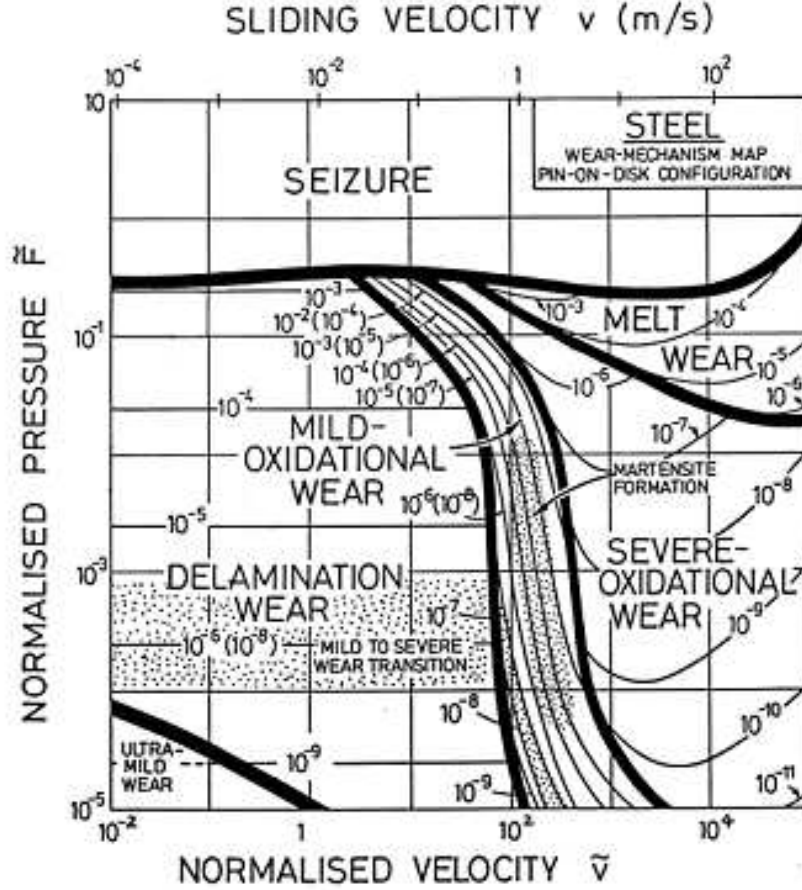
Figure 2.2:   Wear Mechanism Map [26]

$$\tilde{W} = \frac{W}{A_n} \tag{2.2}$$

$$\tilde{F} = \frac{F}{A_n H} \tag{2.3}$$

$$\tilde{v} = \frac{v r_0}{\alpha} \tag{2.4}$$

In these equations, W represents the wear rate, A_n represents the normal contact area, F represents the applied load, H represents the material hardness, v represents the sliding velocity, r_0 represents the radius of the pin used for the experiment, and α represents the thermal diffusivity of the material. The normalization equations are used to relate to studies using different size and shape specimens. Research into the various wear mechanisms has yielded two scenarios of interest for this thesis; abrasive wear and adhesive wear, both of which fall into the classification of mechanical wear. All research presented herein is only considering the phenomenon of mechanical wear. Other wear mechanisms, such as melt wear and oxidation are not considered in this thesis.

2.2.1 Abrasive Wear. Abrasive wear occurs when asperities along the interface of the sliding bodies collide. The tangential force is large enough to cause plastic deformation and eventually remove the asperity. Figure 2.3A represents an abrasive wear scenario. Material from the asperity is being removed by the triangular shaped abrasive particle.

2.2.2 Adhesive Wear. Adhesive wear occurs when two surfaces contact at an asperity and bond together. As the sliding motion continues, and if the bond is strong enough, asperities from the softer material will shear off and adhere to the harder material. The adhered fragments later break free forming worn material. Figure 2.3B depicts the adhesive wear event.

2.3 Coefficient of Friction

As two bodies slide relative to each other, they are inhibited by friction. Friction is a phenomenon resulting from tangential motion between the two sliding bodies, and conventionally is thought of as the force required to initiate or to sustain the
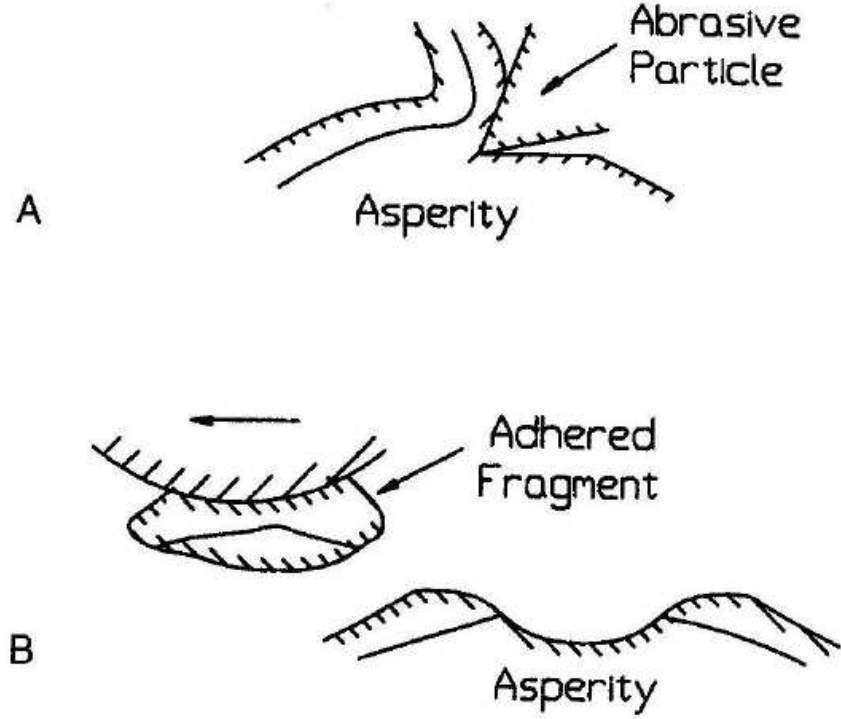
Figure 2.3:   Abrasive Wear and Adhesive Wear [7]

tangential motion [28]. It is important to consider the frictional forces between the rail and slipper, as wear is dominated by the interface of the two materials. The wear mechanisms; abrasive wear, and adhesive wear, discussed in Section 2.2, are relative to the friction in the sliding bodies. Furthermore, the local temperatures of the materials are affected by frictional heating as the sliding motion occurs.

Establishing a coefficient of friction is a common way to represent the frictional forces between two surfaces. The coefficient of friction, μ, relates the frictional force to the normal force applied between the two surfaces. Equation 2.5 is used to solve for the coefficient of friction, where F_f is the frictional force and F is the normal contact force. The equation assumes that the coefficient is independent of the contact area and proportional to the normal load.

$$\mu = \frac{F_f}{F} \tag{2.5}$$

The assumptions listed for Equation 2.5 are generally accepted for mild sliding, or low velocity motion. However, the contact area begins to make a significant contribution to wear as the sliding velocity and loading increases. Research by Montgomery [30], presented in Section 1.3, discusses the relationship between coefficient of friction and Pv. Experimental results show at low Pv values, the coefficient of friction was higher for steel-on-steel sliding. As the Pv value increased, the coefficient of friction decreased exponentially to an asymptotic value. Hale [20] applied a curve fit to the tabulated data from Montgomery for steel sliding on steel. This curve is used to represent the coefficient of friction for the VascoMax 300 slipper sliding along the AISI 1080 steel rail as a function of the Pv term. Figure 2.4 shows the data and curve fit. Equation 2.6 is the exponential curve fit. It is important to note that the curve fit was generated using Pv data with units of MPa $\cdot$ mm/s. Any use of the curve fit requires the same units.
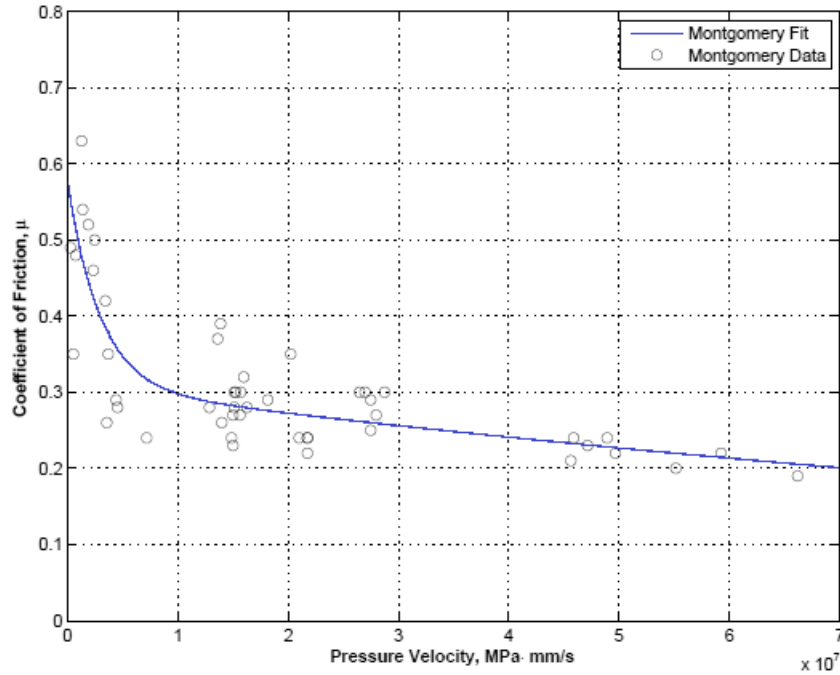
Figure 2.4:   Montgomery Data with Curve Fit [20]

23

$$\mu(Pv) = \begin{cases} 0.2696e^{-3.409 \times 10^7 Pv} + 0.304e^{-6.08 \times 10^{-9} Pv} & : & 0 < Pv < 4.45 \times 10^8 \\ 0.02 & : & Pv \geq 4.45 \times 10^8 \end{cases} \tag{2.6}$$

2.4 Johnson-Cook Viscoplasticity Model

In 1983, Johnson and Cook [23] studied metals subjected to large strains, high strain rates, and high temperatures. Test data for the model was obtained using torsion tests and dynamic Hopkinson bar tensile tests over a range of temperatures. The elevated temperatures were obtained by surrounding the specimen with an oven for several minutes prior to testing. Adiabatic heating resulting from high strains complicated the results because the elevated temperatures showed a reduction in the material strength. Adiabatic heating occurs when the pressure of a material increases due to the motion of surrounding particles. In this case, high strains caused the temperature of the material to increase without adding heat. Johnson and Cook developed Equation 2.7, a constitutive model to solve for the flow stress, σ.

$$\sigma = [A + B\varepsilon_p^n][1 + C\ln(\dot{\varepsilon}_p^*)][1 - T^{*m}] \tag{2.7}$$

This equation is a product of three terms. The first term is the static yield strength and a modification for strain. The second term introduces strain rate dependency and the final term includes temperature effects [20]. A, B, C, m, and n are material constants, ε^p is the equivalent plastic strain, $\dot{\varepsilon}^*$ is the dimensionless plastic strain rate for s^{-1}.

Equation 2.7 is used to represent yielding from the effective stress, von Mises stress. The stress indicates the yield surface when it reaches the Johnson-Cook equation, Equation 2.7. At that point a corresponding plastic strain rate is determined. Since the process is time integrated, the incremental step time of a simulation, Δt, is incorporated in the calculation for the incremental strain. This incremental step time

24

is discussed in Section 3.2. The Bodner-Partom relationship is then used to update stress [35]. This method allows subsequent stress-strain relations to be developed. The homologous temperature, T^*, is defined by Equation 2.8.

$$T^* = \frac{T - T_0}{T_{melt} - T_0} \tag{2.8}$$

Where T is the material temperature, T_0 is the ambient temperature, and T_{melt} is the material melting temperature. The homologous temperature must be defined in order to create strain rate dependent stress-strain curves. Due to the high strain rate deformation applied for this research, the deformation work is considered adiabatic. This implies that the deformation work is transformed into heat with the rise in temperature of the material. This temperature rise is observed in stress-strain curves as thermal softening, a behavior which constitutive equations must account for. Meyers [29] defines the adiabatic temperature rise in a material subjected to high plastic strain rate due to plastic strain energy as Equation 2.9.

$$\Delta T = \frac{\beta}{\rho C_p} \int_0^{\varepsilon_f^p} \sigma d\varepsilon \tag{2.9}$$

where β is the inelastic heat fraction, ρ is density, C_p is the specific heat ratio, and ε_f^p is the final plastic strain. The inelastic heat fraction is set as 0.9 in the analysis based on results from ductile materials [29]. Equation 2.10 is given by replacing the stress term in Equation 2.9 with the Johnson-Cook constitutive equation, Equation 2.7, and assuming the strain rate is constant.

$$\int_{T_0^*}^{T_f^*} \frac{dT^*}{1 - T^{*m}} = \frac{\beta(1 + C \ln(\dot{\varepsilon}_p^*))}{\rho C_p(T_{melt} - T_{ref})} \int_0^{\varepsilon_f^p} (A + B(\varepsilon^p)^n) d\varepsilon^p \tag{2.10}$$

where T_0^* and T_f^* are the initial and final homologous temperatures. Even though m is a material constant, m = 0.8 for VascoMax 300 [15, 16], Meyers proposes an approximation of m $\approx$ 1 to the left hand integral in Equation 2.10. Applying Meyers' approximation, the homologous temperature reduces to Equation 2.11.

$$T^* = 1 - \exp\left[-\frac{\beta(1 + C\ln(\dot{\varepsilon}^{p*}))}{\rho C_p(T_{melt} - T_{ref})}\left(A\varepsilon^p + \frac{B(\varepsilon^p)^{n+1}}{n+1}\right)\right] \qquad (2.11)$$

The true stress-strain curves can now be generated by substituting Equation 2.11 for the homologous temperature in Equation 2.7. Figure 2.5 shows the true stress-strain curves for VascoMax 300 with increasing strain rates. The Johnson and Cook constitutive model uses variables commonly found in computational software which makes it easy to use for simulation.
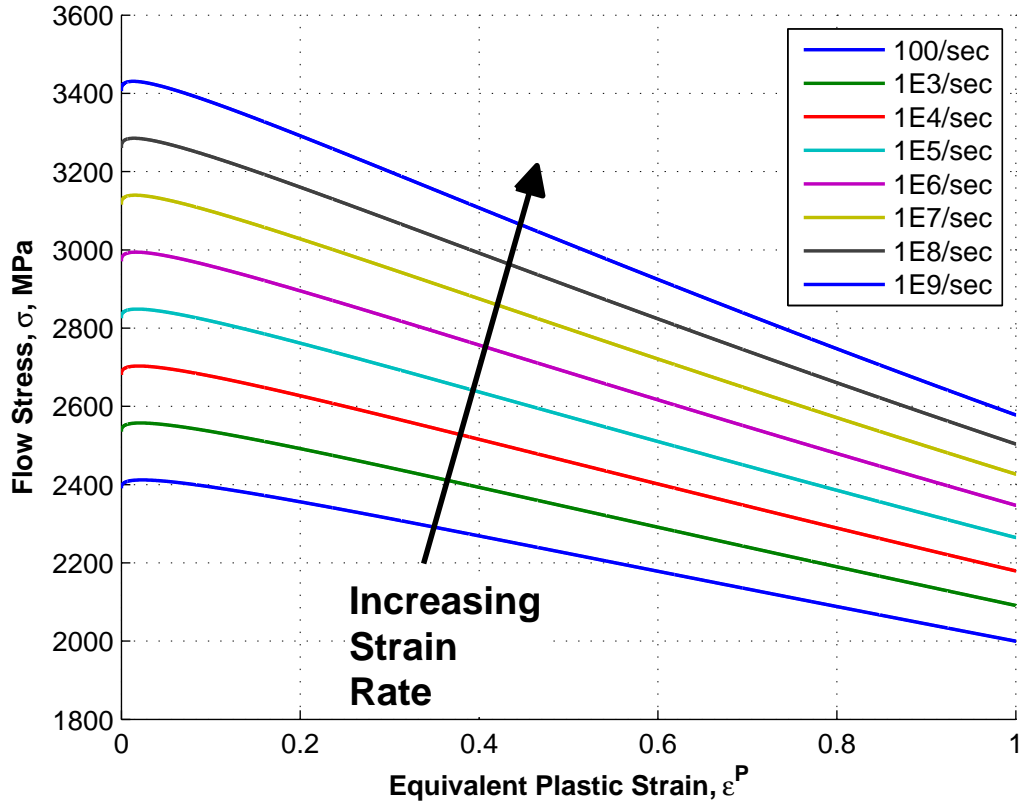
Figure 2.5: True Stress-Strain Curves for VascoMax 300 with Johnson-Cook Constitutive Equation [20]

2.5 Wave Propagation

The research presented in this thesis is an investigation in the wear of VascoMax 300 due to the collision with a surface asperity made of AISI 1080 steel. The goal

is to characterize mechanical wear at high velocities. Analysis of a high velocity collision requires some background information about wave mechanics, specifically the formulation of a shock wave within a solid medium. The next few sub-sections present important information pertaining to the mechanics of wave propagation.

2.5.1 Uniaxial Strain. Common analysis of wave propagation through solid media has been studied while considering uniaxial strain [29]. The yield point for uniaxial strain is referred to as the Hugoniot Elastic Limit, written as σ_{HEL}. This is the maximum elastic stress for one-dimensional elastic wave propagation in plate geometries [37]. The Hugoniot Elastic Limit represents the onset of plasticity in a material under uniaxial conditions. Due to the strain limitations, the onset of plasticity is greater than the yield stress, Y_o, defined for uniaxial stress conditions. The Hugoniot Elastic Limit is given by Equation 2.12, where ν is the poisson ratio.

$$\sigma_{HEL} = Y_o \left(\frac{1 - \nu}{1 - 2\nu} \right) \tag{2.12}$$

It is important to determine the Hugoniot Elastic Limit, because if the stress in the material exceeds this limit, two waves are created. First, an elastic wave will move through the material at the elastic speed, c_E, defined by Equation 2.13, where E is the elastic modulus, and ρ_o is the initial density of the material. Following the elastic wave, a plastic wave will move through the material at the plastic wave speed, c_P, speed defined by Equation 2.14. It is important to note that c_p is a function of the slope of the stress-strain curve at a given point. This means that multiple waves can exist in the material, each with a speed defined by Equation 2.14.

$$c_E = \sqrt{\frac{E(1 - \nu)}{\rho_o(1 - 2\nu)(1 + \nu)}} \tag{2.13}$$

$$c_p = \sqrt{\frac{1}{\rho_o} \frac{d\sigma}{d\varepsilon}} \tag{2.14}$$

Figure 2.6 shows the transition of a pressure wave to a shock wave with increasing time. Point A represents a low pressure region in the wave moving at a low velocity. Points B and C have higher pressures and therefore move at a greater velocity. The four steps in the figure show the pressure wave approaching, and ultimately reaching, a vertical line which represents the onset of a shock within the material. Before the shock is formed, the material properties across the pressure wave are smooth and easily defined. As the shock wave propagates, the material movement becomes discontinuous in front of, and behind the shock. An equation of state, EOS, is used to estimate the pressure and internal energy of the material. Equations of state are discussed in greater detail in Section 2.8.2.
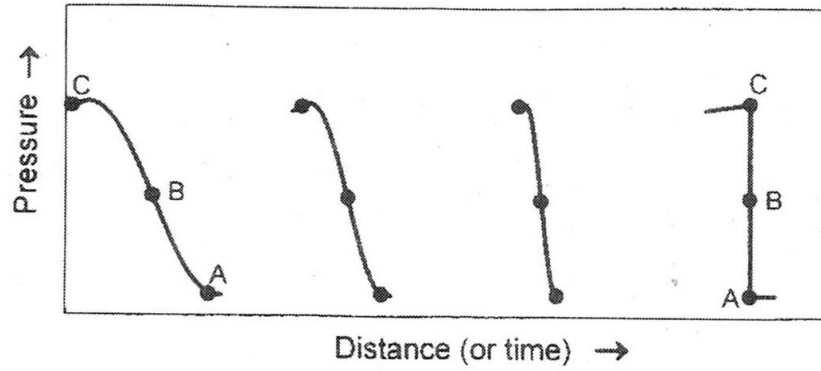
Figure 2.6:   Increasing Pressure Wave with Time [37]

2.5.2 2D Plane Strain.   The analysis in this thesis considers plane strain conditions. The approach used to characterize pressure waves under uniaxial conditions is modified to include strain in two dimensions. In making these modifications, an assumption was made that the strain component can be represented by the summation of the two principal strains. The equivalent Hugoniot Elastic Limit for plane strain conditions, $\sigma_{HEL,PS}$, is given by Equation 2.15. This equation represents the onset of plasticity in a material under plane strain conditions. Appendix A includes the full derivation of the equations presented in this chapter.

$$\sigma_{HEL,PS} = Y_o \left[\frac{3}{8 - 16\nu} + \frac{1}{2} \right] \tag{2.15}$$

This scenario does restrict strain in the third principal axis (z-direction), while allowing strain in the other dimensions. Therefore, the value of $\sigma_{HEL,PS}$ should be less than σ_{HEL} but greater than the yield stress, Y_o. Table 2.1 shows the uniaxial yield stress, Hugoniot elastic limit, and equivalent plane strain Hugoniot elastic limit for VascoMax 300 with a Poisson's ratio ($\nu = 0.283$). The values for yield stress and poisson ratio for VascoMax 300 are taken from Cinnamon [15].

Table 2.1:   VascoMax 300 Hugoniot Limits

Y_o (GPa)	σ_{HEL} (GPa)	$\sigma_{HEL,PS}$ (GPa)
2.1	3.4692	2.8664

The speed of an elastic wave under the plane strain condition, $c_{E,PS}$ is given by Equation 2.16. The speed of the plastic wave under plane strain conditions is still defined by the slope of the stress-strain curve at a point. Multiple plastic waves are still produced in plane strain, each defined by Equation 2.14.

$$c_{E,PS} = \sqrt{\frac{4}{3} \frac{(1 - \nu)}{\rho_o (1 - 2\nu)(1 + \nu)} E} \tag{2.16}$$

2.6   FEA and Hydrocodes

Recent research at AFIT has relied on the use of two codes to model the wear of HHSTT slippers. One is an FEA code called ABAQUS and the other is a hydrocode called CTH. Both codes can be used to create 2-dimensional or 3-dimensional geometry, to represent a wide variety of simulations, and both codes make use of a mesh to solve the numerical analysis. There is one fundamental difference between the FEA approach and the hydrocode approach. The difference stems from the meshes used and frames of reference established in each code.

The FEA method uses a Lagrangian mesh which attaches the mesh to the material. This means the mesh will deform with the material during the analysis, and the frame of reference moves with each successive iteration. This method is an attractive approach for many simulations because the equations are simple to solve. However, if the scenario involves large deformations leading to excessive material displacement, the FEA method begins to fall apart. With large deformations, numerical singularities in the finite element equations can result due to the mesh cell geometry. In some cases, the element can invert under large distortions, resulting in negative volume and negative mass [37]. This gives rise to numerical errors.

Hydrocodes use an Eulerian mesh which fixes the mesh in free space and allows the material to flow through it. The frame of reference does not move during the analysis. Figure 2.7 is a simple depiction of the slipper-rail scenario with a Lagrangian mesh (left) and an Eulerian mesh (right). The Eulerian mesh is commonly referred to as a finite area mesh.
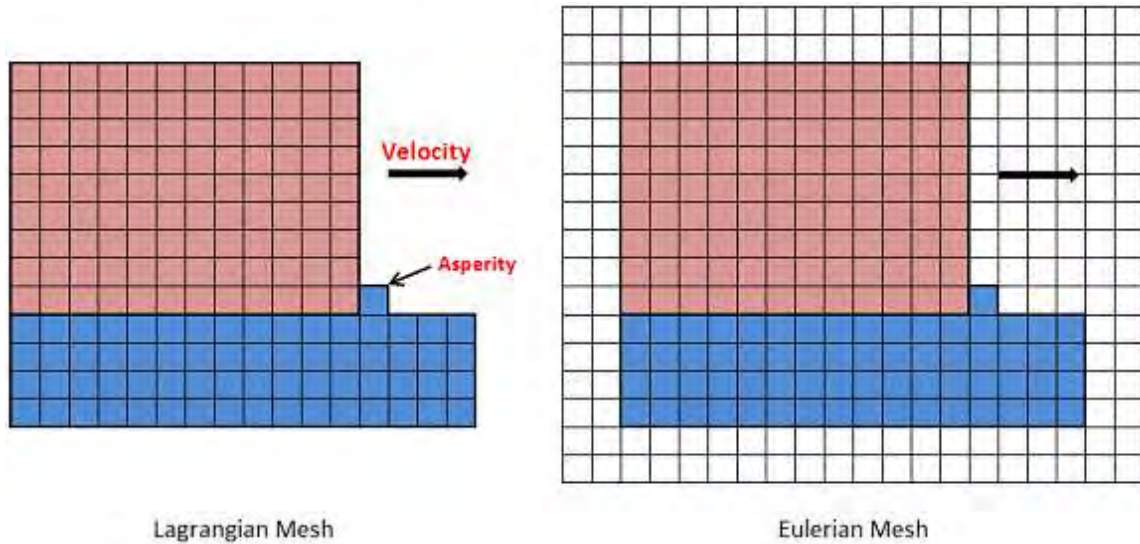
Figure 2.7: Graphical Comparisson of Lagrangian and Eulerian Meshes [28]

30

2.7 ABAQUS

Previous research at AFIT used the Lagrangian FEA approach to model a VascoMax 300 slipper colliding with a AISI 1080 steel surface asperity. Initial work by Chmiel [14] used ABAQUS to evaluate Lagrangian codes as a way to model the wear of HHSTT slippers. The slipper was modeled using 4-node plane strain elements and the rail used 3-node plane strain elements. Chmiel's model is shown in Figure 2.8. The analysis showed material damage as a result of the collision with the asperity. This proved that the FEA method could be used to predict mechanical wear of the HHSTT slippers. However, it has been deemed impractical to run the simulation the entire length of the steel rails at Holloman AFB. Chmiel suggested simulations of single asperity collisions over a range of velocities, and calculating the total wear from these runs.
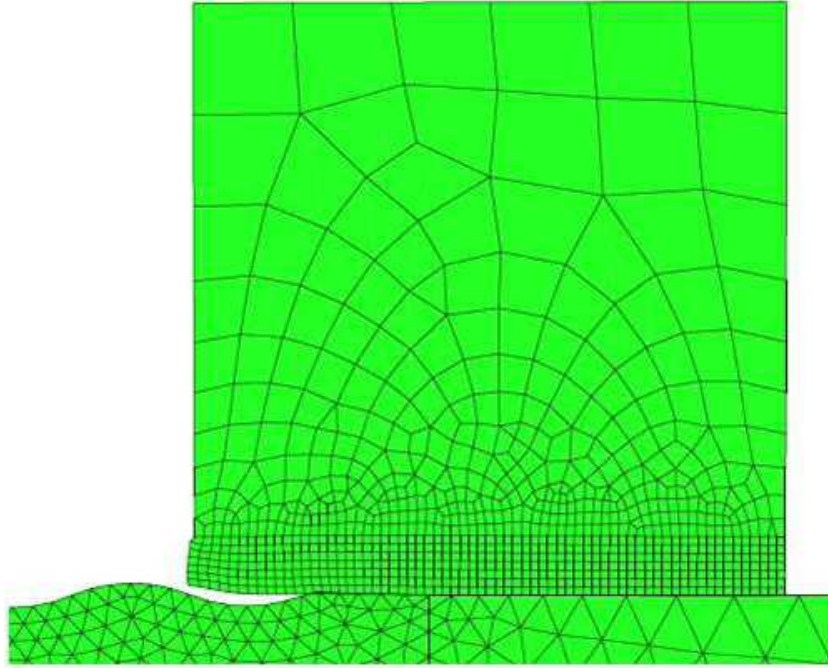
Figure 2.8:   Finite Element Model Used by Chmiel [14]

Hale [20] continued the research of HHSTT slipper wear using ABAQUS to implement Chmiel's suggestion. The asperity collision event is best described as a 3-dimensional event, so a 3-dimensional model was considered. However, complica-

31

tions arose when evaluating a 3-D model. A plane strain model was used to calculate the wear. A 3-dimensional conversion method and scaling factor based on equations developed by Archard were used to extend the plane strain results to a 3-dimensional value. The 3-dimensional conversion method and Archard scaling factor are described in greater detail in Section 3.4. Hale's model, shown in Figure 2.9, used a combination of 3-node linear plane strain triangular elements and 4-node bilinear reduced integration elements to model the slipper and rail.
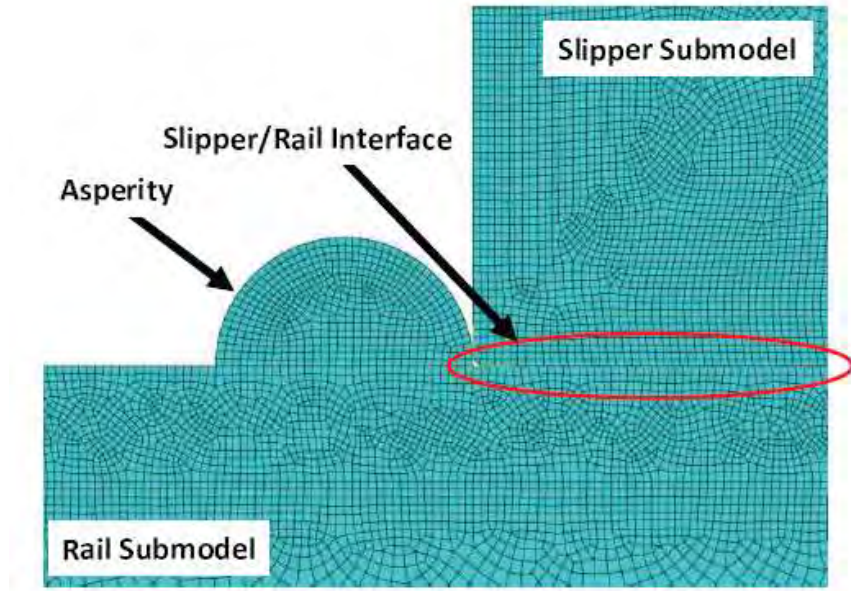
Figure 2.9:   Finite Element Model Used by Hale [20]

2.8   CTH

CTH is a Lagrangian-Eulerian hydrocode developed by Sandia National Laboratories. Hydrocodes can be very useful when evaluating scenarios involving high velocity impact resulting in wave propagation and the possiblity of a shock. The process in solving a hydrocode solution is less straight-forward than the FEA method. However, there are detailed descriptions of CTH features published by Sandia National Laboratories [18] and Palazotto and Meador [31]. Additionally, Zukas [37] and Meyers [29] each wrote books providing descriptions of hydrocodes. The following sec-

32

tions use information taken from these sources to describe in detail the key features of the code, and how it is used to model the HHSTT wear problem.

2.8.1   Lagrangian Step and Eulerian Remap.   The conservation equations of mass, momentum, and energy are satisfied using a two step process in CTH [18,28,31]. First, the Lagrangian step, is used to evaluate the equations across the time step and the mesh deforms with the material. This is followed by an Eulerian remapping step which redefines the mesh to the original Eulerian coordinates. Equations (2.17, 2.18, and 2.19) are the Lagrangian conservation equations for mass, momentum, and energy, respectively, where ρ is the material density, $\overrightarrow{V}$ is velocity, P is pressure, σ is stress, E is energy, and Q represents additive heat as a function of velocity and wave speed, c_s [18]. These equations are a by-product of the Eulerian expression in which the substantial derivative is applied.

$$\frac{d\rho}{dt} = -\rho \nabla \cdot \overrightarrow{v} \tag{2.17}$$

$$\rho \frac{d\overrightarrow{v}}{dt} = -\nabla P - \nabla \cdot [\sigma + Q(\overrightarrow{v}, c_s)] \tag{2.18}$$

$$\rho \frac{dE}{dt} = -P \nabla \cdot \overrightarrow{v} - [\sigma + Q(\overrightarrow{v}, c_s)] \cdot \nabla \overrightarrow{v} \tag{2.19}$$

Since the mesh deforms initially, the conservation of mass is trivially satisfied, because no mass flow occurs across the cell boundaries. The momentum and energy integrals are solved using their explicit finite volume representations [28,31]. Thermal energy of the material must be considered. The conservation of energy equation includes both mechanical and thermal energies, and thus another equation relationship that couples the energies together is needed. This is where an equation of state is used. The conservation equations and equation of state are solved in conjunction with a constitutive model. CTH decomposes the total stress tensor into a spherical

part, solved for using an equation of state, and a deviatoric part, solved for using a constitutive model.

After the conservation equations have been satisfied and the constitutive equation has been applied, the Eulerian remap step is used to return the distorted mesh to the original Eulerian mesh. An interface tracking algorithm internal to CTH is utilized to track locations of material interfaces within mixed cells containing multiple materials. The change in mass is calculated by the geometry of the deformed material compared to the previous step. The mass and internal energy are mapped to the fixed mesh. The results from the interface tracking algorithm are used to map the momentum and kinetic energies to the material in the Eulerian mesh. The equation of state is used to update the pressure, temperature, and density of the cells.

2.8.2 Equation of State. The equation of state is used to relate the internal energy, and pressure, of a material to the density and temperature. There are several equations of state that can be used within CTH. For the purpose of modeling the collision of two solid bodies, CTH provides two separate EOS models, the semi-empirical Mie-Grüneisen EOS, and the tabular Sesame EOS. Vanderhyde's [34] research provides insight to the two EOS models internal to CTH. Much of the information presented in the following sections use information taken from this source.

2.8.2.1 Mie-Grüneisen EOS. The Mie-Grüneisen equation of state is typically used for high velocities ranging from 500 m/s to 2,000 m/s [37]. No phase change is allowed with the Mie-Gruniesen equation of state, which makes it useful for this research. Equation 2.20 is the Mie-Grüneisen equation used by CTH, where P_{ref} and E_{ref} are reference pressure and energy, usually taken from the Hugoniot relations or by assuming a zero-Kelvin isotherm, V is volume, and Γ is the Grüneisen constant defined by Equation 2.21, where K is the bulk modulus, v is the specific volume, α is the thermal coefficient of expansion, and C_v is the specific heat.

$$P - P_{ref} = \frac{\Gamma}{V}(E - E_{ref}) \qquad (2.20)$$

$$\Gamma = \frac{3Kv\alpha}{C_v} \qquad (2.21)$$

2.8.2.2 Sesame EOS. CTH also provides the Sesame equation of state. The Sesame EOS is a set of tabular data collected through experimentation at Sandia National Laboratories primarily using flyer plate impact experiments [15]. When the Sesame EOS is used, CTH interpolates between the tabulated data, or extrapolates outside of the provided data set to estimate the internal energy and pressure within the material.

2.8.3 Boundary Conditions. Boundary conditions are determined using finite volume approximations based on the surrounding cells. However, the cells along the boundary have at least one side with no neighboring cell. Boundary conditions need to be established in order to solve the finite volume problem when using a hydrocode. These conditions are based upon the concepts of sound waves, which is a primary relationship in this research, and thus the boundary conditions must be able to control mass, momentum, and energy fluxes across the boundary. There are four possible boundary conditions in CTH: a symmetrical boundary condition (Type 0), a sound speed based absorbing boundary condition (Type 1), an outflow boundary condition (Type 2), and an extrapolation boundary condition (Type 3). The boundary conditions create additional cells just outside the internal mesh defined in the problem setup.

The Type 0 boundary condition sets parameters of the adjacent cells equal to the cells along the boundary of the internal mesh. The velocity between the two adjacent cells is set to zero and kinetic energy is converted to internal energy. Also, mass flux is restricted across the boundary. The Type 1 boundary condition allows mass to enter the internal mesh, and is used to approximate semi-infinite bodies. The

35

Type 2 boundary condition sets empty cells on the boundary of the internal mesh with user specified pressure. Mass can exit the internal mesh, but no mass is allowed to enter. The Type 3 boundary condition places cells on the boundary of the internal mesh and linearly extrapolates a boundary pressure. No restrictions on mass flux are present in this boundary condition. Previous work by Meador [28] used the type 1 boundary condition. The analysis presented in this thesis used a combination of type 1 and 2.

2.8.4 Data Collection. There are two methods of recording data during a CTH simulation. One method uses locations attached to the stationary mesh to record data as the material deforms through it. The other method uses tracer points that travel with the material during the simulation. For the purpose of this research, the second method is used. Utilizing this method requires the use of a tracer input set defined within the CTH input deck. The tracer input set defines the initial locations of each data point. As the simulation occurs, the tracer points move with the material. This method keeps track of failed material, representing wear, through the entire simulation. If the data were collected at the stationary mesh locations, one cell could be considered damaged, or failed, at a previous time step, when new material has entered the cell. As a result, this new material will not be qualified as damaged, because that cell has previously been defined as damaged. This results in unreasonably low wear predictions.

2.9 Failure Criteria

Properly assessing wear requires established failure criteria to quantify material damage. Meador [28] outlines four failure criteria to determine wear: average strain rate, point-wise strain rate, Johnson-Cook plasticity, and plastic strain. The Johnson-Cook constitutive equation is used to define the plastic strain failure criterion, and was selected to evaluate wear in the model developed for this research. A second

failure criterion was established based upon a critical stress value. The Johnson-Cook fracture model [24, 33] was also evaluated as a failure criterion.

2.9.1   Plastic Strain at Max Stress Failure Criteria.   This method evaluates the plastic strain at maximum stress for a given strain rate from the true stress-strain curves, as given in Figure 2.5. These curves were developed using the Johnson-Cook constitutive equation, Equation 2.7, with Meyer's approximation for the homologous temperature [29], presented in Section 2.4. Each curve on the plot represents the true stress-strain relationship for VascoMax 300 with a given constant strain rate. The critical stress, σ_{crit}, is defined as the maximum stress of each curve. Similarly, the critical plastic strain, ε^p_{crit}, is defined as the strain at maximum stress for each curve. The critical strain can be determined as a function of the strain rate by plotting ε^p_{crit} against the strain rate and applying a curve fit through the data. The curve fit provides a closed form solution for the critical strain, Equation 2.22.

$$\varepsilon_{crit}(x, y, t) = A_{PS}\dot{\varepsilon}(x, y, t)^{B_{PS}} + C_{PS} \tag{2.22}$$

The constants A_{PS}, B_{PS}, C_{PS} are given in Table 2.2. Where the 'PS' subscript is used to identify plastic strain constants. Figure 2.10 shows the plastic strain curve fit for VascoMax 300.

Table 2.2:   Coefficients of Plastic Strain

Coefficient	Value	Units
A_{PS}	2.247×10^{-2}	MPa
B_{PS}	-5.516×10^{-2}	unitless
C_{PS}	6.044×10^{-3}	MPa

CTH calculates and records the plastic strain at each tracer point during the simulation. A MATLAB post-processing code, written to compare the recorded plastic strain against the critical plastic strain from Equation 2.22, is discussed in greater detail in Appendix C.
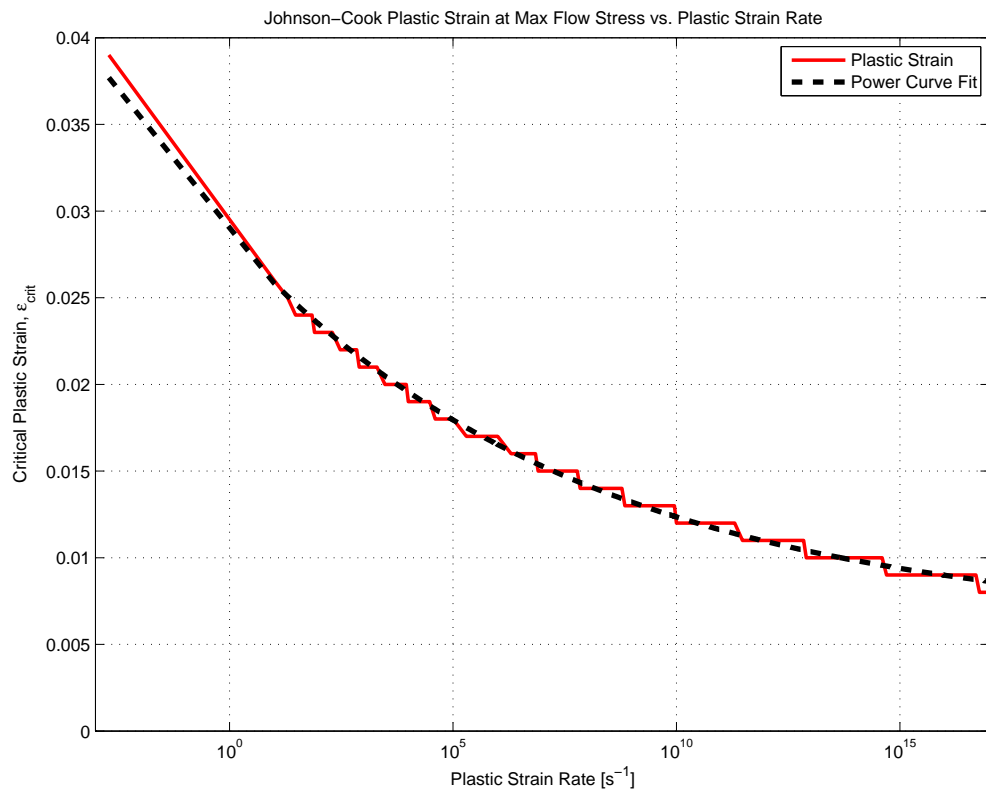
Figure 2.10:   Critical Plastic Strain Curve Fit [28]

2.9.2   Von Mises Stress Failure Criteria.   CTH can be used to calculate the von Mises stress of the material during the simulation. Therefore, a failure criterion can be established based on a critical stress value. This method would allow CTH to do all the calculations in determining material failure. Hale [20] provides maximum stress values for VascoMax 300 based on a dominant strain rate. Table 2.3 shows the dominant strain rates and associated maximum stress from the Johnson-Cook constitutive equation for a range of sliding velocities from the January 2008 test mission. Although the stress levels change from 2,900 MPa to 3,130 MPa, the critical stress value for the von Mises stress failure criterion was chosen to be 3,000 MPa. This means that if the von Mises stress exceeds 3,000 MPa during the simulation, it has failed.

Table 2.3:   VascoMax 300 Maximum Stress Based on Dominant Strain [20]

Velocity Range (m/s)	Dominant Strain Rate	Maximum Stress (MPa)
10 - 200	1×10^5	2,900
300 - 622	1×10^6	3,000
750 - 1,530	1×10^7	3,130

2.9.3   Johnson-Cook Fracture Model.   CTH allows the use of the Johnson-Cook fracture model for evaluating failed material. "It uses a failure criterion based on equivalent plastic strain, taking into account the pressure, temperature, and strain rate along the loading path for each material particle. The model uses one scalar damage variable" [33]. Equation 2.23 defines the plastic strain at failure.

$$\varepsilon^{pf}(p, Y, T, \dot{\varepsilon}) = [D_1 + D_2^{\left(\frac{-D_3 p}{Y}\right)}][1 + D_4 \ln(max(1, \dot{\varepsilon}))][1 + D_5 T^*] \qquad (2.23)$$

Where p is pressure, Y is the material yield stress, T is temperature, $\dot{\varepsilon}$ is the plastic strain rate, D_1, D_2, D_3, D_4, and D_5, are material constants derived from experimentation, and T^* is the homologous temperature previously defined by Equation

39

2.8. The Johnson-Cook scalar damage variable, D, is defined by Equation 2.24. Initially, undamaged material has a D value equal to 0. As the simulation occurs, the material accumulates damage, and the scalar variable, D, increases. When D equals 1, the material is damaged.

$$D = \int \frac{d\varepsilon^p}{\varepsilon^{pf}(p, Y, T, \dot{\varepsilon})} \tag{2.24}$$

2.10 Summary of Theoretical Background

The information presented in this chapter has been crucial in understanding the wear phenomenon. The relations presented will be used to develop a numerical model to predict mechanical wear rates of HHSTT slippers. Previous work by Hale [20] and Meador [28] has made use of a plane strain scenario to model the slipper-rail sliding event. These models allow a VascoMax 300 slipper to collide with a 6 μm surface asperity made of AISI 1080 steel. Damage was recorded per sliding distance to give wear rates. Wave action in a plane strain scenario was also evaluated.

The fundamental approaches to characterizing the onset of plasticity in the uniaxial strain case, σ_{HEL}, were presented. Steps were taken to extend the characteristics to the case of plane strain. This resulted in an equivalent Hugoniot elastic limit for plane strain, $\sigma_{HEL,PS}$, given by Equation 2.15. Due to the limitations of strain in the uniaxial strain case and the plane strain case, it was expected that yield stress, Y_o, would be less than both $\sigma_{HEL,PS}$ and σ_{HEL}. Also, that $\sigma_{HEL,PS}$ would be less than σ_{HEL}. The assumption was validated when the equations derived and solved for VascoMax 300 in Table 2.1. Equation 2.16 was given in this chapter as a method to solve for the speed of an elastic wave through a solid material under plane strain conditions. Appendix A includes the full derivation of the equations used to determine the equivalent Hugoniot elastic limit and plane strain elastic wave speed.

Most of the previous work used a finite element code to simulate the problem. Meador used CTH, a hydrocode discussed in Section 2.8, to model the wear of HHSTT

slippers. This research uses the same code used by Meador, with some modifications mentioned in Chapter III. This chapter discussed in detail the benefits of using a hydrocode as opposed to a finite element code. A primary benefit includes the use of an Eulerian-Lagrangian coordinate system to avoid large mesh distortions, and allow for high velocity impact scenarios.

Hale [20] conducted metallurgical studies on both used and unused test slippers from the HHSTT. The study suggested that mechanical wear results from plastic deformation. This, along with the fact that the micro-level simulation technique, first proposed by Chmiel, is a time-dependent process requires the use of a viscoplastic constitutive model. The Johnson-Cook model, Equation 2.7 was chosen for this research, because it includes considerations of large strains, high strain rates, and elevated temperatures. Furthermore, the equation was intended for use in computational software.

Although wear involves the removal of material, developing a model to remove material during simulation would be complicated. Therefore, a qualitative measure, based on material damage, has been adopted. The Johnson-Cook constitutive model was used to develop failure criteria, discussed in Section 2.9. The failure criterion is used to evaluate material as damaged or undamaged. The amount of damage material for each simulation is computed and divided by the distance slid to give a wear rate. Previous work by Hale and Meador have made use of models developed by Archard [4] to relate the two-dimensional plane strain single asperity collision event to a three dimensional wear scenario.

III. Numerical Model

Developing a numerical model to simulate entire HHSTT missions is an impractical approach to the wear phenomenon, in terms of run-time and simulation cost. However, previous research by Chmiel [14], Burton [10], Hale [20], Meador [28], and Lodygowski [27] has shown results using a simplified plane-strain model. The models in previous research have made use of the DADS data provided by the HHSTT. This chapter will discuss the DADS system and how the recorded data is used to characterize the slipper-rail sliding event. This chapter will also present the hydrocode model used for this research, discussing the input parameters including initial velocity, the viscoplasticity model, and equation of state. The method used to calculate plane strain mechanical wear rates, and total mechanical wear will also be presented.

3.1 DADS Data

Properly characterizing the slipper dynamics as it slides along the rail is necessary to create an accurate model. The HHSTT provides data using a program called Dynamic Analysis and Design System (DADS). DADS is a commercial-off-the-shelf software developed by Computer Aided Design Software, Inc. The HHSTT uses the software to simulate a rocket sled run and predict vertical forces of each slipper, vertical velocity of the sled, and horizontal velocities of the slippers, as a function of time.

A model has been developed to represent the HHSTT sled and rail as a complicated system of masses, springs, and dampers, while the sled forward velocity and rail undulations are supplied as inputs to the system [21]. The simulations have been validated using accelerometers attached to test sleds [22]. Given the complexity of the model, and the validation by HHSTT engineers, the DADS model is assumed to be valid within the context of this research [28].

The geometry of the sled influences the dynamics of the sled and slipper as it slides along the steel rail. According to the HHSTT Design Manual [1], the nominal

slipper gap is 0.125 inches. This corresponds to the nominal max clearance between the slipper and rail. The slipper gap allows the slipper to bounce along the rail during the test missions. Due to this gap and bouncing effect, the slipper is not in total contact with the rail for the entire run. The bouncing effect is included in the calulation of total mechanical wear in Section 3.4.

3.2 *Plane Strain Simulation Using a Hydrocode*

The plane strain simulations for this thesis used CTH, a hydrocode discussed in Section 2.8. The model simulates the collision of VascoMax 300 with a 6 μm radius hemispherical surface asperity made of AISI 1080 steel, as shown in Figure 3.1. In this figure, the slipper (yellow) moves to the right at a given input velocity and collides with the green asperity and rail. Several inputs must be defined to run the two-dimensional analysis. These inputs include sliding velocities, simulation time, mesh and domain sizing, boundary conditions, and geometry. This research made use of an existing CTH code developed by Meador [28] with some modifications.

The sliding distance was chosen to be 110% of the 6 μm radius to allow the leading edge of the slipper to go past the maximum height of the asperity. The simulation time is found as a function of the input sliding velocity, v_{slide}, and asperity radius, r_a. Equation 3.1 was used to determine the simulation time for each run. The simulation times are shown in Table 3.1.

$$t_{sim} = \frac{(1.1)(r_a)}{v_{slide}} \tag{3.1}$$

The size of the domain and slipper were selected to reduce boundary effects and pressure wave interactions along the edges. Since the simulation time is known for each case, and the velocity of the elastic pressure wave and plastic pressure waves are given by Equations (2.13) and (2.14), the distance traveled by a pressure wave can be found. Meador determined that a domain size of 850 μm by 850 μm, and a slipper size of approximately 700 μm by 125 μm were sufficient. However, for his research, Meador

43
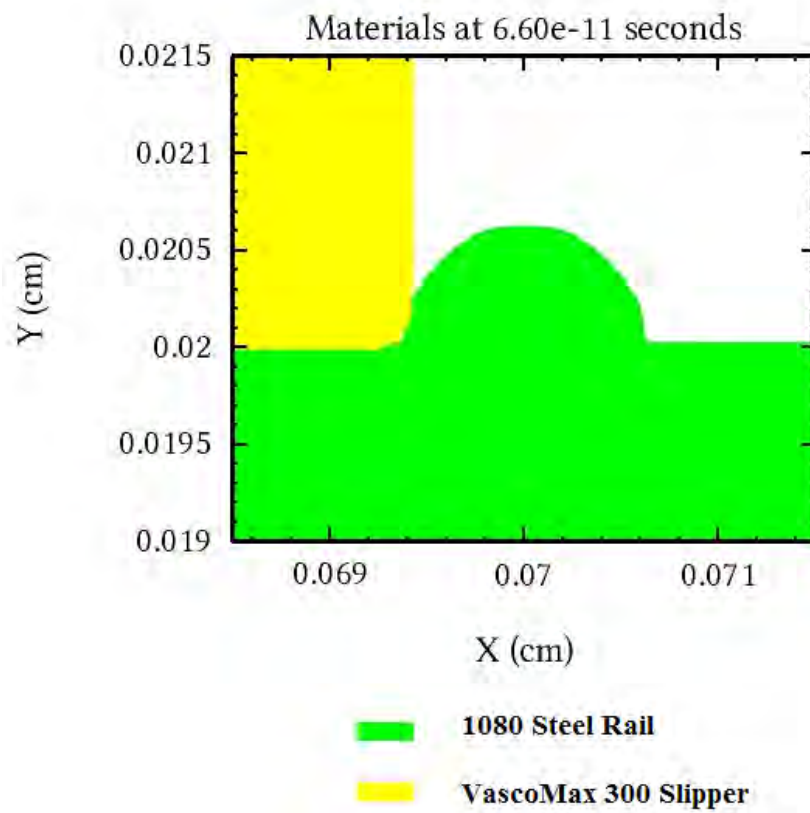
Figure 3.1:   Slipper-Asperity Interface of Current Model

Table 3.1: Simulation Time for Given Velocity Based on Equation 3.1

Horizontal Velocity (m/s)	Simulation Time (s)
100	6.60×10^{-8}
200	3.30×10^{-8}
300	2.20×10^{-8}
400	1.65×10^{-8}
500	1.32×10^{-8}
600	1.10×10^{-8}
700	9.43×10^{-9}
800	8.25×10^{-9}
900	7.33×10^{-9}
1,000	6.60×10^{-9}
1,100	6.00×10^{-9}
1,200	5.50×10^{-9}
1,300	5.08×10^{-9}
1,400	4.71×10^{-9}
1,500	4.40×10^{-9}

considered velocities ranging from 750 m/s to 3,000 m/s. This research considers a velocity range from 200 m/s to 1,500 m/s, corresponding with the velocity profile of the third sled from the January 2008 test mission (1.12). Decreasing the sliding velocity increases the simulation time, Equation 3.1, which increases the distance traveled by the stress waves. This means at velocities less than 750 m/s, the stress waves may reach the boundaries of the slipper or domain.

To reduce the wave interactions along the boundary of the domain, the boundary conditions were modified. A combination of Type 1 and Type 2 boundary conditions were used to simulate a semi-infinite boundary (Type 1 and 2) and allow material to flow out of the domain (Type 2 only). Figure 3.2 shows the domain created with the materials defined and boundary conditions selected.

Additional consideration was given to the leading edge of the slipper, specifically at the point of contact with the surface asperity. The concern was that the corner would result in a singularity. Previous research by Cameron [13], Hale [20], and Meador [28] alleviated this issue by replacing the corner with a 2 μm radius fillet.
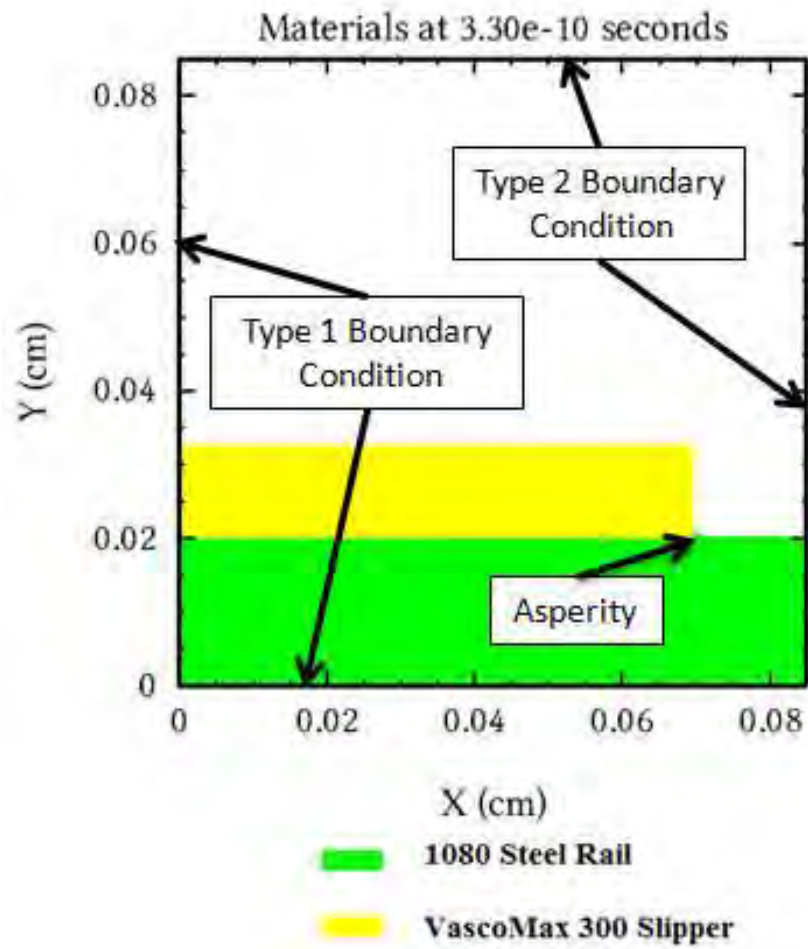
Figure 3.2:　　Entire Domain of Current Model

This research uses the filleted edge to stay consistent with the previous work. The mesh was selected to create a grid of cells with size 1 μm by 1 μm throughout the entire domain. Figure 3.3 shows the mesh used for the simulations.
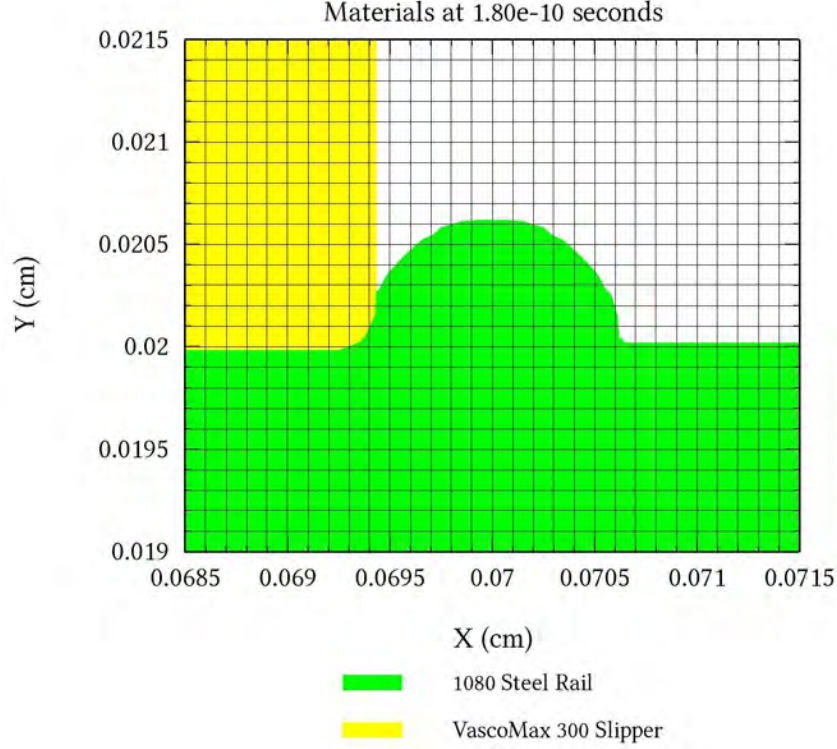
Figure 3.3:   Eulerian Mesh Applied to Current Model

The tracer points, discussed in Section 2.8.4 are attached to the material throughout the entire simulation. This method of data collection allows each cell to be affected by the previous iteration, meaning if a cell has failed at one time step it will remained failed for the rest of the simulation. The tracer points are initially placed at the center of each cell, so the area allocated to each tracer is the same as the cell area. MATLAB was used to create a post-processing code to compute the wear rates from each CTH run. The post-processing code is provided with explanation in Appendix C.

3.2.1 Material Interface Conditions.   The model developed in this thesis allows one material to slide along another surface. Therefore, friction along the interface must be considered. However, CTH does not allow an input coefficient of friction.

47

There are two interface conditions that can be defined in the model to represent friction in the surface. The first is called a "slide line" condition which sets the shear stress along the interface to zero. This condition is used to simulate a frictionless surface. The second condition is called "no slide". This condition will not allow the material to move until a user defined pressure is reached. This user defined pressure is the fracture pressure defined in the fracture input set of the CTH code in Appendix B. The CTH code was run with these two conditions representing two extremes in terms of friction; one being a frictionless surface, and the other representing a semi-infinite coefficient of friction.

3.2.2 Input Velocity. Since the simulation is evaluating a two-dimensional scenario, velocity can be defined in two directions: horizontal and vertical. The horizontal component of velocity is determined by the sliding velocity. Values are chosen from 200 m/s to 1,500 m/s to represent the increasing velocity of the slipper along the rail. The vertical velocity component can be determined using the DADS data. The vertical velocity is positive going up and negative going down. Therefore, the negative represents the slipper moving toward the rail. Figure 3.4 plots the vertical velocity of the third stage aft right slipper from the 2008 mission against the horizontal velocity of the sled. The figure shows that the maximum vertical velocity of the slipper into the rail is approximately -3.45 m/s. The horizontal velocity component is always much larger than the vertical component. This means that vertical velocity has very little effect on the velocity vector. All simulations have a constant vertical velocity of -0.5 m/s, which helps to keep the slipper in contact with the rail throughout the simulation. The idea of creating a more realistic simulation of the HHSTT environment is continued with the addition of a dead load to represent the effective mass of the slipper as it slides along the rail at increasing velocity. The addition of the dead load is discussed in detail in Section 4.1.

3.2.3 Viscoplasticity Model. The Johnson-Cook constitutive equation, discussed in Section 2.4, is used as the viscoplasticity model for this research. The model

48
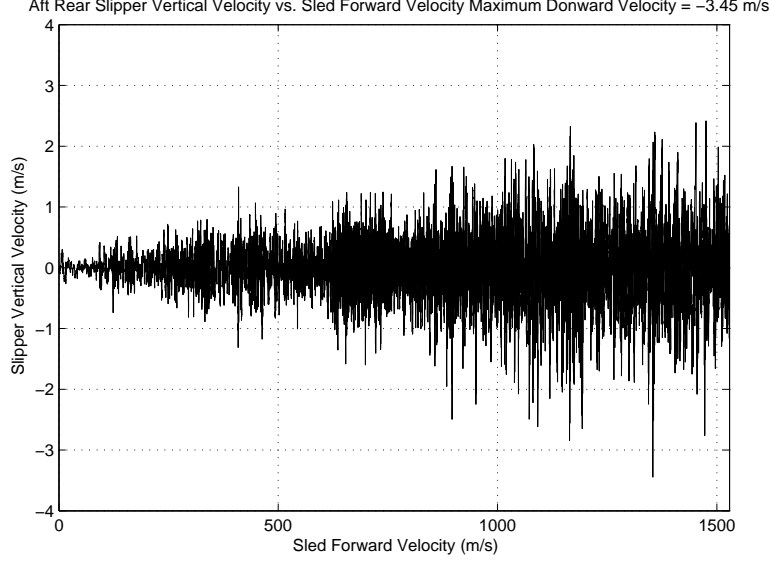
Figure 3.4:   Slipper Vertical Velocity from DADS

was developed to handle large strains, high strain rates, and high temperatures. The material constants need to be defined for the VascoMax 300 slipper and AISI 1080 steel rail in order to use the Johnson-Cook model. Cinnamon [15–17] determined these constants, shown in Table 3.2, using flyer plate experiments. It is also necessary to define the initial temperature of the materials because the Johnson-Cook model carries the homologous temperature term, Equation 2.8.

Table 3.2:   Johnson-Cook Coefficients for VascoMax 300 and AISI 1080 Steel

Coefficient	VascoMax 300	AISI 1080 Steel
A (GPa)	2.1	0.7
B (GPa)	0.124	3.6
C (Unitless)	0.03	0.17
m (Unitless)	0.8	0.25
n (Unitless)	0.3737	0.6
T_{melt} (K)	1,685	1,630

3.2.4 Equation of State.   Hydrocodes make use of an equation of state to relate internal energy and pressure of a material to the density and temperature. It serves as an additional equation to relate the conservation equations to the constitutive equation. The equation of state is also useful when a shock is present within

the material. The shock creates discontinuities and an EOS can be used to solve for material properties.

The Mie-Grüneisen EOS, presented in Section 2.8.2.1, was initially considered for use in this research. This EOS model is typically used for high velocities ranging from 500 m/s to 2,000 m/s [37]. Therefore, some issues arose when modeling at the lower sliding velocities. These errors included numerical inconsistencies in calculated mechanical wear rates and pressure wave propagation. These low velocity issues and a modified approach are discussed in greater detail in Section 4.5.

Due to the inconsistent results using the Mie-Grüneisen equation of state at low velocities, the Sesame EOS is used for this research. The Sesame EOS is a tabular set of experimental data. The experiments are typically a high velocity impact scenario under uniaxial strain conditions. VascoMax 300 is defined in the Sesame tables and is used to represent the slipper for this research. However, AISI 1080 steel is not defined in the Sesame tables, so iron is used to represent the rail. The two materials have similar properties as shown in Table 3.3.

Table 3.3:   Iron and AISI 1080 Steel Properties

Property	Iron	AISI 1080 Steel
Density (g/cm^3)	7.28	7.85
Yield Stress (MPa)	50	585
Elastic Modulus (GPa)	200	205
Melt Temperature (K)	1,181	1,630
Poisson's Ratio	0.28	0.25

3.3   *Mechanical Wear Rate Calculation*

The post-processing code uses CTH output to determine the wear rate per unit width, W_{uw}, given by Equation 3.2, where A_d is the damage area computed from the plane strain simulation based on the failure criteria used, and the distance slid is the product of sliding velocity, v_{slide}, and simulation time, t_{sim}.

$$W_{uw} = \frac{A_d}{v_{slide} t_{sim}} \tag{3.2}$$

The plane strain simulation, along with this equation gives wear rates in units of area of damaged, or worn, material per distance slid. Since wear is defined as the volume of material worn per distance slid, it is best represented as a three-dimensional problem. As such, a conversion factor must be established to represent a three-dimensional hemispherical surface asperity using the two-dimensional semi-circular asperity in plane strain.

3.3.1 Semi-spherical Coefficient. Hale [20] determined the semi-spherical coefficient by running plane strain simulations with 2 μm, 4 μm, and 6 μm asperities and integrating across the width to determine a volume of damaged material per distance slid. Figure 3.5 shows how the plane strain models are related to the three-dimensional analysis. The red areas in Figure 3.5(b) represent the damaged material due to the collision with the various asperities. For a given sliding velocity, the area of damaged material increases as the size of the asperity increases.

The 2 μm and 4 μm asperity collisions are related to the 6 μm asperity by assuming an off-center collision. Since the analysis is under plane strain conditions and the z-axis is eliminated, the actual height of the asperity does not affect the simulation. Equation 3.3 is used to determine the location of the 2 μm and 4 μm asperity along the z-axis in the three-dimensional hemispherical asperity, where r is the 6 μm asperity radius.

$$z = \sqrt{r^2 - y^2} \tag{3.3}$$

This places the 2 μm and 4 μm asperities at z-locations of 4.47 μm and 5.66 μm, respectively. These locations are illustrated by the dashed line in Figure 3.5(a). The single asperity wear rate, W_{sa}, is determined by Equation 3.4, where the integral is multiplied by two to represent the symmetrical asperity.

51

(a) Hemispherical Asperity

(b) Plane Strain Analyses Illustration
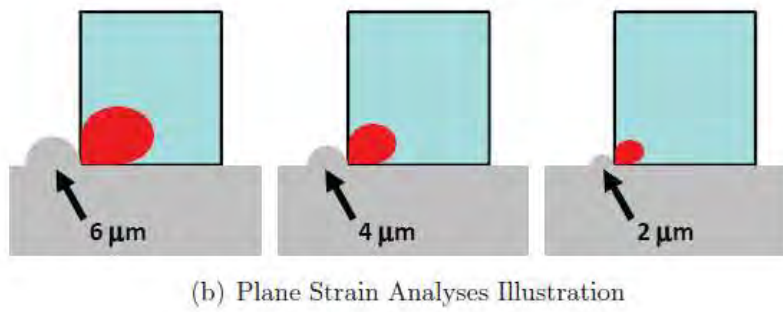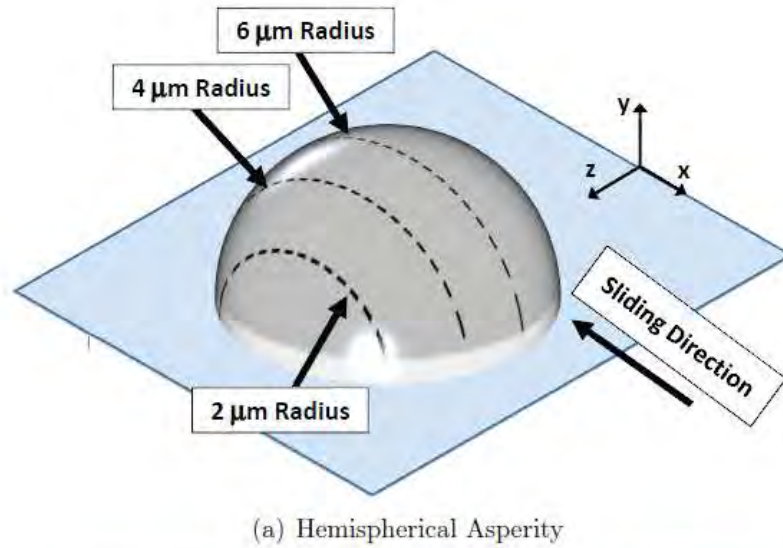
Figure 3.5:   Plane Strain Representation of a Semi-Spherical Surface Asperity [20]

$$W_{sa} = 2\int_0^r W_{uw}(z)dz \tag{3.4}$$

Equation 3.4 gives the plane strain wear rate for a collision with a single semi-spherical asperity. Hale solved this equation for a range of sliding velocities, and then divided the single asperity wear rates by their respective plane strain wear rates to get an average effective width, w_{eff}, of 8.29 μm. Equation 3.5 uses this average effective width to calculate the single asperity wear rates, as opposed to using the integral in Equation 3.4.

$$W_{sa} = w_{eff}W_{uw} \tag{3.5}$$

3.3.2   Archard Scaling Factor.   The plane strain models developed by Hale [20] and Meador [28] make use of a scaling factor to account for collisions with multiple asperities as the slipper sides along the rail. This equation is derived by relating wear rates to Archard's wear model at low velocities [2–4]. Equation 3.6 is used to relate Archard's wear rate, W_A, to the single asperity wear rate.

$$W_A = \frac{k_A F}{H} = NW_{sa} \tag{3.6}$$

where k_A is Archard's wear coefficient, F is the applied load, H is the material hardness, and N is the scaling factor. The applied load in Archard's equation relates to the force applied by the pin in a pin-on-disk experiment. The scaling factor is found by Equation 3.7. Hale [20] solved for N = 11.77, at a sliding velocity of 10 m/s, with k_A equal to 4.45×10^{-5}, and with F given from the DADS data.

$$N = \frac{k_A F}{W_{sa}H} \tag{3.7}$$

3.4 Total Mechanical Wear Calculation

Calculating total wear of the HHSTT slippers allows for a comparison to be made between experimental data and simulation results. The experimental data for this research is a used slipper retrieved from the January 2008 test mission at Holloman AFB. To evaluate total wear, the single asperity wear rates are integrated with respect to sliding distance. The DADS data is used to determine at what distance along the track the slipper reaches a certain velocity. The wear rates are then plotted as a function of sliding distance. Before the values are integrated, an additional scaling factor must be included.

This scaling factor represents the amount of time the slipper and rail are in contact. The CTH simulations assume the slipper and rail are in contact throughout the entire simulation. The percentage of contact, d_{pc}, is set to 0.3. That assumes that the slipper and rail are in contact for 30% of the test run. This assumption, first used by Hale [20], comes from the comparison of test data between the January 2008 mission and a simulation designated by the HHSTT as 80X-A1. DADS data for the 80X-A1 simulation was supplied to Cameron [13] for his research in 2007.

Equation 3.8 calculates total mechanical wear, W_{TOTAL}, where d_{max} is the total sliding distance. This equation includes the single asperity wear rate, W_{sa} from Equation 3.5, the Archard scaling factor, N, from Equation 3.7, and the percentage of contact coefficient, d_{pc}.

$$W_{TOTAL} = N d_{pc} \int_0^{d_{max}} W_{sa}(s)ds \qquad (3.8)$$

3.5 Summary of Numerical Modeling

This chapter discussed the dynamic data, DADS, used to characterize position, velocity, and forces of the rocket sled system. This dynamic data, along with the theoretical background presented in Chapter II, was used to create a hydrocode model capable of estimating mechanical wear of HHSTT slippers. Equations were given in

this chapter to represent multiple semi-spherical asperity collisions with a single semi-circular asperity in plane strain. The model developed in this thesis evaluates pressure and internal energy of a material due to this collision. The next chapter will discuss the results of the simulation, calculated mechanical wear rates, total mechanical wear, and compare these to the experimental data.

IV. Results and Discussion

This chapter will present the results of the numerical model discussed in Chapter III. First, the equivalent plane strain Hugoniot elastic limit, discussed in Section 2.5.2, will be compared against CTH simulations. The calculated wear rates will be presented for various failure criteria and interface conditions. Finally, the results of the total wear calculation will be presented and compared against experimental wear from the HHSTT January 2008 test mission.

4.1   Dead Load

In order to develop a model that represents the HHSTT environment, a variable vertical force was considered. Since the concept of a hydrocode is to include kinetic energy as a basic function, it was felt that at least an investigation of the vertical movement should be included. This is considered by characterizing a vertical force. This variable force represents the vertical force of the slipper as it bounces along the rail. Figure 4.1 is a plot of the vertical force of the aft right slipper from the third sled during the January 2008 test from the DADS data. When the force is zero, the slipper is not in contact with the rail.

CTH does not allow a force input. However, the force can be represented with an appropriate dead load fixed to the top of the slipper. DADS does not provide data representing vertical acceleration of the slipper as it travels down the rail. Therefore, a modified force equation, Equation 4.1, was developed to represent the effective dead load as a function of vertical velocity and vertical force using Newton's second law, F=ma.

$$m = \frac{F_{avg}\Delta t}{\Delta v} \tag{4.1}$$

where Δv is the maximum change in vertical velocity within a window enclosing the desired horizontal velocity, Δt is the size of the window, and F_{avg} is the average
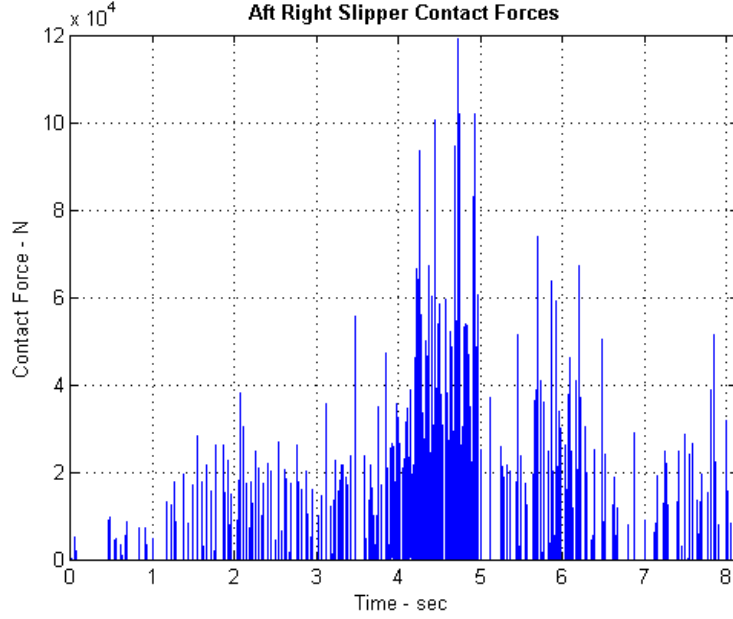
Figure 4.1:   HHSTT Third Stage Vertical Force, January 2008
Test Mission

slipper force during the window. The velocity profile of the third stage from the
HHSTT January 2008 test mission, Figure 4.2, is used to determine the time at
which a desired velocity is reached. Figures 4.3 and 4.4 show the method of applying
windows surrounding a time representing a target sled velocity of 500 m/s enclosing
the vertical force and vertical velocity.

The size of the window, Δt, is the time between two peaks enclosing the desired
velocity. These two peaks are shown in Figure 4.3 with red circles. The black circle
represents the time at which the sled reaches the desired velocity. The average force,
F_{avg}, is the average of the two peaks in Figure 4.3. The same window applied to
the vertical force plot is applied to the vertical velocity. A maximum and minimum
velocity is found in this window and shown on Figure 4.4 with two red circles. The
maximum change in velocity, Δv is the change in velocity between these two points.

The dead load is calculated with respect to sliding velocity and plotted in Fig-
ure 4.5. It is important to note that there are many sudden changes in vertical velocity
and vertical force of the slipper as it travels along the rail. The scattered data results

57
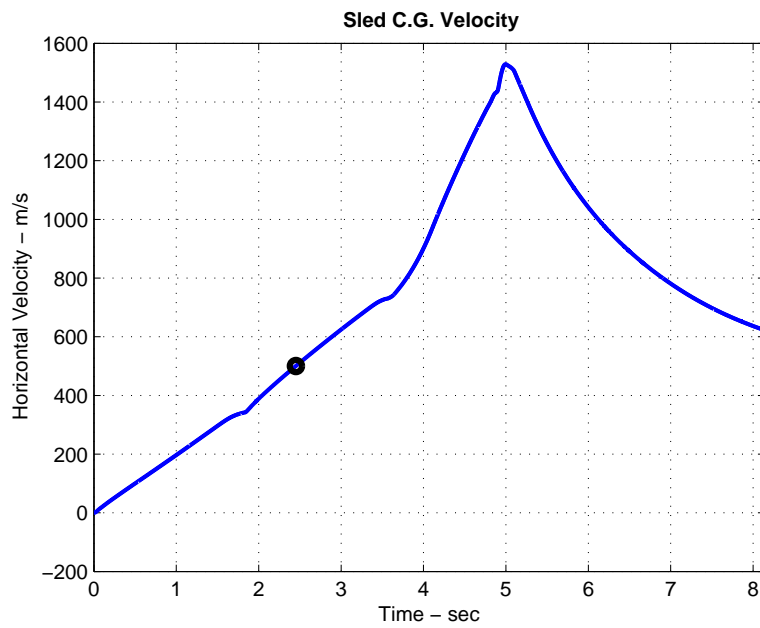
Figure 4.2: HHSTT Third Stage Velocity Profile, January 2008 Test Mission
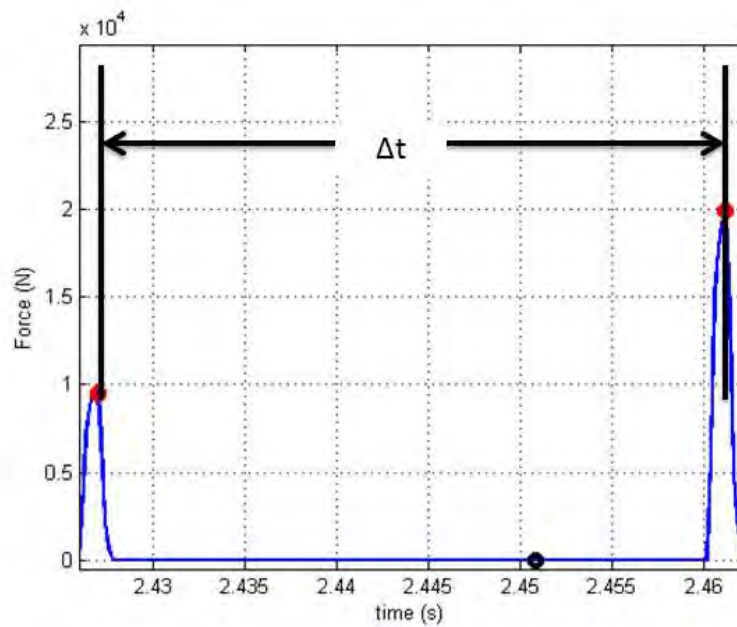
Figure 4.3: Windowed Vertical Force Data at 500 m/s

58
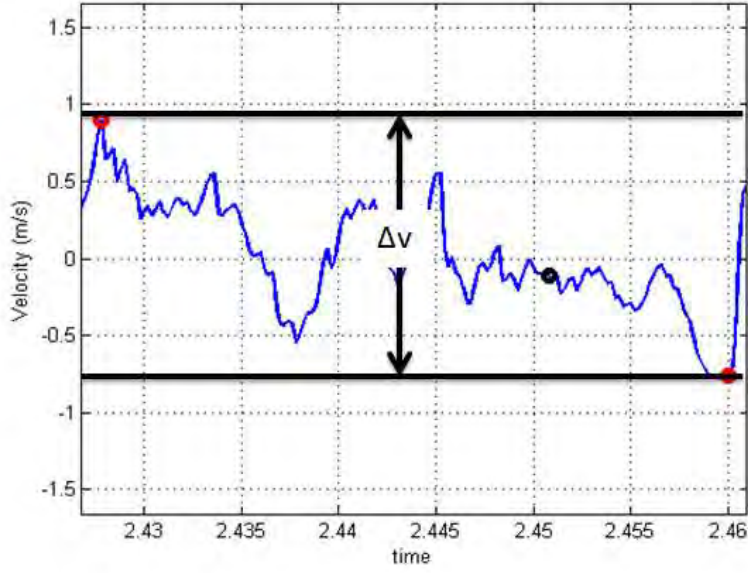
Figure 4.4:   Windowed Vertical Velocity Data at 500 m/s

in a scattered function of dead load with respect to sliding velocity. Also, there is an outlying maximum dead load at 1,000 m/s. This is probably due to the increased acceleration down the track due to the firing of the third rocket sled.

The model developed in this thesis is a local submodel of the slipper colliding with a surface asperity. As such, the entire slipper is not represented in the model. Therefore, a mass fraction, δ_M, was found that related the mass of the actual slipper to the mass of the slipper in the CTH model. This mass fraction is applied to the calculated dead load when added to the CTH input deck. Data from Holloman AFB states that the weight of the aft right slipper is 19 pounds. This is converted to grams, assuming gravity, g, = 9.81 m/s^2 using Equation 4.2. This equation gives a slipper mass of approximately 8,615 grams. The mass of the CTH slipper is given by the product of its density, 8.091 g/cm^3 and volume, 8.63×10^{-4} cm^3, to be approximately 7.02×10^{-3} grams. Therefore, the mass fraction, δ_M, is 8.15×10^{-7}.

$$Mass_{grams} = Weight_{lb_f} \frac{4.448N}{lb_f} \frac{kg \cdot m}{N \cdot s^2} \frac{1}{9.81m/s^2} \frac{1000g}{1kg} \tag{4.2}$$

59
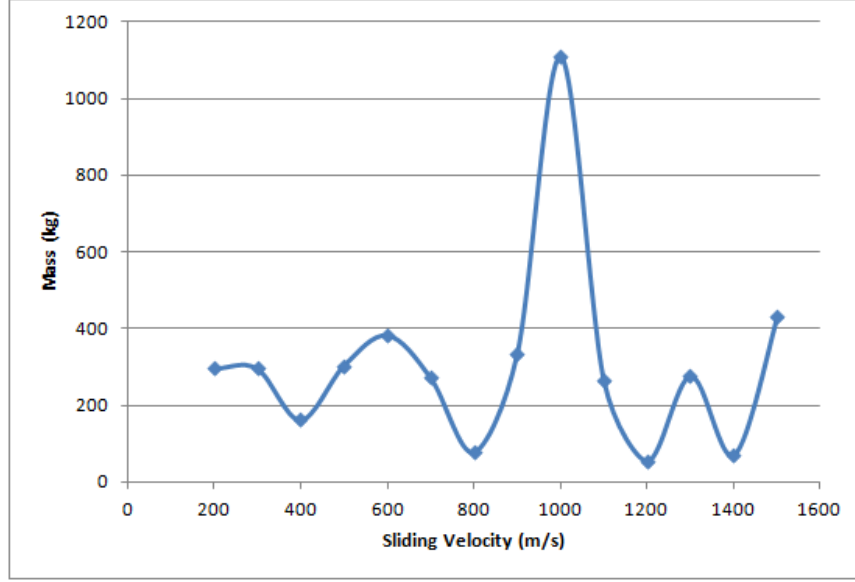
Figure 4.5:   Change in Dead Load with Respect to Velocity

To add the calculated dead load to the CTH model, a block of platinum was fixed to the top of the VascoMax 300 slipper. Platinum was selected, because it is the most dense material in CTH. Since the dead load sits atop the entire slipper, the dead load dimension along the X-axis is known. Because a plane strain model was developed, the thickness is also known. Since the mass of any material is given by the product of its density and volume, the height of the platinum dead load is found using Equation 4.3, where h is the dead load height, m is the dead load mass, ρ is the dead load density, w is the width of the dead load along the X-axis, and t is the thickness of the dead load in the z-axis.

$$h = \frac{m\delta_M}{\rho w t} \tag{4.3}$$

The investigation of the dead load effect was carried out by running two simulations with the dead load at 800 m/s and 1,200 m/s with a "no slide" boundary condition. The results of these simulations, shown in Table 4.1, are identical to the simulations without the dead load. This is probably due to the fact that the contact area between the slipper and asperity is so small that the added mass does not

60

have a siginificant effect. The dead load was dropped from the simulation, and is not considered in any more simulations.

Table 4.1:   Dead Load Wear Rates

Horizontal Sliding Velocity (m/s)	800	1,200
Dead Load Height (cm)	4.30×10^{-2}	3.04×10^{-2}
Dead Load Strain at Max Stress (mm^3/mm)	2.66×10^{-4}	2.86×10^{-4}
Dead Load Critical Von Mises Stress (mm^3/mm)	3.54×10^{-4}	3.73×10^{-4}
No Dead Load Strain at Max Stress (mm^3/mm)	2.66×10^{-4}	2.86×10^{-4}
No Dead Load Critical Von Mises Stress (mm^3/mm)	3.54×10^{-4}	3.73×10^{-4}

4.2   Failure Criteria Selection

Three failure Criteria were presented in Section 2.9, plastic strain at max stress, critical von Mises stress, and the Johnson-Cook fracture model. The plastic strain at max stress criteria, developed by Meador [28], has provided reliable results in previous research and is considered a valid failure criteria. The critical von Mises stress criteria is a modified approach used by Hale [20] and Meador. The benefit of this criteria is in the fact that the von Mises stress can be calculated from the CTH simulation. This removes the need for the curve fit, Equation 2.22. The number of cells exceeding the critical von Mises stress value is used to determine the amount of material damage for this criteria. A critical stress value of 3,000 MPa was selected based upon Hale's strain rate analysis [20].

Preliminary evaluation of the Johnson-Cook fracture model suggest that it does not work well with the plane strain collision studied in this research. This method produced zero wear in most cases. Recall that the Johnson-Cook fracture model is dependent upon an integral given by Equation 4.4. As damage accumulates in the material, the integral goes to 1. When the integral is equal to 1, the material is said to have failed. For most cases, the model developed for this research does not allow the integral to reach the critical value of 1. However, some cells do reach the critical value resulting in some wear. This number tends to be two to three orders of magnitude less than the other models.

$$D = \int \frac{d\varepsilon^p}{\varepsilon^{pf}(p, Y, T, \dot{\varepsilon})} \tag{4.4}$$

One seemingly obvious reason for the poor results of the model is the fact that the coefficients of the Johnson-Cook fracture model for VascoMax 300 and AISI 1080 steel are not defined in CTH. Several steels are defined in CTH. For the purposes of this research, Iron was used to represent the AISI 1080 steel rail, and AISI 4340 steel was used to represent the VascoMax 300 slipper. The Johnson-Cook fracture coefficients used are given in Table 4.2. Previous work by Lee [25] has shown the utility of the Johnson-Cook fracture model in CTH. If the coefficients for the materials were defined in CTH, the model may produce satisfactory results.

Table 4.2:   Johnson-Cook Fracture Coefficients for
Iron and AISI 4340 Steel Defined in CTH [24]

Coefficient	Iron	AISI 4340 Steel
D_1	-2.2	-0.8
D_2	5.43	2.1
D_3	-0.47	-0.5
D_4	0.016	0.002
D_5	0.63	0.61
T_{melt} (eV)	0.1581885	0.1566566

4.3   Validation of Plane Strain Hugoniot Limit

Table 2.1 provides the predicted equivalent plane strain Hugoniot elastic limit for VascoMax 300 as 2.8664 GPa. This value can be validated by checking for an equivalent Hugoniot limit from the CTH simulation. This is done by plotting the evolution of pressure through time at a point in the VascoMax 300 slipper. Cinnamon [15] did this under uniaxial strain conditions using a flyer plate test. The experiment fired VascoMax 300 projectiles at a target at high velocites. Stress was measured using a stress gauge attached to the projectile approximately 2 mm from the leading edge. Since the experiment represented uniaxial strain, the pressure was set to the measured stress. The pressure was plotted against time to check for the Hugoniot

elastic limit. Cinnamon also created a CTH simulation of the impact event. To keep in line with the experiment, the pressure from Cinnamon's CTH simulation was recorded 2 mm from the interface of the projectile and target. The dimensions of the slipper-rail simulation created for this thesis are much smaller than Cinnamon's model. Therefore, the pressure is recorded from the CTH simulation at 2 μm vertically from the interface of the slipper and rail, and 2 μm horizontally from the interface of the slipper and asperity. The black dot in Figure 4.6 shows the point in the model where the pressure data is recorded to locate the equivalent plane strain Hugoniot elastic limit. Figure 4.7 shows the increase of pressure, in a slipper sliding at 1,000 m/s, to a value in which the pressure drops and increases to a max value. The value at which the pressure stops increasing is referred to as the equivalent plane strain Hugoniot elastic limit. When loading exceeds this value, deformation is no longer purely elastic. Multiple plastic waves are produced when the loading exceeds the limit, which explains the cyclic behavior at max pressure after the equivalent plane strain Hugoniot limit is reached.

It should be noted that the equivalent plane strain Hugoniot limit from Figure 4.7 does not equal the calculated value (2.8664 GPa) exactly. However, the value from the simulation is close to the predicted value. Figures 4.8 and 4.9 show the pressure evolution in the VascoMax 300 slipper at 1,200 m/s and 1,500 m/s, respectively. Although the simulation implies that equivalent plane strain Hugoniot elastic limit is influenced by sliding velocity, an implication that is easily accepted, the predicted value of 2.8664 GPa is an approximate value representing this limit.

4.4 *Validation of Plane Strain Elastic Wave Speed*

An equation to determine the elastic wave speed through a solid material under plane strain conditions was provided in Section 2.5.2. Equation 4.5, derived from equations presented by Zukas [37] and Saada [32], is a function of Poisson's ratio, ν and elastic modulus, E.
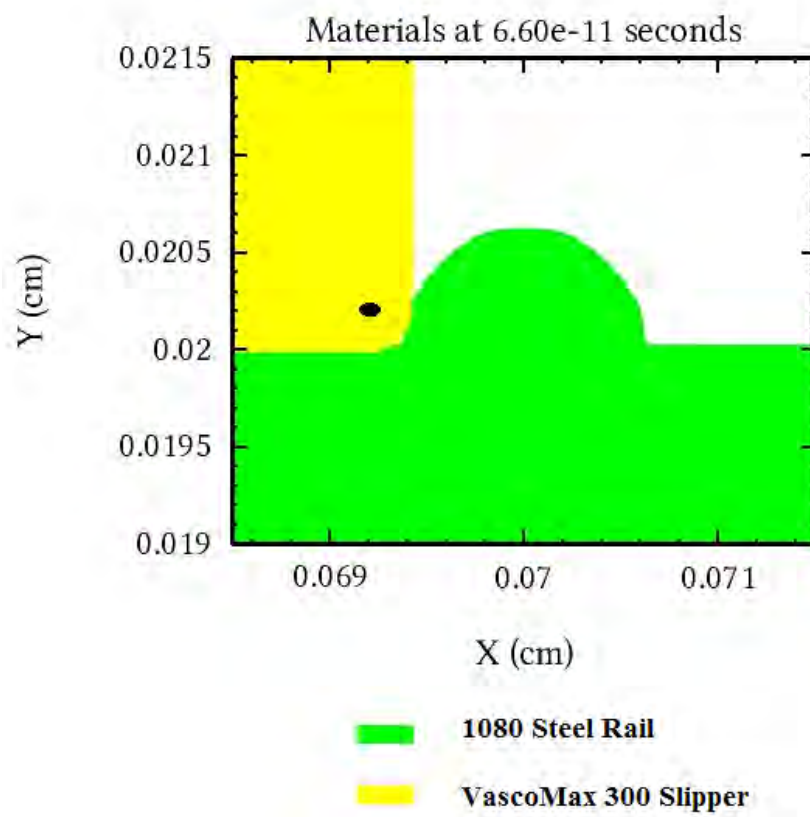
Figure 4.6:   Location in Model Where Pressure Data is Recorded
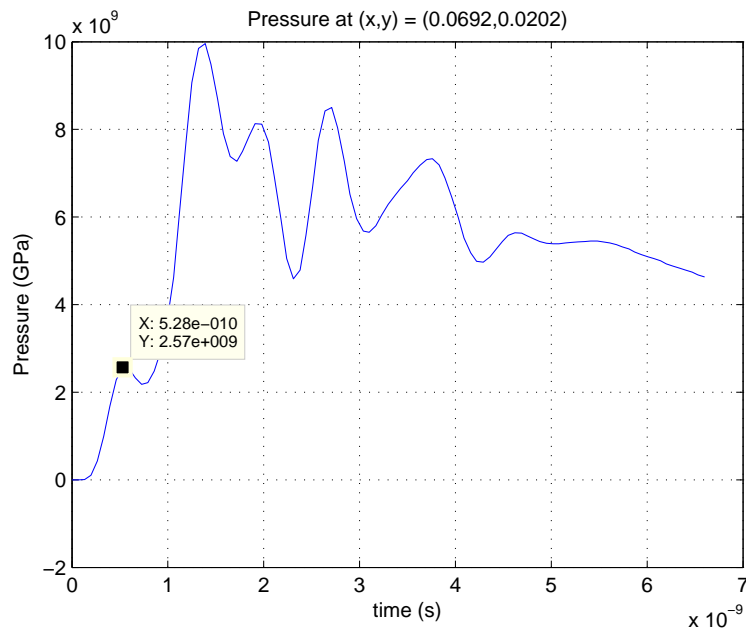
Figure 4.7: Pressure Evolution in VascoMax 300 Slipper at 1,000 m/s Sliding Velocity
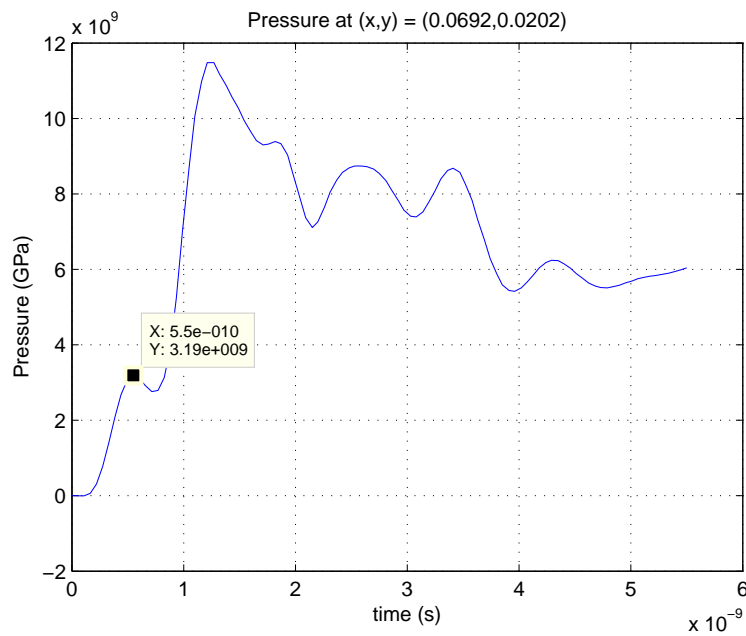
Figure 4.8: Pressure Evolution in VascoMax 300 Slipper at 1,200 m/s Sliding Velocity
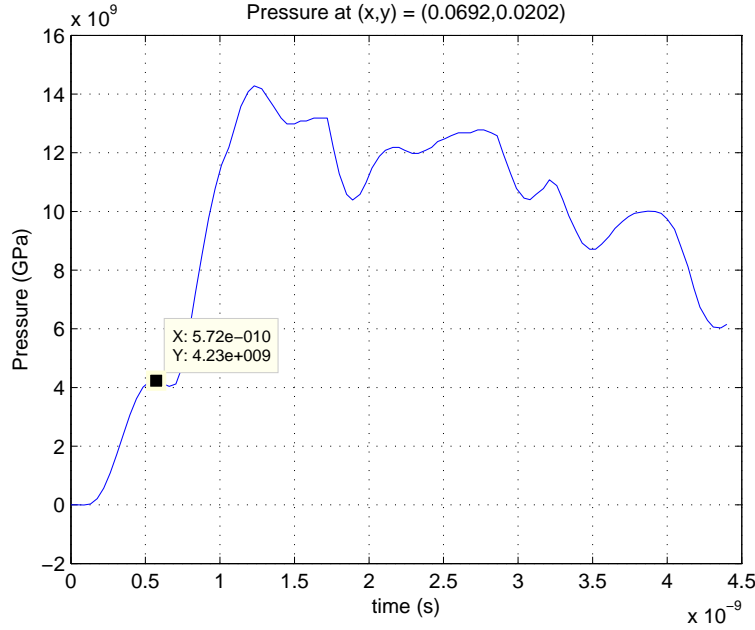
Figure 4.9: Pressure Evolution in VascoMax 300 Slipper at 1,500 m/s Sliding Velocity

$$c_{E,PS} = \sqrt{\frac{4}{3} \frac{(1-\nu)}{\rho_o(1-2\nu)(1+\nu)} E} \qquad (4.5)$$

Solving the equation for VascoMax 300, with Poisson's ratio equal to 0.283 and elastic modulus of 180.7 GPa, gives an elastic wave speed under plane strain conditions approximately 6,230 m/s. This can be validated by tracing a pressure wave through the material with respect to distance and time. This is done by plotting the pressure along a diagonal from the point of impact with respect to distance at each time step. A MATLAB code was created to do this. Before the MATLAB code is used, the CTH input deck needed to be modified. This modification and MATLAB code is discussed in Appendix D. The MATLAB code calculates and plots the change in pressure at a point along the three diagonals with respect to time.

Figure 4.10 shows the change in pressure in the VascoMax 300 slipper with respect to time on a 45° diagonal at 30 μm from the point of impact with a sliding velocity of 1,000 m/s. Figure 4.11 shows a similar plot along the 45° diagonal at

66

60 μm. These two plots can be used to determine the speed of the elastic-plastic wave generated during the CTH simulation. The speed of the wave is determined by dividing the difference in distance along the diagonals by the difference in time at which a constant value of pressure is achieved in the two figures. In this case, the speed of a wave with a constant pressure of -5 GPa was selected. The change in distance along the diagonal is 30 μm, and the change in time is approximately 4.90×10^{-9} seconds. This gives an elastic-plastic wave speed of 6,120 m/s.
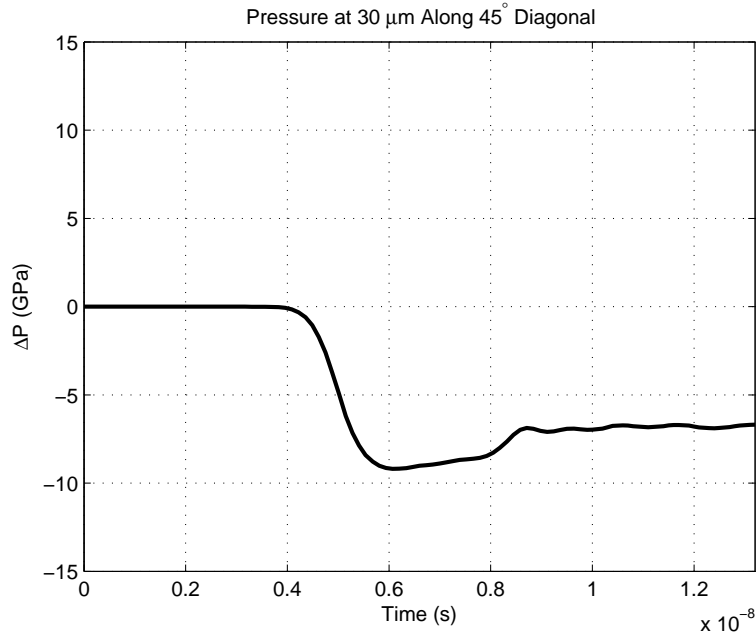
Figure 4.10: Pressure at 30 μm on a 45° diagonal at 1,000 m/s Sliding Velocity

The predicted elastic speed wave through VascoMax 300 under plane strain conditions, given by Equation 4.5, is 6,230 m/s. This is the speed of a purely elastic wave. The wave speed calculated from the CTH simulations represents an elastic-plastic wave. Introducing plasticity reduces the speed of the wave. Therefore, an elastic-plastic wave speed through the VascoMax 300 slipper of 6,120 m/s suggests that Equation 4.5 is a valid approach to calculating the speed of an elastic wave through a solid material.
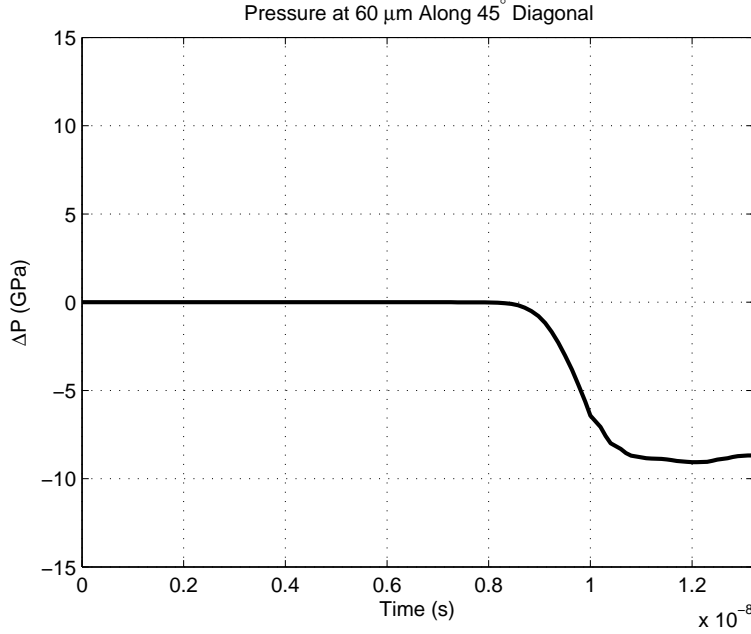
Figure 4.11:   Pressure at 60 μm on a 45° diagonal at 1,000 m/s Sliding Velocity

4.5   Equation of State at Low Velocities

Section 3.2.4 discussed modeling issues when using an equation of state in low velocity impact problems. Numerical inconsistencies were observed when solving for the mechanical wear rates at 50 m/s and 100 m/s. These wear rate values were two to three times greater than simulations at higher velocities. The low velocity simulations also produced an inconsistent state of pressure in the materials. When the slipper collides with the asperity, a pressure wave is created. Figure 4.12 shows a pressure wave generated by the collision of the VasocoMax 300 slipper sliding at 1,500 m/s into the surface asperity. This pressure wave extends into both the VascoMax 300 slipper and the AISI 1080 steel rail. Figure 4.13 shows the inconsistent state of pressure at sliding velocity of 50 m/s. Since the equation of state is used to solve for pressure, it can be assumed that the inconsistencies are a result of an improper EOS model.

An EOS must be defined for each material in CTH. Zukas [37] suggests a modification to the Mie-Grüneisen for low velocity impact. This modification, shown in Equation 4.6), sets the pressure to a product of the bulk modulus, K, and plastic
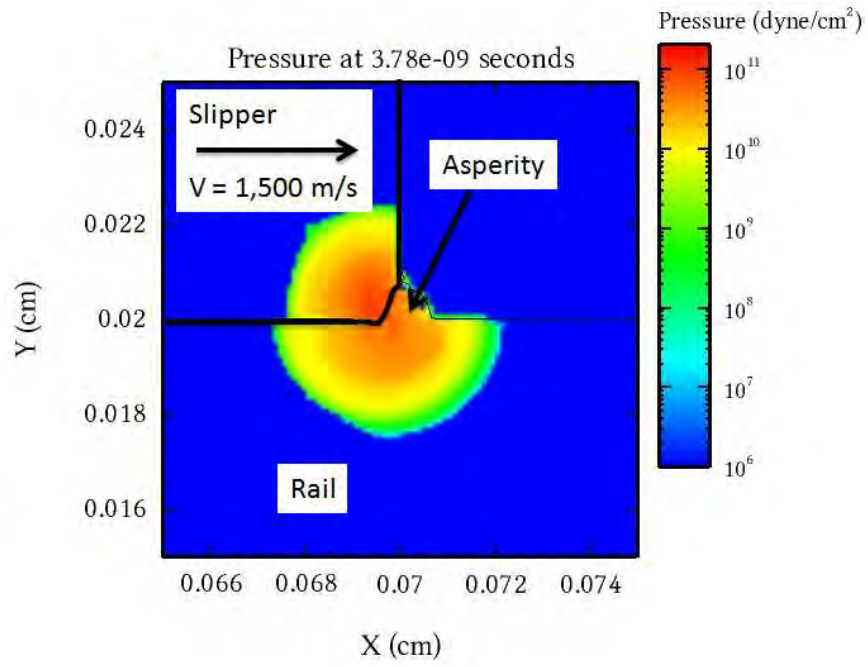
Figure 4.12:   Pressure Wave Generated by 1,500 m/s Collision
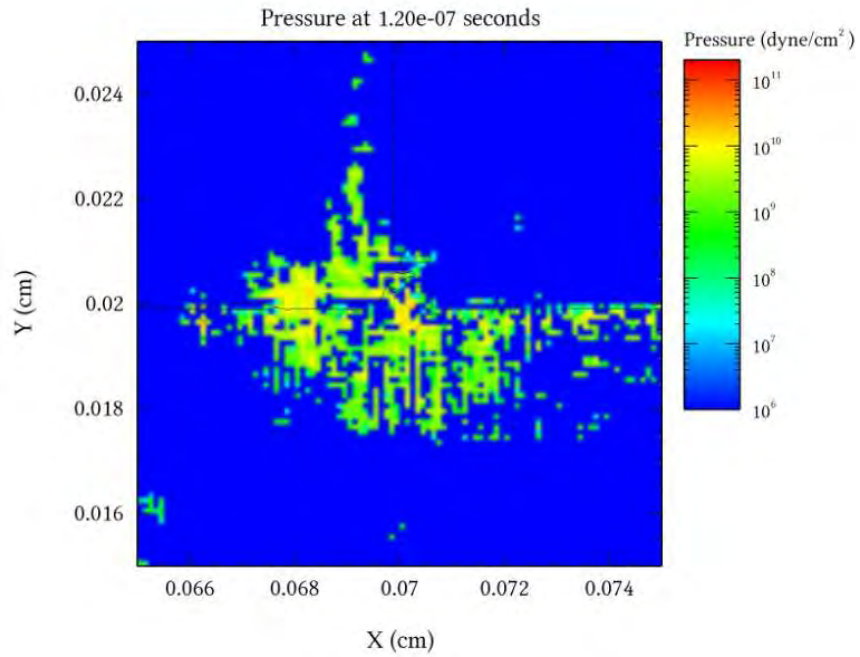
Figure 4.13:   Inconsistent State of Pressure at 50 m/s Sliding Velocity

69

strain, μ. It is reasonable to expect that a low velocity impact will produce less deformation in the material. The proposed equation is used to ensure that a state of zero pressure is achieved with zero compression.

$$P = K\mu \tag{4.6}$$

Based on a review of the CTH user's manual [18] and discussions with the author, an approach was developed to use the modified Mie-Grüneisen EOS by altering user input variables for the existing CTH Mie-Grüneisen model. A user defined Mie-Grüneisen EOS in CTH must define the material density, ρ_0, sound speed through the material, c_s, a linear coefficient in the Hugoniot fit, S, the Grüneisen constant, Γ, and the specific heat, c_v. The material density and sound speed do not change for the proposed modification. However, if the S value is set to a small value, but not zero, the sound speed dependence on pressure is removed. Also, if the Grüneisen constant is set to a small number, but not zero, and the specific heat is set to a large number, the material should be prevented from changing temperature during compression or expansion. This results in a model that should allow the material to respond elastically with respect to its bulk modulus and remove the thermal portion of the EOS. This attempt at implementing the modified Mie-Grüneisen EOS did not remove the numerical inconsistencies at low velocities.

It was decided that the Mie-Grüneisen EOS is not adequate for the model developed in this research. The Sesame equation of state, discussed in Section 2.8.2.2 was selected for use in this research because the model uses experimental data. It should be noted that the Sesame EOS interpolates data between experimental data when the sliding velocity falls within two points. When the sliding velocity is outside the range of experimental data, the Sesame EOS extrapolates using experimental data. The accuracy of the model at varying velocity is dependent on the amount of experimental data. The lower velocities are certainly extrapolated from the experimental

70

data, and therefore some error may be introduced when running simulations outside of the experimental range.

4.6 Wolfson Data

As discussed in Section 1.3, Wolfson [36] ran experiments to study the wear of materials in high speed track applications. Of the sixty tests, the results of two can be used to compare against the model presented in this thesis. The two tests both use specimens made of stainless steel, and a bare steel track with welded joints. This is a close representation of the VascoMax 300 on AISI 1080 steel sliding scenario studied in this research. Table 4.3 shows the results of the two experiments. The experimental average wear rates are given in units of in/ft. This was measured on specimens with a constant contact area, A_n, of 1 square inch (645.16 mm^2). Equation 4.7 is used to convert the experimental average wear rates to units of mm^3/mm.

$$\bar{W} = W_{wolfson} A_n \qquad (4.7)$$

Table 4.3:   Data From Wolfson's Experiments [36]

Sliding Velocity (ft/s)	Average Wear Rate (in/ft)	Average Wear Rate (mm^3/mm)
825	9.50×10^{-6}	5.11×10^{-4}
2,500	7.50×10^{-6}	4.03×10^{-4}

It is important to note that Wolfson's experiments produce three dimensional wear rates. Therefore, a conversion method must be applied to better represent a plane strain environment. To do this, Archard's equation [3,4], Equation 4.8 is used, which solves for the volume of worn material at low velocities, W_A. In this equation, P is the applied normal pressure, A_n is the contact area, k_A is the dimensionless Archard wear coefficient, and H is the material hardness. An Archard wear coefficient of 4.40$\times 10^{-5}$ is used for low speed wear, and the VascoMax 300 material hardness is 0.5$\times 10^3$ Pa.

$$W_A = \frac{k_A P A_n}{H} \tag{4.8}$$

When solving for Equation 4.8 using data from Wolfson's experiments, which applied a constant normal pressure of 300 psi, using a pin with a constant contact area of 1 square inch, a wear rate value of 1.17×10^{-4} mm^2 is found. Results from Hale's dissertation [20] at 10 m/s give an area of worn material equal to 2.65×10^{-5} mm^2. Dividing Wolfson's worn area by Hale's provides a constant, $N_{wolfson}$, which is used to relate Wolfson's experimental data [36] to the plane strain model using Equation 4.9.

$$W_{PS,wolfson} = \frac{\bar{W}}{N_{wolfson}} \tag{4.9}$$

where $W_{PS,wolfson}$ is the plane strain equivalent of Wolfson's experimental data and $\bar{W}$ is the Wolfson's experimental wear data converted from English to metric units. The two experiments were run at different velocities (252 m/s and 762 m/s). This provides two data points representing Wolfson's experiments converted to plane strain wear. These two data points are provided in Table 4.4 and will be plotted along with estimated wear rates from the CTH simulation in Section 4.7.

Table 4.4:   Wolfson Plane Strain Wear Rates

Sliding Velocity (m/s)	Mechanical Wear Rate (mm^3/mm)
252	1.16×10^{-4}
762	9.13×10^{-5}

4.7   Mechanical Wear Rate Results

Mechanical wear rates are calculated by passing output data from CTH into the MATLAB code described in Appendix C. Figure 4.14 is a plot of the calculated mechanical wear rates due to the collision with a single semi-circular surface asperity in plane strain conditions. The figure shows four lines representing the two failure

criteria, strain at max stress and critical von Mises stress, with a "slide" line interface condition, and a "no slide" condition. The Wolfson data [36], converted to the plane strain scenario in Section 4.6, is included in Figure 4.14 along with the wear rate results from Hale's FEA model [20]. Including the Wolfson data provides a validation to the simulation results because it shows the calculated values are on the same order of magnitude as an experimental set of data. The wear rate data are given in Table 4.5.

There are two failure criteria and two interface boundary conditions evaluated in this thesis. The boundary condition has an obvious effect on the calculated wear rates. The "slide line" condition simulates a frictionless surface by setting the shear stress along the surface to zero, whereas the "no slide" condition represents a surface with a semi-infinite coefficient of friction. The "no slide" boundary condition estimates a higher wear rate than the "slide line" condition for both failure criteria. This is due to the fact that the "no slide" condition requires pressure along the interface to reach a threshold before the material can move. Some of this additional pressure is captured within the data collection and adds damaged material to the calculation resulting in a higher wear rate.

Regardless of the interface boundary condition, the critical von Mises stress criteria tends to result in a higher calculated mechanical wear rate than the strain at max stress criteria. The critical von Mises stress failure criteria causes the wear rate to increase with sliding velocity up to 1,300 m/s, then a slight decrease is observed. Wear rates calculated using the strain at max stress failure criteria appear to level off at velocities above 1,200 m/s. Both failure criteria follow a similar curve provided by Hale until the wear rate calculated by the FEA approach decreases with increasing velocity above 600 m/s. Although each curve provides a different estimation for mechanical wear rates based on velocity, they all are on the same order of magnitude. The total mechanical wear, presented in Section 4.8, provides a better overall analysis of the models presented in this thesis.
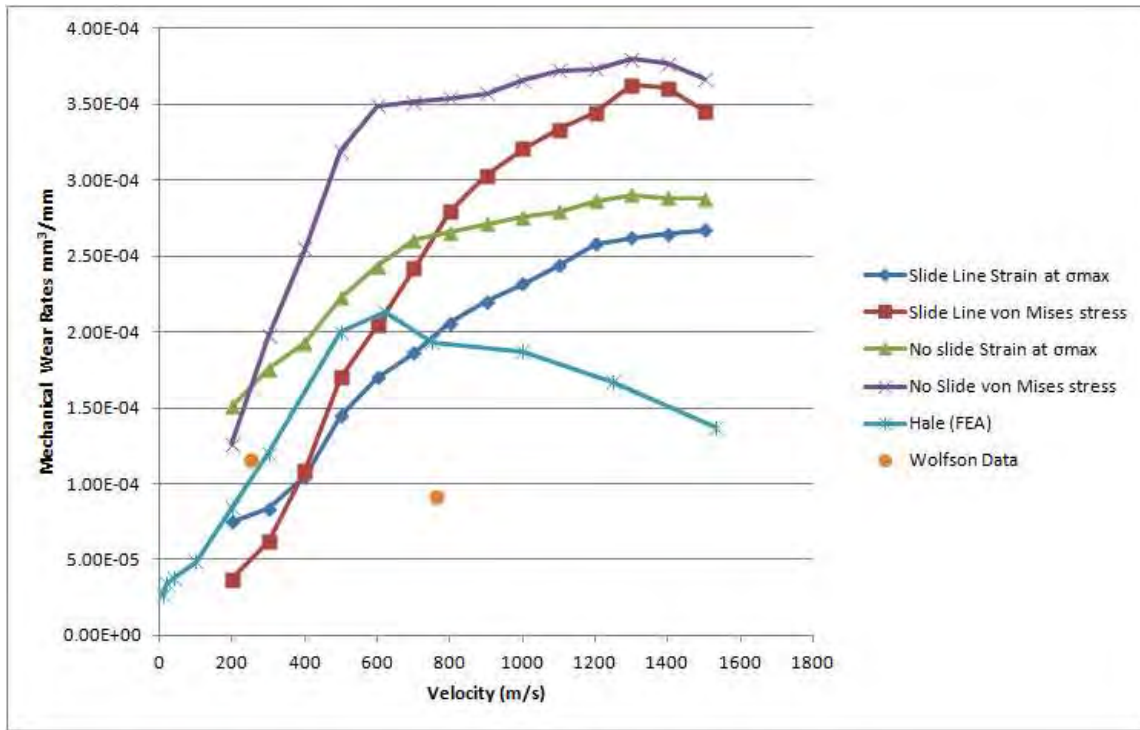
Figure 4.14:   Plane Strain Mechanical Wear Rates

Table 4.5:   Tabulated Wear Rates

Horizontal Sliding Velocity (m/s)	No Slide Strain at Max Stress (mm³/mm)	Slide Line Strain at Max Stress (mm³/mm)	No Slide Critical Von Mises Stress (mm³/mm)	Slide Line Critical Von Mises Stress (mm³/mm)
200	1.51×10^{-4}	7.49×10^{-5}	1.26×10^{-4}	3.71×10^{-5}
300	1.76×10^{-4}	8.34×10^{-5}	1.97×10^{-4}	6.16×10^{-5}
400	1.93×10^{-4}	1.05×10^{-4}	2.55×10^{-4}	1.09×10^{-4}
500	2.23×10^{-4}	1.45×10^{-4}	3.19×10^{-4}	1.70×10^{-4}
600	2.43×10^{-4}	1.70×10^{-4}	3.49×10^{-4}	2.04×10^{-4}
700	2.61×10^{-4}	1.86×10^{-4}	3.52×10^{-4}	2.42×10^{-4}
800	2.66×10^{-4}	2.06×10^{-4}	3.54×10^{-4}	2.79×10^{-4}
900	2.71×10^{-4}	2.20×10^{-4}	3.57×10^{-4}	3.03×10^{-4}
1,000	2.76×10^{-4}	2.32×10^{-4}	3.66×10^{-4}	3.21×10^{-4}
1,100	2.79×10^{-4}	2.44×10^{-4}	3.72×10^{-4}	3.33×10^{-4}
1,200	2.86×10^{-4}	2.58×10^{-4}	3.73×10^{-4}	3.44×10^{-4}
1,300	2.91×10^{-4}	2.62×10^{-4}	3.80×10^{-4}	3.63×10^{-4}
1,400	2.89×10^{-4}	2.64×10^{-4}	3.77×10^{-4}	3.61×10^{-4}
1,500	2.88×10^{-4}	2.67×10^{-4}	3.67×10^{-4}	3.45×10^{-4}

4.8   Total Mechanical Wear Results

As mentioned in Section 3.4, the total mechanical wear of an HHSTT slipper can be determined by plotting the wear rates as a function of distance along the track and integrating with respect to distance. Figure 4.15 shows the estimated total mechanical wear for the four cases presented in Section 4.7 as well as the total experimental wear from the January 2008 test mission. The experimental wear was determined by measuring the thickness of the slipper at the end of the test compared to the design nominal thickness. There are two things to consider when using this experimental value. The first is that the third sled reaches a maximum velocity close to 1,500 m/s and then decelerates to approximately 600 m/s (1,342 miles per hour) at the end of the track, at which point the sled and slippers leave the track, bouncing along the ground. It is not unreasonable to assume that some wear occurs during this time. The second thing to consider is that the slippers are not measured prior to the test. The initial thickness of the slippers is assumed to be the nominal thickness from the HHSTT design manual [1]. Since the total volume of worn material is determined as units of mm^3, a slight deviation from the nominal thickness can have an effect on the experimental wear value. Hale [20] gives the total wear volume from the aft right slipper on the third stage sled from the January 2008 test mission as 10,516 mm^3. The total volume of worn material and percentage of experimental wear for each criteria is given in Table 4.6.

Table 4.6:   Estimated Total Mechanical Wear

Failure Criteria	Volume of Worn Material (mm^3)	Percentage of Experimental Wear
No Slide Strain at Max Stress	6,418	61.03
Slide Line Strain at Max Stress	5,186	49.31
No Slide Critical Von Mises Stress	8,504	80.87
Slide Line Critical Von Mises Stress	6,857	65.20
Hale FEA method [20]	4,298	40.87
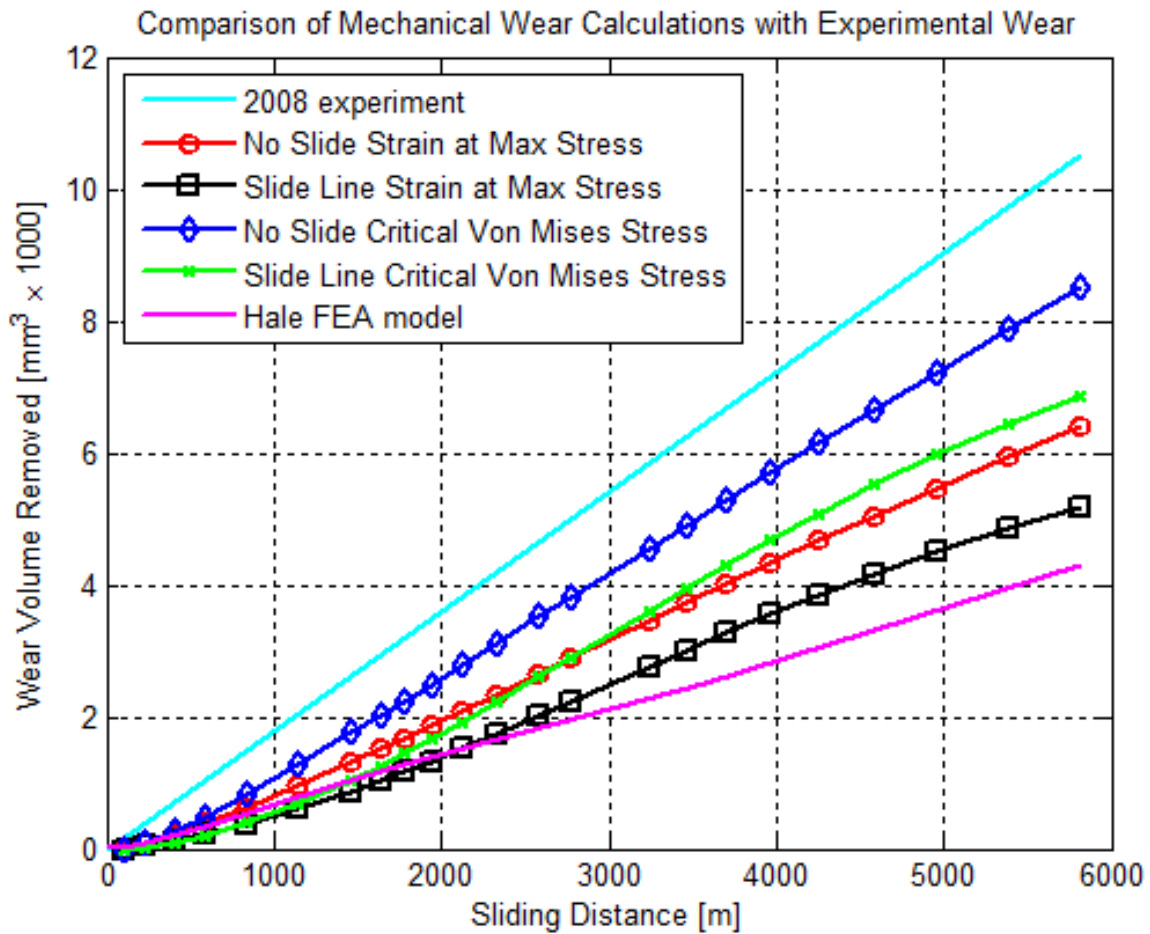
Figure 4.15:   Total Mechanical Wear

4.9 Summary of Results

This chapter discussed the addition of a dead load to the plane strain model to represent the variable vertical force of the slipper as it slides along the rail. The addition of the dead load produced wear rates identical to simulations without the dead load. Therefore, the dead load was dropped from the model and not included in the analysis. It is possible that the dead load is not adequately represented in the submodel developed for this thesis. It may produce results if a larger-scale model was developed with an entire slipper and dead load attached to the top.

The equivalent plane strain Hugoniot elastic limit, derived in Section 2.5.2, was evaluated and compared to values obtained from CTH simulations. The equation used to determine $\sigma_{HEL,PS}$, Equation 2.15, assumes it is independent of sliding velocity, and gives a value of 2.8664 GPa for VascoMax 300. The CTH simulations suggest that the onset of plasticity is influenced by the sliding velocity of the slipper. However, 2.8664 GPa appears to be a good approximation for VascoMax 300 $\sigma_{HEL,PS}$. This chapter also presented a validation of the plane strain elastic wave speed, Equation 2.16, derived in Section 2.5.2.

This chapter included a discussion of issues encountered during low velocity simulations. It is believed that these issues are a result of the use of an improper equation of state. A modified EOS was attempted based on suggestions by Zukas [37]. However, this modified EOS did not provide a substantial improvement over the existing models. Hydrocodes are typically used to model high energy problems, such as explosives or high velocity impact problems. Therefore, the low velocity issues were not a significant surprise. The simulations ran with no errors over a velocity range from 200 m/s to 1,500 m/s. Simulations with a sliding velocity below 200 m/s resulted in numerical inconsistencies described in Section 4.5.

This chapter also presented the results of the CTH simulation for four scenarios; "No slide" strain at max stress, "slide line" strain at max stress, "no slide" critical von Mises stress, and "slide line" critical von Mises stress. The mechanical wear rate

results are presented in Figure 4.14 and the total mechanical wear can be found in Figure 4.15. The wear rate data are given in Table 4.5.

V. Summary and Conclusions

The chapter is a summation of the material presented in this thesis. The literature search and theoretical background will be discussed first, followed by a brief description of the hydrocode model developed and the results obtained. Finally, conclusions will be presented on the results of the thesis, and suggestions for future work will be presented.

5.1 Summary

Research into the onset of wear of sliding bodies has produced low-velocity models capable of estimating worn material. One model in particular, the Archard Wear model [2–4], has been used to establish relationships between wear in plane strain to three-dimensional wear. Previous work by Hale [20] and Meador [28] has made use of a plane strain scenario to model the slipper-rail sliding event.

Based on the previous research, a hydrocode model was developed using CTH to estimate plane strain mechanical wear rates. The model allows a VascoMax 300 slipper to collide with a 6 μm radius surface asperity made of AISI 1080 steel. Damage was recorded per sliding distance to give wear rates. Two failure criteria were evaluated (Section 2.9): critical von Mises stress and strain at max stress. These failure criteria were established by the Johnson-Cook viscoplasticity model presented in Section 2.4. The model also has two distinctly different interface boundary conditions between the slipper and rail. One boundary condition, "slide line", simulates a frictionless surface by setting the shear stress along the surface to zero. The second boundary condition, "no slide", simulates a surface with a semi-infinite coefficient of friction by establishing a pressure threshold that must be exceeded for the material to move. These two boundary conditions represent two extremes along the surface in terms of friction.

Since the model developed in this thesis simulates a collision between two metals at high velocities, and establishes failure criteria based on the material response due

to the collision, fundamentals of wave mechanics were researched. Previous research of high velocity impact has considered uniaxial strain conditions. As such, equations exist that are used to estimate the onset of plasticity in the material, called the Hugoniot elastic limit, and to calculate the speed of pressure waves propagating through a solid material under uniaxial strain conditions. However, the scenario of interest for this research is plane strain. Therefore, equations were derived in Chapter II to evaluate the plane strain elastic wave speed through a solid, Equation(2.16), and the equivalent plane strain Hugoniot elastic limit, Equation 2.15.

The CTH model was run at velocities ranging from 200 m/s to 1,500 m/s. The results of the simulations were presented in Chapter IV. The estimated mechanical wear rates were used to determine the total mechanical wear of the aft right slipper from the third sled of the January 2008 test mission.

5.2   Conclusions

The plane strain derivations presented in Chapter II were validated in Chapter III using results obtained from CTH simulations. The derived equations imply they are independent of sliding velocity. However, the CTH simulations suggest that onset of plasticity and elastic wave speed through the slipper are effected by the sliding velocity. This effect appears to be minimal, and the derived equations present an adequate estimation of these values.

The addition of a dead load to represent the vertical force of the slipper into the rail was presented in Section 4.1. The dead load was added to provide a more accurate representation of the HHSTT environment. CTH does not allow a force input. Therefore, Equation 4.1 was used to calculate the effective mass representing the vertical force from the DADS data. The simulations with the dead load produced mechanical wear rates that were identical to simulations without. One possible reason for these results is the fact that a submodel of the slipper was developed, only representing a small part of the slipper in the simulation. It may be necessary to develop a full model of the slipper with an attached dead load to get an accurate

respresentation of the vertical force. Such a model was not developed for this thesis, because the simulation time would drastically increase.

The mechanical wear rates obtained from the CTH simulation appear to be an accurate estimation of the HHSTT slipper-rail sliding event. Data from Wolfson [36] was converted to the plane strain scenario in Section 4.6 and plotted with the estimated mechanical wear rates in Figure 4.14. The two data points are of the same order of magnitude as the estimated values from the CTH simulation. The total mechanical wear was calculated and plotted in Figure 4.15. The total experimental wear from the January 2008 test mission was determined by Hale [20] to be 10,516 mm^3. The results of the total mechanical wear predict between 49.31% and 80.87% of the experimental wear. However, due to the uncertainty of the true experimental wear, discussed in Section 4.8, the results of the simulation are acceptable. The results of the simulation and total wear calculation suggest that the model developed is an adequate method to model mechanical wear.

5.3   Future Work Suggestions

The model presented in this thesis has been developed and modified based on previous research. There are however, simplifications made to allow the plane strain model to represent a three-dimensional scenario. One significant simplification to this research is the absence of a thermal model. Previous work by Meador [28] has shown that melt wear plays an important role in the slipper - rail sliding event. Mrs. Gracie Paek, as part of her PhD dissertation is developing a thermodynamic model to represent melt wear of HHSTT slippers.

The Johnson-Cook fracture model, discussed in Section 2.9.3, can be used to model material damage. This failure criteria was evaulated for use in the current model. However, the simulations estimated zero wear when this criteria was used. The fracture model requires five coefficients to be defined for each material. These fracture coefficients are not known for VascoMax 300 or AISI 1080 steel. AISI 4340 steel and iron were used to represent the VascoMax 300 slipper and AISI 1080 steel

rail, respectively. With properly defined fracture coefficients, obtained through experimentation, the Johnson-Cook fracture model may yield worn material.

Appendix A. Plane Strain Derivations of Hugoniot Elastic Limit and Elastic Wave Speed

An approach for considering the uniaxial Hugoniot elastic limit is outlined in Meyers [29] and Zukas [37]. A similar process is applied, but in this process a Hugoniot elastic limit is determined considering plane strain conditions. The speed of the elastic-plastic wave generated due to plane strain collision is also determined. The following equations show the derivation of Equations (2.15) and (2.16).

A.1 Equivalent Hugoniot Elastic Limit for Plane Strain

Since plane strain is considered, one can say

$$\varepsilon_1 = \varepsilon_1^e + \varepsilon_1^p \tag{A.1}$$

$$\varepsilon_2 = \varepsilon_2^e + \varepsilon_2^p \tag{A.2}$$

$$\varepsilon_3 = \varepsilon_3^e + \varepsilon_3^p = 0 \tag{A.3}$$

$$\varepsilon_3^e = -\varepsilon_3^p \tag{A.4}$$

where ε_i^e = elastic strain and ε_i^p = plastic strain. The next step is to consider the plastic portion to be incompressible, thus

$$\varepsilon_1^p + \varepsilon_2^p + \varepsilon_3^p = 0 \tag{A.5}$$

$$\varepsilon_1^p + \varepsilon_2^p = \varepsilon_3^p \tag{A.6}$$

If Equations (A.1) through (A.6) are combined, the result is an equation for the summation of principal strains ε_1 and ε_2.

$$\varepsilon_1^p + \varepsilon_2^p = \varepsilon_3^e = \varepsilon_1 - \varepsilon_1^e + \varepsilon_2 - \varepsilon_2^e \qquad (A.7)$$

$$(\varepsilon_1 + \varepsilon_2) = \varepsilon_1^e + \varepsilon_2^e + \varepsilon_3^e \qquad (A.8)$$

Saada [32] provides constitutive equations for plane strain.

$$\varepsilon_1^e = \frac{1+\nu}{E}[(1-\nu)\sigma_1 - \nu\sigma_2] \qquad (A.9)$$

$$\varepsilon_2^e = \frac{1+\nu}{E}[(1-\nu)\sigma_2 - \nu\sigma_1] \qquad (A.10)$$

$$\varepsilon_3^e = 0 \qquad (A.11)$$

The Tresca yield theory is used to get $\sigma_2 = f(\sigma_1, Y_o)$ [32].

$$Y_o = \sigma_1 - \sigma_2 \qquad (A.12)$$

$$\sigma_2 = \sigma_1 - Y_o \qquad (A.13)$$

where Y_o is the yield stress for a uniaxial elastic - perfectly plastic material. The constiutive equations along with Tresca yield theory are used to reduce Equation A.8 to a form for σ_1.

$$\sigma_1 = \frac{(\varepsilon_1 + \varepsilon_2)E}{(1+\nu)(1-2\nu)2} + \frac{Y_o}{2} \qquad (A.14)$$

The next step is to consider loading of an elastic - perfectly plastic material, starting with the pressure.

$$P = \frac{\sigma_1 + \sigma_2 + \sigma_3}{3} \tag{A.15}$$

$$P = \frac{\sigma_1 + \sigma_2 + \nu(\sigma_1 + \sigma_2)}{3} \tag{A.16}$$

where ν is the Poisson's ratio, and $\sigma_3 = \nu(\sigma_1 + \sigma_2)$ in a plane strain scenario. If one solves again for σ_1,

$$\sigma_1 = \frac{3}{2} \frac{P}{(1+\nu)} + \frac{Y_o}{2} \tag{A.17}$$

σ_1 becomes the stress of importance for the analysis as it is in a uniaxial strain situation. When pressure, P, equals zero

$$\sigma_1 = \frac{Y_o}{2} \tag{A.18}$$

Figure A.1 shows the loading of an elastic-perfectly plastic material. For the case of zero pressure

$$\alpha = \frac{Y_o}{2} \tag{A.19}$$

For our purposes, we assume $\beta = \frac{4}{3}\mu$, as related to a uniaxial stress situation [32], where $\mu = \frac{E}{2(1+\nu)}$. The summation of principal strain term $\varepsilon_1 + \varepsilon_2$, is evaluated in terms of α and β to get

$$(\varepsilon_1 + \varepsilon_2) = \frac{3Y_o}{4E}(1+\nu) \tag{A.20}$$

Equations (A.14) and (A.20) are combined to solve for the equivalent Hugoniot elastic limit for the case of plane strain.
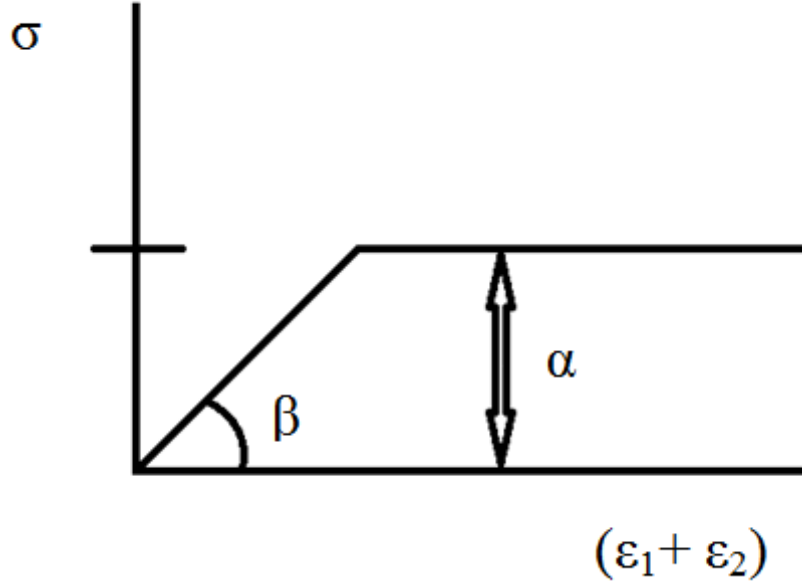
Figure A.1: Loading of an Elastic-Perfectly Plastic Material

$$\sigma_{HEL,PS} = Y_o \left[\frac{3}{8 - 16\nu} + \frac{1}{2} \right] \tag{A.21}$$

A.2 Plane Strain Elastic Wave Speed

Combining equations (A.13) and (A.20), the result for $(\varepsilon_1 + \varepsilon_2)$ is

$$(\varepsilon_1 + \varepsilon_2) = \frac{3(1 + \nu)}{4E}(\sigma_1 + \sigma_2) \tag{A.22}$$

and

$$\sigma_2 = \frac{\nu}{1 - \nu}\sigma \tag{A.23}$$

Combining equations (A.22) and (A.23), and solving for σ_1, the following is obtained

$$\sigma_1 = \frac{4(1-\nu)}{3(1+\nu)(1-2\nu)}(\varepsilon_1 + \varepsilon_2)E \qquad (A.24)$$

The speed of sound through any medium can be represented as the square root of pressure divided by density. Through a solid media, the pressure term is replaced by the elastic modulus. For the case of plane strain, the elastic modulus carries an added term representing the summation of strain, $(\varepsilon_1 + \varepsilon_2)$. The elastic wave speed for the case of plane strain is given by Equation A.25

$$c_{E,PS} = \sqrt{\frac{4}{3}\frac{(1-\nu)}{\rho_o(1-2\nu)(1+\nu)}E} \qquad (A.25)$$

Appendix B. CTH Input Deck

B.1 Discussion of CTH Input

The sample CTH input deck provided in this appendix is used to estimate the wear rate of VascoMax 300 sliding at 1,000 m/s into a 6 μm radius surface asperity made of AISI 1080 steel. This input deck can be altered to represent an event with a different sliding velocity. To do this, the total simulation time, "tstop", and intermediate step time need to be updated. The "tstop" variable is found on line 36 of the input deck. There are nine variables in the input deck that use the intermediate step time, and all nine must be updated for each run. The variables are: "dt", "dtfrequency", "PlotTime", "SaveTime", and "HisTime". The "dt" variable is listed four times on lines 244, 247, 318, and 322. The "dtfrequency" variable is listed twice on lines 250 and 253. The "PlotTime" variable is found on line 330, the "SaveTime" variable is found on line 331, and the "HisTime" variable is found on line 406.

The initial velocity also needs to be updated when changing the sliding velocity of the VascoMax 300 slipper. The initial velocity vector is found in the diatom input set, starting on line 124. Since the VascoMax 300 slipper is the only moving body for this analysis, it is the only velocity that needs to be changed. The initial velocity input for the VascoMax 300 slipper is found on line 152 of the input deck. The initial velocities of the other materials should remain at zero for all simulations. It is important to note that the base unit of length in CTH is cm. This means that all velocities and distances must be input having dimensions of cm/s and cm, respectively. This is seen on line 152 of the included input deck, the initial velocity is given as 100,000 cm/s which gives 1,000 m/s.

In CTH, the units of pressure and stress are expressed as dynes/cm^2 and temperature in electron volts, eV. This is accounted for in the post-processing code provided in Appendix C. However, the implementation of the Johnson-Cook viscoplastic model requires the conversion of a couple material constants. Pressure and stress is converted to GPa from dynes/cm^2 using Equation (B.1), and temperature

is converted from K to eV using Equation (B.2) [23]. Table B.1 shows the material constants in units compatible with CTH.

$$P_{dynes/cm^2} = P_{GPa} \times 10^{10} \qquad \text{(B.1)}$$

$$T_{eV} = T_K/11604.505 \qquad \text{(B.2)}$$

Table B.1:   Johnson-Cook Coefficients for VascoMax 300 and AISI 1080 Steel in CTH Units [15, 20, 28]

Coefficient	VascoMax 300	AISI 1080 Steel
A ($dynes/cm^2$)	2.1×10^{10}	0.7×10^{10}
B ($dynes/cm^2$)	0.124×10^{10}	3.6×10^{10}
C (Unitless)	0.03	0.17
m (Unitless)	0.8	0.25
n (Unitless)	0.3737	0.6

B.2   Example CTH Input Deck

```
1  ***********************************************
   *eor* cthin
   ***********************************************
   *
   * cthin input with Spymaster graphics for slipper wear simulation
6  *
   * filename: slipperwear.in
   *
   * 1. File modified by Steve Meador (MS-10M)
   * 2. File converted to CTH v8.1 by Maj Chad Hale, PhD-09S, Aug ...
     2008
11 * 3. new format based on CTH Course (4-7 Aug 08) in Albuquerque, ...
     NM
   * 4. modifies Cameron's 393 m/s, No Coating, Asperity, T=297 input...
     file
   *
   *          ----------------
   *         |      ----->    |
16 *        |       |         |
   *        |       v         /
   *  ------------------------------
   *
   *
```

89

```
21 *   vx=varies, vy=-1 m/s  V300 Steel Slider, 1080 Steel Rail, No ...
      Atm.
   *   No Slide line. mix=1 frac=1 Rounded corner.
   *   Added mass on top to simulate sled mass

      **************************************************
26 * title record set
   **************************************************

   Horizontal Velocity = 1000 m/s, Vertical Velocity = -0.50 m/s

31 **************************************************
   * control input set
   **************************************************
   control
     mmp3                    * enable multiple material temperatures and...
         pressures in each cell
36   tstop = 6.60e-9        * stopping criteria for time level - this ...
        is total simulation time
     nscycle = 100000      * maximum number of cycles to be run
   *  rdumpf = 3600.         * time for back-ups of restart file ...
      updates
     tbad = 1e30           * maximum number of thermodynamics warnings
   *  dtcourant = 0.6       * Courant condition multiplier
41   ygravity = -980       * Acceleration due to gravity = -9.80 m/s^2
   endcontrol


   **************************************************
   * mesh input set
46 **************************************************
   *   geom=2DR(rectangular x,y)
   *   geom=2DC(cylindrical x=radius, y=axis)
   *   geom=3DR(rectangular x,y,z)
   *   type=e (Eulerian)   now the default (CTHv8.1)
51 *   x#=coordinate range for plot
   *   y#=coordinate range for plot
   *   dxf=width of first cell in the region
   *   dxl=width of last cell in the region
   *   n=number of cells added in this region
56 *   w=total width of this region in centimeters
   *   r=ratio of adjacent cell widths
   **************************************************

   mesh
61   block 1  geom=2dr                * coordinates for 2D rectangular ...
         Eulerian mesh
       x0 = 0.0000
         x1 w = 850e-4 dxf = 1.0e-4 dxl = 1.0e-4
       endx

66     y0 = 0.0000
         y1 w = 850e-4 dyf = 1.0e-4 dyl = 1.0e-4
```

```
      endy
    endblock
  endmesh
71
  **********************************************
  * EOS input set
  **********************************************
  eos
76  material1 ses grepxy1        * epoxy rail coating (Cinnamon/...
        Cameron)
    material2 ses iron           * 1080 steel rail
  *   MAT3 MGRUN=user R0=8.13 CS=3.63e5 S1=1e-3 G0=1e-3 CV=1e15 * ...
      modified Mei-Gruneisen for VM300 slipper
    material3 ses steel_v300     * VascoMax 300 slipper
    material4 mgr platinum       * platinum for simulated sled mass
81 endeos

  **********************************************
  * elastic-plastic input set
  **********************************************
86 epdata
    vpsave          * cell yield stress and plastic strain rate data ...
        is saved
    lstrain         * compute and save Lagrangian strain tensor ...
        components
    mix = 3         * volume averaged yield strength normalized by sum...
        of volume fractions

91  matep = 1      *Epoxy Glider Coating
      poisson 0.46
      yield 1.0e8

   matep = 2      * 1080 Steel rail
96     JO USER
       AJO 0.7e10            * A
       BJO 3.6e10            * B
       CJO 0.17             * C
       MJO 0.25             * m
101    NJO 0.6              * n
       TJO 0.14391          * Melting temperature
       poisson 0.27

   matep = 3      * VascoMax 300 slipper
106    JO USER
       AJO = 2.1e10          * A
       BJO = 0.124e10        * B
       CJO = 0.03           * C
       MJO = 0.8            * m
111    NJO = 0.3737         * n
       TJO = 0.145202       * Melting temperature
       poisson 0.283
```

```
        matep = 4                    * platinum simulated sled mass
116     poisson 0.2
        yield 10e10

    * SLI 2 3

121 endepdata

    ***********************************************
    * diatom input set
    ***********************************************
126 diatom
      block 1

            package '1080 steel rail'
            material 2
131         numsub 100
            temperature = 2.55935e-2 * eV = 74.93F = 297 K
            velocity 0.0, 0.0
            insert box
               p1 0 0
136            p2 850e-4 200e-4
            endinsert
            delete circle
               center 700e-4 200e-4
               radius 6e-4
141         enddelete
            insert circle
               center 700e-4 200e-4
               radius 6e-4
            endinsert
146       endpackage

         package 'slipper'
            material 3
            numsub 100
151         temperature = 0.0184558
            velocity = 1000e2, -0.50e2
            insert box
               p1 0.0 200e-4
               p2 694e-4 325e-4
156         endinsert
            delete box
               p1 692e-4 200e-4
               p2 694e-4 202e-4
           enddelete
161        delete circle
               center 692e-4 202e-4
               radius 2e-4
            enddelete
           insert circle
166            center 692e-4 202e-4
```

```
              radius 2e-4
          endinsert
        endpackage

171   endblock
      enddiatom


      ************************************************
      * tracer input set
176   ************************************************
      tracer
              add 0.06755, 0.01905 to 0.07115, 0.01905 n=37
              add 0.06755, 0.01915 to 0.07115, 0.01915 n=37
              add 0.06755, 0.01925 to 0.07115, 0.01925 n=37
181           add 0.06755, 0.01935 to 0.07115, 0.01935 n=37
              add 0.06755, 0.01945 to 0.07115, 0.01945 n=37
              add 0.06755, 0.01955 to 0.07115, 0.01955 n=37
              add 0.06755, 0.01965 to 0.07115, 0.01965 n=37
              add 0.06755, 0.01975 to 0.07115, 0.01975 n=37
186           add 0.06755, 0.01985 to 0.07115, 0.01985 n=37
              add 0.06755, 0.01995 to 0.07115, 0.01995 n=37
              add 0.06755, 0.02005 to 0.07115, 0.02005 n=37
              add 0.06755, 0.02015 to 0.07115, 0.02015 n=37
              add 0.06755, 0.02025 to 0.07115, 0.02025 n=37
191           add 0.06755, 0.02035 to 0.07115, 0.02035 n=37
              add 0.06755, 0.02045 to 0.07115, 0.02045 n=37
              add 0.06755, 0.02055 to 0.07115, 0.02055 n=37
              add 0.06755, 0.02065 to 0.07115, 0.02065 n=37
              add 0.06755, 0.02075 to 0.07115, 0.02075 n=37
196           add 0.06755, 0.02085 to 0.07115, 0.02085 n=37
              add 0.06755, 0.02095 to 0.07115, 0.02095 n=37
              add 0.06755, 0.02105 to 0.07115, 0.02105 n=37
              add 0.06755, 0.02115 to 0.07115, 0.02115 n=37
              add 0.06755, 0.02125 to 0.07115, 0.02125 n=37
201           add 0.06755, 0.02135 to 0.07115, 0.02135 n=37
              add 0.06755, 0.02145 to 0.07115, 0.02145 n=37
              add 0.06755, 0.02155 to 0.07115, 0.02155 n=37
              add 0.06755, 0.02165 to 0.07115, 0.02165 n=37
              add 0.06755, 0.02175 to 0.07115, 0.02175 n=37
206           add 0.06755, 0.02185 to 0.07115, 0.02185 n=37
              add 0.06755, 0.02195 to 0.07115, 0.02195 n=37
              add 0.06755, 0.02205 to 0.07115, 0.02205 n=37
              add 0.06755, 0.02215 to 0.07115, 0.02215 n=37
              add 0.06755, 0.02225 to 0.07115, 0.02225 n=37
211           add 0.06755, 0.02235 to 0.07115, 0.02235 n=37
              add 0.06755, 0.02245 to 0.07115, 0.02245 n=37
      endtracer


216   ************************************************
      * convection control input set
      ************************************************
```

```
     Convct                    * enable convection of internal energy
       convection = 1          * use slope of internal energy and mass ...
          density, discard KE residual
221    interface = smyra       * scheme for interface tracker
     endconvct


     ************************************************
226  * fracture input set
     ************************************************
     Fracts                    * enable fracture data (dynes/cm^2)
       pressure
       pfrac1 = -1.0e8         * fracture stress or pressure for nth ...
          material
231    pfrac2 = -2.0e10
       pfrac3 = -7.45e10
       pfrac4 = -1.2e10
       pfmix = -1.20e10        * fracture stress or pressure in a cell ...
          with no void present
       pfvoid = -1.20e10       * fracture stress or pressure in a cell ...
          with a void present
236  endfracts
     ************************************************
     * edits input set
     ************************************************

241  edit
       exact
       shortta                 * short edits based on time
         time = 0.0  , dt = 6.60e-11
       ends
246    longt                   * long edits based on time
         time = 0.0e0  , dt = 6.60e-11
       endl
       plott                   * plot dumps based on time
         time  0.0e-6  dtfrequency 6.60e-11
251    endp
       histt                   * tracer history based on time
         time  0.0e-6  dtfrequency 6.60e-11
         htracer all
       endhistt
256  ende


     ************************************************
     * boundary condition input set
     ************************************************
261  * 0=symmetry
     * 1=sound speed based absorbing
     * 2=extrapolated pressure with no mass allowed to enter
     * 3=extrapolated pressure but mass is allowed to enter
     ************************************************
266
```

```
      boundary                            * enable boundary condition data
        bhydro                            * enable hydrodynamic boundary ...
            conditions
          block 1
            bxbot = 1 , bxtop = 2
271         bybot = 1 , bytop = 2
          endb
        endh
      endb

276 * CSH: cleaned up to here...


      *heatconduction                     * enable heat conduction
      *   MAT1 TABLE = 3                   * conductivity tables defined in ...
            DEFTABLE list below
281 *   MAT2 TABLE = 1
      *   MAT3 TABLE = 2
      *endh

      *   DEFTABLE=1              * 1080 STEEL
286   *T(eV)     k(erg/s/eV/cm)
      *  1.4684e-3 4.7700e10
      *  1.0377e-2 4.8100e10
      *  1.9090e-2 4.5200e10
      *  2.7900e-2 4.1300e10
291 *  3.6711e-2 3.8100e10
      *  4.5521e-2 3.5100e10
      *  5.4332e-2 3.2700e10
      *  6.3142e-2 3.0100e10
      *  7.1953e-2 2.4400e10
296 *  8.9574e-2 2.6800e10
      *  1.1111e-1 3.0100e10
      *  endd

      *   DEFTABLE=2              * VascoMax 300 Steel
301   *T(eV)     k(erg/s/eV/cm)
      *  3.6711e-3 2.4715e10
      *  1.4684e-2 2.7424e10
      *  2.9369e-2 2.9794e10
      *  3.9158e-2 3.0132e10
306 *  endd

      *   DEFTABLE=3              * Epoxy
        *T(eV)     k(erg/s/eV/cm)
      *  3.6711e-3 6.5e8
311 *  1.4684e-2 6.5e8
      *  2.9369e-2 6.5e8
      *  3.9158e-2 6.5e8
      *  endd

316
```

```
    *mindt                      * minimum allowable time step in mesh
    *   time = 0.0 dt = 6.60e-11
    *endm

321 maxdt                       * maximum allowable time step in mesh
        time = 0.0 dt = 6.60e-11
    endm


326 * CSH: Attempt to get data for Spymaster

    spy

     PlotTime(0.0, 6.60e-11);
331  SaveTime(0.0, 6.60e-11);
     Save("VOID,VOLM,M,P,XXDEV,YYDEV,XYDEV,VX,VY,T,TK,PM,TM,YLD,Q3,J2P...
        ");

    define main()
     {
336 %    pprintf(" PLOT: Cycle=%d, Time=%e\n",CYCLE,TIME);
    %    XLimits(400e-4,725e-4);
    %    YLimits(175e-4,300e-4);
    %    Image("Materials");
    %     Window(0,0,0.75,1);
341 %     Label(sprintf("Materials at %6.2e seconds", TIME));
    %     Plot2DMats(0.3);
    %     ULabel("Test: (cm)");
    %     Draw2DMesh();                % toggle on/off mesh
    %     MatColors(RED,GREEN,YELLOW,NO_COLOR);
346 %     MatNames("Epoxy Coating","1080 Steel Rail","VascoMax 300 ...
        Slipper","");
    %     DrawMatLegend("",0.71,0.2,0.99,0.9);
    %    EndImage;

        XLimits(650e-4,750e-4);
351     YLimits(150e-4,250e-4);
        Image("VonMisesStress");
         Window(0,0,0.75,1);
         ColorMapRange(0,4000);
         ColorMapClipping(OFF,OFF);
356     Label(sprintf("von Mises Stress at %6.2e seconds", TIME));
        Plot2D("J2P");
        Draw2DMatContour;
        DrawColorMap("vonMises Stress (MPa)", 0.7,0.4,0.9,0.9);
        EndImage;
361
    %    XLimits(650e-4,750e-4);
    %    YLimits(150e-4,250e-4);
    %    Image("PlasticStrainRate");
    %     Window(0,0,0.75,1);
366 %     ColorMapRange(1e6,1e15,LOG_MAP);
```

96

```
%      ColorMapClipping(OFF,OFF);
%      Label(sprintf("Plastic Strain Rate at %6.2e seconds", TIME));
%      Plot2D("PSR");
%      Draw2DMatContour;
371 %      DrawColorMap("Plastic Strain Rate (1/sec)", 0.7,0.4,0.9,0.9);
%     EndImage;

     XLimits(685e-4,715e-4);
     YLimits(190e-4,215e-4);
376    Image("Materials_small");
       Window(0,0,0.75,1);
       Label(sprintf("Materials at %6.2e seconds", TIME));
       Plot2DMats(0.3);
       Label( "Test Label: Distance (cm)" );
381 %      Draw2DMesh();                % toggle on/off mesh
       MatColors(NO_COLOR,GREEN,YELLOW,NO_COLOR);
       MatNames("","1080 Steel Rail","VascoMax 300 Slipper","");
       DrawMatLegend("",0.71,0.2,0.99,0.9);
     EndImage;
386
     XLimits(650e-4,750e-4);
     YLimits(150e-4,250e-4);
     Image("Pressure");
       Window(0,0,0.75,1);
391    ColorMapRange(1e6,2e11,LOG_MAP);
       ColorMapClipping(OFF,OFF);
       Label(sprintf("Pressure at %6.2e seconds", TIME));
       Plot2D("P");
       Draw2DMatContour;
396    DrawColorMap("Pressure (dyne/cm^2)", 0.7,0.4,0.9,0.9);
     EndImage;

   }


401 SaveHis("POSITION,YLD,Q3,PSR,VOLM+3,P,XXDEV,YYDEV,XYDEV,J2P");
   % SaveHis("POSITION,YLD,VOLM+3,P,XXDEV,YYDEV,XYDEV");
   % SaveHis("POSITION,Q3,PSR,VOLM+3");
   % SaveHis("POSITION,VOLM+3,DMG3");
    SaveTracer(ALL);
406  HisTime(0,6.60e-11);

   define spyhis_main()
   {
    HisLoad(1,"hscth");
411  Label("EFP Velocity (Tracer 1)");
    TPlot("VY.1",1,AUTOSCALE);
   }

   endspy
```

Appendix C. MATLAB Post Processing Code

C.1   CTH Data Extraction

Output data from CTH are stored a text file called "hscth." The output file is comma-delimited, and is easily opened and converted to tab-delimited using Excel. The "hscth" file includes data pertaining to the CTH cycle number and current step time. This is found in the second and third column. This data needs to be removed before passing the file through the MATLAB post-processing file. The first three rows of the "hscth" file needs to be removed as well. These header rows give the titles for each column and are unnecessary.

After the two columns and three rows are removed, the data set should consist of columns containg data in this order: time, x-position, y-position, von Mises stress, z-position, xy-stress deviator, yy-stress deviator, xx-stress deviator, material pressure (hydrostatic stress), volume fraction of the slipper, plastic strain rate, and plastic strain of the slipper. The default filename for this code is "cthData.txt" but this can be modified.

C.2   MATLAB Post Processing Code

```
%% CTH DATA POST PROCESS - PLANE STRAIN EVALUATION

% Stephen Meador - AFIT/GAE/ENY/10M-16
% Master's Student
% CTH Slipper Wear Post Process Code
% Written Sept 2009-Mar 2010

clear all; close all; clc

% HOW TO USE THIS POST-PROCESS FILE:
%{
This file is divided into several cells.  The first cell clears ...
   the
workspace and closes any open windows.  This cell also has two ...
   variables
that must be defined by the user: "aspRad" and "velocity."  aspRad...
    is the
plane strain asperity radius with units of micrometers, and ...
   velocity is the
collision velocity in meters per second.
```

The second cell defines the poisson's ratio of the slipper ...
material and the

19 mesh size used for CTH simulations defined with units of ...
centimeters
squared. This code assumes a uniform CTH cell arrangement where ...
the cells
are all squares of equal size. This is important for calculating ...
damage
area later in the code. Additionally, the directory containing ...
the CTH
data is defined based on the simulation asperity radius and ...
slipper

24 velocity defined in the first cell.

The third cell imports the CTH data, and the fourth cell ...
categorizes as
individual arrays and matrices. The data should be organized such...
that
each row represents the data extracted for a given time step of ...
the CTH

29 simulation, and the columns are the data extracted from the CTH ...
tracer
points. The user should note the order in which the variables are...
arranged
by the xxxLoc variables in cell four.

Cell five calculates the sliding distance for a given simulation. ...
This

34 distance is assumed to be 110*% of the asperity radius and is ...
calculated*
based on the velocity and simulation time. The sixth cell ...
calculates the
ZZ-deviatoric stress based on the other deviatoric stresses output...
from
CTH. The seventh cell then converts all stress components to ...
Pascals.

39 The eighth cell evaluates the strain rates at every tracer point ...
during
the simulation. The Johnson-Cook constitutive model defines the ...
minimum
strain rate as 0.002 1/s, so any strain rate below this value is ...
reset.
Also, if any strain rate exceeds 10^17 1/s then the code ...
terminates
because the stress and strain curve fits have not been evaluated ...
for data

44 above this level.

Cells nine and ten evaluate the stress tensor components and ...
calculate the

```matlab
    von Mises stresses, respectively.  Cells eleven through fourteen ...
        evaluate
    the various failure criteria.  And, finally, cell fifteen saves ...
        the wear
49 rate data to text files.
   %}

   aspRad = 6;           % microns

54 velocity = 700;       % meters per second

   VMcrit = 3.00e9;
   Yo = 1.897e9;
   SigHEL = 2.8664e9;
59
   tic

   %% POISSON'S RATIO, MESH SIZE,

64 nu = 0.283;                            % Poisson's ratio of material

   meshSize = 1.0e-4*1.0e-4;      % Area of a single mesh cell in cm...
       ^2

   if velocity < 100
69     newDirectory = ['Data/00' num2str(velocity) ...
           'mps/0' num2str(aspRad) 'micron'];
   elseif velocity <1000
       newDirectory = ['Data/0' num2str(velocity) ...
           'mps/0' num2str(aspRad) 'micron'];
74 else
       newDirectory = ['Data/' num2str(velocity) ...
           'mps/0' num2str(aspRad) 'micron'];
   end

79 cd(newDirectory)

   disp(' ')

   %% IMPORT DATA
84
   dataFile = 'cthData.txt';

   data = load(dataFile);

89 disp('Data Imported...')

   %% CATEGORIZE DATA

   time = data(:,1);
94
   numCycles = length(time);
```

```matlab
    numPoints = (size(data,2)-1)/12;

    xPoints = zeros(numCycles,numPoints);
    yPoints = zeros(numCycles,numPoints);
    pressureData = zeros(numCycles,numPoints);
    vonMisesData = zeros(numCycles,numPoints);
    xxdevData = zeros(numCycles,numPoints);
    yydevData = zeros(numCycles,numPoints);
    xydevData = zeros(numCycles,numPoints);
    vfData = zeros(numCycles,numPoints);
    srData = zeros(numCycles,numPoints);
    strainData = zeros(numCycles,numPoints);
    jcpData = zeros(numCycles,numPoints);

    xLoc = 2;
    yLoc = 3;
    vmLoc = 5;
    xyLoc = 6;
    yyLoc = 7;
    xxLoc = 8;
    pLoc = 9;
    vfLoc = 10;
    srLoc = 11;
    sLoc = 12;
    jcpLoc = 13;

    for iter = 1:numPoints
        xPoints(:,iter) = data(:,xLoc);
        yPoints(:,iter) = data(:,yLoc);
        pressureData(:,iter) = data(:,pLoc);
        vonMisesData(:,iter) = data(:,vmLoc);
        xxdevData(:,iter) = data(:,xxLoc);
        yydevData(:,iter) = data(:,yyLoc);
        xydevData(:,iter) = data(:,xyLoc);
        vfData(:,iter) = data(:,vfLoc);
        srData(:,iter) = data(:,srLoc);
        strainData(:,iter) = data(:,sLoc);
        jcpData(:,iter) = data(:,jcpLoc);

        xLoc = xLoc + 12;
        yLoc = yLoc + 12;
        vmLoc = vmLoc + 12;
        xyLoc = xyLoc + 12;
        yyLoc = yyLoc + 12;
        xxLoc = xxLoc + 12;
        pLoc = pLoc + 12;
        vfLoc = vfLoc + 12;
        srLoc = srLoc + 12;
        sLoc = sLoc + 12;
        jcpLoc = jcpLoc + 12;
    end
```

```matlab
    disp('Data Categorized...')

    %% CALCULATE DISTANCE SLID

    distanceSlid = velocity*time(end)*1000;      % mm

    disp('Distance Slid Calculated...')

    %% CALCULATE ZZDEV (GIVEN XXDEV, YYDEV, AND POISSON'S RATIO)

    zzdevData = (xxdevData+yydevData)*nu;

    disp('ZZ Deviator Calculated...')

    %% CONVERT DATA TO Pa

    pressureData = pressureData/10;
    xxdevData = xxdevData/10;
    yydevData = yydevData/10;
    xydevData = xydevData/10;
    zzdevData = zzdevData/10;
    jcpData = jcpData/10;
    vonMisesData = vonMisesData/10;

    %% EVALUATE STRAIN RATES FOR ZEROS

    for r = 1:size(srData,1)
        for c = 1:size(srData,2)
            if srData(r,c)<.002
                srData(r,c) = .002;
            end

             if srData(r,c)>10e17
                 disp('Temp:'),disp(temp)
                 disp('H Vel:'),disp(velocity)
                 disp('V Vel:'),disp(vVel)
                 disp('Row:'),disp(r)
                 disp('Col:'),disp(c)
                 disp('Strain Rate'),disp(srData(r,c))
                 error('Strain Rate Out of Range')
             end
        end
    end


    %% EVALUATE STRAIN AT MAX STRESS FAILURE AREA

    failureSMS = zeros(numCycles,numPoints);

    failureSumSMS = zeros(numCycles,1);

    A = 2.24700e-2;
```

```
    B = -5.5160e-2;
    C = 6.04400e-3;

    failureCritSMS = A*(srData.^B) + C;
204
    for row=1:r
        for col=1:c
            if row>1 && failureSMS(row-1,col)==1

209             failureSMS(row,col)=1;

            end

            if strainData(row,col)>=failureCritSMS(row,col)
214             failureSMS(row,col)=1;

            end
        end
219 end

    failureSMS = failureSMS.*vfData;

    for iter = 1:length(failureSumSMS)
224     failureSumSMS(iter,1) = sum(failureSMS(iter,:));
    end

    damAreaSMS = failureSumSMS*meshSize;

229 WR_SMS = 100*damAreaSMS(end)/distanceSlid;

    disp('Strain at Max Stress Failure Mechanism Evaluated...')

    %% Evaluate CTH J2P data
234
    failureSumVMS = zeros(numCycles,1);

    VONMISESDATA = zeros(numCycles,numPoints);

239 for row=1:r
        for col=1:c
            if row>1 && VONMISESDATA(row-1,col)==1

                VONMISESDATA(row,col)=1;
244
            end

            if row>1 && vonMisesData(row-1,col)>=VMcrit

249             VONMISESDATA(row,col)=1;
            end
        end
```

```matlab
    end

254 VonMisesFracData = VONMISESDATA.*vfData;

    for iter = 1:length(failureSumVMS)
        failureSumVMS(iter,1) = sum(VonMisesFracData(iter,:));
    end
259

    damAreaVMS = failureSumVMS*meshSize;

    WR_VMS = 100*damAreaVMS(end)/distanceSlid;

264 disp('VonMises Stress Failure Mechanism Evaluated...')

    %% SAVE WEAR RATES TO .txt FILE

    if velocity < 100
269     fileName = ['WearRates_00' num2str(velocity) ...
            'mps_0' num2str(aspRad) 'micron.txt'];
    elseif velocity <1000
        fileName = ['WearRates_0' num2str(velocity) ...
            'mps_0' num2str(aspRad) 'micron.txt'];
274 else
        fileName = ['WearRates_' num2str(velocity) ...
            'mps_0' num2str(aspRad) 'micron.txt'];
    end

279 fid=fopen(fileName,'wt');
    fprintf(fid,'%6.5e\t%6.5e\t%6.5e\t%6.5e\t',...
        WR_SMS*8.29e-3,...
        WR_VMS*8.29e-3);
    fclose(fid);
284
    disp('Failure Data Saved...')

    %% END PROGRAM

289 disp('PROGRAM COMPLETE...')

    toc

    %% Plot Pressure Time Data for points @ (x,y) = (0.0692,0.0204)
294
    Pressure(1:numCycles,1) = pressureData(1:101,424)-pressureData...
        (1,424);


    figure
299 plot(time,Pressure(1:numCycles,1))
    xlabel('time (s)')
    ylabel('Pressure (GPa)')
    title('Pressure at (x,y) = (0.0692,0.0202)')
```

```
grid on
```

Appendix D. MATLAB Code for Pressure Along a Diagonal

The MATLAB code presented in this appendix is used to plot the pressure along a 30° 45° and 60° diagonal from the point of contact between the slipper and asperity with respect to the horizontal rail. The CTH input deck must be modified before the MATLAB code can be used. The tracer input set, line 177 to line 213 of the example CTH input deck in Appendix B, defines the initial locations of the data points. This section must be modified to only include data points along the diagonals. Replacing lines 177 to 213 with the following lines records data along the 30° diagonal. This input deck must be run three times to record the data, with each run capturing one diagonal. The asterisks at the begining of a line comments that line out of the input deck. To capture data along the 45° diagonal, an asterisk needs to be added to line 2 to comment the 30° out, and the asterisk on line 6 should be removed. Removing the asterisk on line 9 captures the data along the 60° diagonal.

D.1   Modified Tracer Input Set

```
tracer
* 30 degrees
        add 693.4e-4, 200.6e-4 to 578.45e-4, 266.64e-4 n=500

* 45 degrees
*       add 693.4e-4, 200.6e-4 to 600e-4, 294e-4 n=500

* 60 degrees
*       add 693.4e-4, 200.6e-4 to 627.36e-4, 315.53e-4 n=500
endtracer
```

When the three simulations are finished, the first two columns and first three rows need to be removed in Excel using the process outlined in Appendix C. The MATLAB code plots the change in pressure along the three diagonals with respect to distance for each time step. These images are used to determine the elastic-plastic wave speed through the VascoMax 300 slipper in Section 4.4.

D.2   MATLAB Post Processing Code

```
clear all; close all; clc

%% VELOCITY TO PLOT
```

```matlab
 5 velocity = 500;

   angle = 45;

   %% LOAD DATA
10
   if velocity <100
       datafile = ['00' num2str(velocity) 'mps30degData.txt'];
   elseif velocity <1000
       datafile = ['0' num2str(velocity) 'mps30degData.txt'];
15 else
       datafile = [num2str(velocity) 'mps30degData.txt'];
   end

   data30 = load(datafile);
20
   if velocity <100
       datafile = ['00' num2str(velocity) 'mps45degData.txt'];
   elseif velocity <1000
       datafile = ['0' num2str(velocity) 'mps45degData.txt'];
25 else
       datafile = [num2str(velocity) 'mps45degData.txt'];
   end

   data45 = load(datafile);
30
   if velocity <100
       datafile = ['00' num2str(velocity) 'mps60degData.txt'];
   elseif velocity <1000
       datafile = ['0' num2str(velocity) 'mps60degData.txt'];
35 else
       datafile = [num2str(velocity) 'mps60degData.txt'];
   end

   data60 = load(datafile);
40
   %% ORGANIZE 30 DEGREE DATA

   time30 = data30(:,1);

45 nCycles30 = size(data30,1);
   nPoints30 = (size(data30,2)-1)/4;

   xPos30 = 2;
   yPos30 = 3;
50 zPos30 = 4;
   pPos30 = 5;

   xData30 = zeros(nCycles30,nPoints30);
   yData30 = zeros(nCycles30,nPoints30);
55 zData30 = zeros(nCycles30,nPoints30);
```

```matlab
    pData30 = zeros(nCycles30,nPoints30);

    for iter = 1:nPoints30
        xData30(:,iter) = data30(:,xPos30);
        yData30(:,iter) = data30(:,yPos30);
        zData30(:,iter) = data30(:,zPos30);
        pData30(:,iter) = data30(:,pPos30);

        xPos30 = xPos30 + 4;
        yPos30 = yPos30 + 4;
        zPos30 = zPos30 + 4;
        pPos30 = pPos30 + 4;
    end

%% ORGANIZE 45 DEGREE DATA

    time45 = data45(:,1);

    nCycles45 = size(data45,1);
    nPoints45 = (size(data45,2)-1)/4;

    xPos45 = 2;
    yPos45 = 3;
    zPos45 = 4;
    pPos45 = 5;

    xData45 = zeros(nCycles45,nPoints45);
    yData45 = zeros(nCycles45,nPoints45);
    zData45 = zeros(nCycles45,nPoints45);
    pData45 = zeros(nCycles45,nPoints45);

    for iter = 1:nPoints45
        xData45(:,iter) = data45(:,xPos45);
        yData45(:,iter) = data45(:,yPos45);
        zData45(:,iter) = data45(:,zPos45);
        pData45(:,iter) = data45(:,pPos45);

        xPos45 = xPos45 + 4;
        yPos45 = yPos45 + 4;
        zPos45 = zPos45 + 4;
        pPos45 = pPos45 + 4;
    end

    %% ORGANIZE 60 DEGREE DATA

    time60 = data60(:,1);

    nCycles60 = size(data60,1);
    nPoints60 = (size(data60,2)-1)/4;

    xPos60 = 2;
    yPos60 = 3;
```

```matlab
    zPos60 = 4;
    pPos60 = 5;

    xData60 = zeros(nCycles60,nPoints60);
    yData60 = zeros(nCycles60,nPoints60);
    zData60 = zeros(nCycles60,nPoints60);
    pData60 = zeros(nCycles60,nPoints60);

    for iter = 1:nPoints60
        xData60(:,iter) = data60(:,xPos60);
        yData60(:,iter) = data60(:,yPos60);
        zData60(:,iter) = data60(:,zPos60);
        pData60(:,iter) = data60(:,pPos60);

        xPos60 = xPos60 + 4;
        yPos60 = yPos60 + 4;
        zPos60 = zPos60 + 4;
        pPos60 = pPos60 + 4;
    end

    %% CONVERT UNITS

pInt30 = mean(pData30(1,:));    % Initial Pressure

    pData30 = pData30-pInt30;        % Pressure Change

    pData30 = pData30/10;        % Pa
pData30 = pData30/10^9;        % GPa

    xData30 = xData30*10^4;        % microns
    yData30 = yData30*10^4;        % microns

pInt45 = mean(pData45(1,:));    % Initial Pressure

    pData45 = pData45-pInt45;        % Pressure Change

    pData45 = pData45/10;        % Pa
pData45 = pData45/10^9;        % GPa

    xData45 = xData45*10^4;        % microns
    yData45 = yData45*10^4;        % microns

pInt60 = mean(pData60(1,:));    % Initial Pressure

    pData60 = pData60-pInt60;        % Pressure Change

    pData60 = pData60/10;        % Pa
pData60 = pData60/10^9;        % GPa

    xData60 = xData60*10^4;        % microns
    yData60 = yData60*10^4;        % microns
```

```
160 %% DEFINE LENGTH

    minX30 = min(xData30(1,:));
    maxX30 = max(xData30(1,:));
    minY30 = min(yData30(1,:));
165 maxY30 = max(yData30(1,:));

    deltaX30 = maxX30 - minX30;
    deltaY30 = maxY30 - minY30;

170 length30 = sqrt(deltaX30^2 + deltaY30^2);

    tracerPoints30 = linspace(0,length30,nPoints30);

    minX45 = min(xData45(1,:));
175 maxX45 = max(xData45(1,:));
    minY45 = min(yData45(1,:));
    maxY45 = max(yData45(1,:));

    deltaX45 = maxX45 - minX45;
180 deltaY45 = maxY45 - minY45;

    length45 = sqrt(deltaX45^2 + deltaY45^2);

    tracerPoints45 = linspace(0,length45,nPoints45);
185
    minX60 = min(xData60(1,:));
    maxX60 = max(xData60(1,:));
    minY60 = min(yData60(1,:));
    maxY60 = max(yData60(1,:));
190
    deltaX60 = maxX60 - minX60;
    deltaY60 = maxY60 - minY60;

    length60 = sqrt(deltaX60^2 + deltaY60^2);
195
    tracerPoints60 = linspace(0,length60,nPoints60);

    %% PLOT

200

    figNum = 0;

    plotTracers = 0;
205 if plotTracers
        for index = 1%:100:nCycles

            x = [500 693.4];
            y30 = [200*tand(30)+200.6 200.6];
210         y45 = [200*tand(45)+200.6 200.6];
            y60 = [200*tand(60)+200.6 200.6];
```

```
            testX = xData30 ( index ,:);
            testY = yData30 ( index ,:);
215         testP = pData30 ( index ,:);

            figNum = figNum + 1;
            figure ( figNum )
            hold on
220         plot ( testX , testY , 'd ')
            plot (x , y30 , 'k ')
            plot (x , y45 , 'k ')
            plot (x , y60 , 'k ')
            axis ( 'square ')
225         xLim ([500 700])
            yLim ([200 400])


        end
    end
230
    plotPressures = 1;
    if plotPressures
        for index = 1:1: min ([ nCycles30 nCycles45 nCycles60 ])

235         titleText = sprintf ( '%4.0 f m/s | Pressure Change Along ...
                Diagonal at %1.2 e seconds ', velocity , time30 ( index ));

            p30 = pData30 ( index ,:);
            p45 = pData45 ( index ,:);
            p60 = pData60 ( index ,:);
240
            figNum = figNum + 1;
            figure ( figNum )
            subplot (1 ,7 ,[3 7])
            hold on
245         plot ( tracerPoints30 ,p30 , 'r ', 'LineWidth ',2)
            plot ( tracerPoints45 ,p45 , 'k ', 'LineWidth ',2)
            plot ( tracerPoints60 ,p60 , 'b ', 'LineWidth ',2)
%                    plot ([6 6] ,[ -10 15] , 'r -- ', 'LineWidth ',2)
            xlim ([ min ( min ([ tracerPoints30 ; tracerPoints45 ; ...
                tracerPoints60 ])) max ( max ([ tracerPoints30 ; ...
                tracerPoints45 ; tracerPoints60 ]))])
250         ylim ([ -15 15])
%            title ({[ num2str ( velocity ) ' m/s | Pressure Change Along ...
     Diagonal at Time ' num2str ( time30 ( index )) ' seconds ']})
            title ( titleText )
            xlabel ( 'Distance Along Diagonal (\ mum ) ')
            ylabel ( '\ DeltaP ( GPa ) ')
255         grid on
            legend ( '30 deg ', '45 deg ', '60 deg ', 'Location ', 'NorthEast ')
            subplot (1 ,7 ,1)
            bar (( index -1) /( min ([ nCycles30 nCycles45 nCycles60 ]) -1)...
                *100 , 'k ', 'BarWidth ',1)
```

111

```matlab
            ylim([0 100])
260         ylabel('Percentage of Simulation Time Completed')

            if index<10
                if velocity<100
                    saveas(gcf,['00' num2str(velocity) 'mps00' num2str...
                        (index) '.bmp'])
265             elseif velocity<1000
                    saveas(gcf,['0' num2str(velocity) 'mps00' num2str(...
                        index) '.bmp'])
                else
                    saveas(gcf,['0' num2str(velocity) 'mps00' num2str(...
                        index) '.bmp'])
                end
270         elseif index<100
                if velocity<100
                    saveas(gcf,['00' num2str(velocity) 'mps0' num2str(...
                        index) '.bmp'])
                elseif velocity<1000
                    saveas(gcf,['0' num2str(velocity) 'mps0' num2str(...
                        index) '.bmp'])
275             else
                    saveas(gcf,['0' num2str(velocity) 'mps0' num2str(...
                        index) '.bmp'])
                end
            else
                if velocity<100
280                 saveas(gcf,['00' num2str(velocity) 'mps' num2str(...
                        index) '.bmp'])
                elseif velocity<1000
                    saveas(gcf,['0' num2str(velocity) 'mps' num2str(...
                        index) '.bmp'])
                else
                    saveas(gcf,['0' num2str(velocity) 'mps' num2str(...
                        index) '.bmp'])
285             end
            end

            close(gcf)

290     end
    end

    figNum = figNum + 1;
    figure(figNum)
295 plot(time30,pData30(:,114),'k','LineWidth',2)
    xlim([0 max(time30)])
    ylim([-15 15])
    title('Pressure at 30 \mum Along 30^{\circ} Diagonal')
    xlabel('Time (s)')
300 ylabel('\DeltaP (GPa)')
```

```matlab
    figNum = figNum + 1;
    figure(figNum)
    plot(time30,pData30(:,227),'k','LineWidth',2)
305 xlim([0 max(time30)])
    ylim([-15 15])
    title('Pressure at 60 \mum Along 30^{\circ} Diagonal')
    xlabel('Time (s)')
    ylabel('\DeltaP (GPa)')
310
    figNum = figNum + 1;
    figure(figNum)
    plot(time45,pData45(:,115),'k','LineWidth',2)
    xlim([0 max(time45)])
315 ylim([-15 15])
    title('Pressure at 30 \mum Along 45^{\circ} Diagonal')
    xlabel('Time (s)')
    ylabel('\DeltaP (GPa)')

320 figNum = figNum + 1;
    figure(figNum)
    plot(time45,pData45(:,229),'k','LineWidth',2)
    xlim([0 max(time45)])
    ylim([-15 15])
325 title('Pressure at 60 \mum Along 45^{\circ} Diagonal')
    xlabel('Time (s)')
    ylabel('\DeltaP (GPa)')

    figNum = figNum + 1;
330 figure(figNum)
    plot(time60,pData60(:,114),'k','LineWidth',2)
    xlim([0 max(time60)])
    ylim([-15 15])
    title('Pressure at 30 \mum Along 60^{\circ} Diagonal')
335 xlabel('Time (s)')
    ylabel('\DeltaP (GPa)')

    figNum = figNum + 1;
    figure(figNum)
340 plot(time60,pData60(:,227),'k','LineWidth',2)
    xlim([0 max(time60)])
    ylim([-15 15])
    title('Pressure at 60 \mum Along 60^{\circ} Diagonal')
    xlabel('Time (s)')
345 ylabel('\DeltaP (GPa)')
```

Bibliography

1. *Holloman High Speed Test Track Design Manual.* Technical report, 846th Test Squadron, 46th Test Group, Holloman AFB, New Mexico, 2008.

2. Archard, J. F. "Contact and Rubbing of Flat Surfaces". *Journal of Applied Physics*, 24(8):981–988, August 1953.

3. Archard, J. F. "The Temperature of Rubbing Surfaces". *Wear*, 2(6):438–455, October 1959.

4. Archard, J. F. and W. Hirst. "The Wear of Metals Under Unlubricated Conditions". *Proceedings of the Royal Society of London. Series A, Mathematical and Physical Sciences*, 236:397 – 410, 1956.

5. ASTM. *Standard Terminology Relating to Wear and Erosion.* ASTM, 2001.

6. Bayer, R. G. *Wear Analysis for Engineers.* HNB Publishing, New York, 2002.

7. Bayer, R. G. *Engineering Design for Wear.* Marcel Dekker, Inc., New York, 2004.

8. Bayer, R. G. *Mechanical Wear Fundamentals and Testing.* Marcel Dekker, Inc., New York, 2004.

9. Bhushan, Barat. *Introduction to Tribology.* John Wiley and Sons, 2002.

10. Burton, Chad A. *A Finite Element Study Of Sliding Friction Between Two Rough Surfaces.* Master's thesis, University of Dayton, Dayton, Ohio, 2009.

11. Burton, Chad A. and Robert A. Brockman. "Frictional Interactions in High-speed Sliding Contact". *Proceedings of the 50th AIAA/ASME/ASCE/AHS/ASC Structures, Structural Dynamics and Materials Conference*, 2009.

12. Cameron, G. and A. Palazotto. "An Evaluation of High Velocity Wear". *Wear*, In Press, Corrected Proof.

13. Cameron, G. J. *An Evaluation of High Velocity Wear, AFIT/GAE/ENY/07-M06.* Master's thesis, Air Force Institute of Technology, Wright Patterson AFB, OH, 2007.

14. Chmiel, A. J. *Finite Element Simulation Methods for Dry Sliding Wear, AFIT/GAE/ENY/08-M03.* Master's thesis, Air Force Institute of Technology, Wright Patterson AFB, OH, 2008.

15. Cinnamon, J. D. *Analysis and Simulation of Hypervelocity Gouging Impacts, AFIT/DS/ENY/06-01.* Ph.D. thesis, Air Force Institute of Technology, Wright Patterson AFB, OH, 2006.

16. Cinnamon, J. D., A. N. Palazotto, and Z. Keenan. "Material Characterization and Development of a Constitutive Relationship for Hypervelocity Impact of 1080

Steel and VascoMax 300". *International Journal of Impact Engineering*, 33(1-12):180–189, December 2006.

17. Cinnamon, J. D., A. N. Palazotto, and A. G. Szmerekovsky. "Further Refinement and Validation of Material Models for Hypervelocity Gouging Impacts". *AIAA Journal*, 46(2):317–327, 2008.

18. Crawford, D. A. and R. L. Bell. *CTH User's Manual and Input Instructions Version 8.1*. Technical report, CTH Development Project Sandia National Laboratories, 2007.

19. Farrell, R. M. and T. S. Eyre. "The Relationship Between Load and Sliding Distance in the Initiation of Mild Wear in Steels". *Wear*, 15:359 – 372, 1970.

20. Hale, Chad S. *Consideration of Wear Rates at High Velocities, AFIT/DS/ENY/10-08*. Ph.D. thesis, Air Force Institute of Technology, Wright Patterson AFB, OH, 2009.

21. Hooser, M. D. "Simulation of 10,000 Foot per Second Ground Vehicle". *Proceedings of the 21st AIAA Advanced Measurement Technology and Ground Testing Conference*, 2000.

22. Hooser, M. D. "Validation of Dynamic Simulation Techniques at the Holloman High Speed Test Track". *Proceedings of the 38th AIAA Aerospace Sciences Meeting and Exhibit*, 2000.

23. Johnson, Gordon R. and William H. Cook. "A Constitutive Model and Data for Metals Subjected to Large Strain, High Strain Rates and High Temperatures". *Proceedings of the 7th International Symposium on Ballistics*, 1983.

24. Johnson, Gordon R. and William H. Cook. "Fracture Characteristics of Three Metals Subjected to Various Strains, Strain Rates, Temperatures and Pressures". *Engineering Fracture Mechanics*, 21:31 – 48, 1985.

25. Lee, Jason K. *Analysis of Multi-Layered Materials Under High Velocity Impact Using CTH, AFIT/GAE/ENY/08-M19*. Master's thesis, Air Force Institute of Technology, Wright Patterson AFB, OH, 2008.

26. Lim, S. C. and M. F. Ashby. "Wear-Mechanism Maps". *Acta Metallurgica*, 35:1 – 24, 1987.

27. Lodydgowski, Adam. *Friction and Wear at Elevated Velocities*. Ph.D. thesis, Louisiana State University, Baton Rouge, Louisiana, 2010.

28. Meador, Stephen P. *Consideration of Wear at High Velocities, AFIT/GAE/ENY/10-M16*. Master's thesis, Air Force Institute of Technology, Wright Patterson AFB, OH, 2010.

29. Meyers, Marc A. *Dynamic Behavior of Materials*. John Wiley and Sons, New York, 1994.

30. Montgomery, R. S. "Friction and Wear at High Sliding Speeds". *Wear*, 36:275 – 298, 1976.

31. Palazotto, Anthony N. and Stephen P. Meador. "Consideration of Wear at High Velocities Using a Hydrocode". *AIAA*, Accepted for publication 2011.

32. Saada, Adel S. *Elasticity Theory and Applications*. Krieger Pub Co, 1993.

33. Silling, Stewart. *Use of the Johnson-Cook Fracture Model in CTH*. Technical report, Sandia National Laboratories, 1996.

34. Vanderhyde, Michael J. *Comparison of Thermodynamic Equilibrium and Non-Equilibrium Representations of Materials, AFIT/GAE/ENY/07-M25*. Master's thesis, Air Force Institute of Technology, Wright Patterson AFB, OH, 2007.

35. Wilson, Roy and Anthony Palazotto. "Viscoplastic Fatigue in a Superalloy at Elevated Temperatures". *Engineering Fracture Mechanics*, 22:927 – 937, 1985.

36. Wolfson, M. R. *Wear, Solid Lubrication, and Bearing Material Investigation for High-Speed Track Applications*. Technical Report AFMDC-TR-60-7, Test Track Division, Air Force Missile Development Center, Holloman AFB, New Mexico, March 1960.

37. Zukas, Jonas A. *Introduction to Hydrocodes*. Elsevier, Amsterdam, 2004.

REPORT DOCUMENTATION PAGE

Form Approved
OMB No. 0704–0188

1. REPORT DATE *(DD–MM–YYYY)*	2. REPORT TYPE	3. DATES COVERED *(From — To)*
15–12–2011	Master's Thesis	Oct 2010 — Dec 2011

4. TITLE AND SUBTITLE

The Use of Various Failure Criteria
As Applied
To High Speed Wear

5a. CONTRACT NUMBER

5b. GRANT NUMBER

5c. PROGRAM ELEMENT NUMBER

6. AUTHOR(S)

David Huber

5d. PROJECT NUMBER

5e. TASK NUMBER

5f. WORK UNIT NUMBER

7. PERFORMING ORGANIZATION NAME(S) AND ADDRESS(ES)

Air Force Institute of Technology
Graduate School of Engineering and Management (AFIT/EN)
2950 Hobson Way
WPAFB OH 45433-7765

8. PERFORMING ORGANIZATION REPORT NUMBER

AFIT/GAE/ENY/11-D01

9. SPONSORING / MONITORING AGENCY NAME(S) AND ADDRESS(ES)

Air Force Office of Scientific Research
Attn: Dr. Michael Kendra
875 Randolph St., Suite 325
Arlington, VA 22203
(703)588-0671
michael.kendra@afosr.af.mil

10. SPONSOR/MONITOR'S ACRONYM(S)

AFOSR

11. SPONSOR/MONITOR'S REPORT NUMBER(S)

12. DISTRIBUTION / AVAILABILITY STATEMENT

APPROVED FOR PUBLIC RELEASE; DISTRIBUTION UNLIMITED

13. SUPPLEMENTARY NOTES

This material is declared a work of the U.S. Government and is not subject to copyright protection in the United States.

14. ABSTRACT

This research has been aimed at developing methods to predict mechanical wear of sliding bodies at high velocities. Specifically, wear of test sled slippers at the Holloman High Speed Test Track at Holloman AFB, NM, is being considered. Developing a numerical model to represent the velocity range achieved at the test track is infeasible, so numerical modeling techniques must be adopted. Previous research has made use of finite element codes to simulate the high velocity sliding event. However, the extreme velocities at the test track can create numerical errors in the finite element codes. To avoid the numerical errors, an Eulerian-Lagrangian hydrocode called CTH has been used to allow for a velocity range of 200 to 1,500 meters per second. The CTH model used in this research performs plane strain analysis of a slipper colliding with a 6 μm radius semi-circular surface asperity. The slipper-asperity collision event creates pressure waves in the slipper which leads to failed cells and worn material. Equations have been derived to represent the onset of plasticity and elastic wave speed through a material under plane strain conditions. These equations were validated using the CTH model. Several failure criteria were evaluated as possible methods to estimate damaged material from the sliding body. The Johnson and Cook constitutive model was selected because of its ability to handle high strains, strain rates, and temperatures. The model developed in this thesis calculates total mechanical wear between 49.31% and 80.87% of the experimental wear from the HHSTT January 2008 test mission.

15. SUBJECT TERMS

High Velocity Wear, Plane Strain Hugoniot Elastic Limit, Plane Strain Elastic Wave Speed, Holloman High Speed Test Track, Hydrocode, CTH

16. SECURITY CLASSIFICATION OF:			17. LIMITATION OF ABSTRACT	18. NUMBER OF PAGES	19a. NAME OF RESPONSIBLE PERSON
a. REPORT	b. ABSTRACT	c. THIS PAGE			Dr. Anthony N. Palazotto
U	U	U	UU	133	19b. TELEPHONE NUMBER *(include area code)* (937) 255–3636, ext 4599

Standard Form 298 (Rev. 8–98)
Prescribed by ANSI Std. Z39.18